

# Physical mechanisms providing formation of ohmic contacts metal–semiconductor (Review)

A.V. Sachenko\*, R.V. Konakova, A.E. Belyaev

V. Lashkaryov Institute of Semiconductor Physics, National Academy of Sciences of Ukraine  
45, prospect Nauky, 03680 Kyiv, Ukraine

\*E-mail: sach@isp.kiev.ua

**Abstract.** This review is devoted to presentation and analysis of physical mechanisms of ohmic contacts formation in semiconductors. In addition to the classical mechanisms known for decades, new mechanisms for current flow in ohmic contacts researched for the recent decade are described. Used in this review were the original results of the authors, which they described earlier in various papers of recent years. Current flow through dislocations combined with metal shunts, realized, in particular, on the lapped semiconductor surface; detailed current flow mechanism in the presence of doping step and current flow through the heavily doped semiconductor surface charge states reduction should be noted among the new mechanisms of current flow. These current flow mechanisms are characterized by the presence of specific contact resistance growth with temperature increase in some temperature intervals and contacts ohmicity up to helium temperatures.

**Keywords:** ohmic contacts, helium temperatures, metal–semiconductor contact, surface states current flow mechanisms specific contact resistance.

doi: <https://doi.org/10.15407/spqeo21.01.005>

PACS 61.72.Ft, 61.72.Hh, 61.72.Lk, 73.30.+y, 73.40.cg, 73.40.Ns

Manuscript received 22.12.17; revised version received 18.03.18; accepted for publication 29.03.18; published online 29.03.18.

## Contents

1. Historical background	6	5.2. The specimens and methods of investigation	19
2. Classical current flow mechanisms ensuring ohmic contact realization	6	5.3. The results of measurements and discussion	19
3. Mechanism of contact resistance formation in ohmic contacts with high dislocation density	7	5.4. Conclusions	23
3.1 Introduction	7	6. The temperature dependence of contact resistivity for ohmic contacts to $n$ -Si with an $n^+$ - $n$ doping step	23
3.2. Theoretical basis for the concept development	8	6.1. Introduction	23
3.2.1. Distribution of potentials	8	6.2. Model of the ohmic contact with a doping step	23
3.2.2. Calculation of currents	9	6.3. Conclusions	26
3.2.3. General relations and limit cases	10	7. On the ohmicity of Schottky contacts	26
3.3. Discussion of results and comparison with experiment	12	7.1. Introduction	26
3.4. Conclusions	15	7.2. General expressions for the current of majority and minority carriers through the Schottky contact with a dielectric gap	26
4. Features of temperature dependence of contact resistivity in ohmic contacts on lapped $n$ -Si	15	7.3. Criteria for Schottky-contact ohmicity	28
4.1. Introduction	15	7.4. Analysis of currents through the Schottky contacts with allowance for the minority-carrier current	29
4.2. Theoretical notions	16	7.5. Results and discussion	31
4.3. The specimens and methods of measurement	16	7.6. Conclusions	32
4.4. Experimental results and discussion	17	8. A new mechanism for realization of ohmic contacts	32
4.5. Conclusions	18	8.1. Introduction	32
5. Some features of temperature dependence of contact resistivity for ohmic contacts to $n^+$ -InN	18	8.2. Problem statement	32
5.1. Introduction	18	8.3. Analysis of results	33
		8.4. Conclusions	35
		9. General conclusions	36
		References	36

## 1. Historical background

An ohmic contact is such metal–semiconductor contact at which an applied voltage decreases linearly, and the contact resistance  $R_c$  is low as compared with that of bulk semiconductor  $R_b$ . Ohmic contacts are integral parts of any semiconductor device. Regular experimental investigations of metal–semiconductor contacts began about eighty years ago. A considerable part of the studies deals with the so-called Schottky (or rectifying) contacts at which boundaries there is a potential barrier. In the same years, the pioneer theoretical works were performed that dealt with mechanisms of current flow in contacts – mainly, in the Schottky ones (Mott, Davydov, Pekar, Schottky) [1-7]. Somewhat later, the work by Bardeen appeared [8], in which it was shown that in most cases presence of barrier is not due to contact difference of metal and semiconductor work functions,  $\varphi_{ms}$ , but owes to density and energy distribution of semiconductor surface states. The latter, in Spicer’s opinion [9], are formed because of presence of foreign atoms on semiconductor surface.

The studies of ohmic contacts have been developing simultaneously with the physical investigations of Schottky contacts. Their stages are rather minutely presented in the review by Gol’dberg [10]. By now, there are many monographs and reviews dealing with presenting the physical processes of current flow in the Schottky contacts as well as their applied applications. Some of them contain chapters or sections dealing with the properties of ohmic contacts [11-19]. At the same time, the monographs describing current flow mechanisms in ohmic contacts are few in number, and the material presented in them is mostly of descriptive character (see, *e.g.* [20]). By now, the physical mechanisms that explain Schottky contacts functioning are principally understood. Contrary to this, the mechanisms of ohmic contacts operation still are being specified. In particular, several physical mechanisms explaining temperature growth of ohmic contacts resistivity were proposed in the recent 10–15 years. Among them, there are current flow through metal shunts coupled with extensive defects in semiconductors [20-26], current flow in ohmic contacts with a doping step [27] and the mechanism of partial screening of surface charge states at high doping levels [28].

Returning to the background, we firstly dwell upon an analysis of ohmic contact formation mechanisms given in [11-19] and then go to description of physical features that ensure realization of ohmic contacts, contact resistivity of which increases with temperature. At the end, criteria for ohmicity of metal–semiconductor contacts are considered in detail.

## 2. Classical current flow mechanisms ensuring ohmic contact realization

In this section, a brief description is given for classical mechanisms of current flow in a metal–semiconductor contact that lead to ohmic contact realization. (For the

most part, the description uses the approach considered in the monograph [19] and the review [10].) They are, first of all, thermionic, thermal-field and tunnel (field) current flow mechanisms.

Shown in Fig. 1 is the energy diagram illustrating these mechanisms. If the thermionic, thermal-field or tunnel (field) mechanism is realized, then the current of majority charge carriers flows over the barrier, through the barrier over the Fermi level or through the barrier at the Fermi energy level, respectively.

The criteria for realization of the above cases were considered by Padovani and Stratton [30]. They introduced the parameter  $E_{00}$ , the physical meaning of which is the tunneling energy. For  $n$ -semiconductor, this parameter is

$$E_{00} = \frac{\hbar}{2} \sqrt{\frac{N_d}{\epsilon_0 \epsilon_s m^*}}, \quad (1)$$

where  $\hbar$  is the reduced Planck constant,  $N_d \cong n_0$  – concentration of shallow ionized donors (equal to the equilibrium concentration of majority charge carriers in a semiconductor),  $\epsilon_0$  – vacuum permittivity,  $\epsilon_s$  – semiconductor permittivity, and  $m^*$  – effective mass of tunneling charge carriers.

It was shown in [30] that at  $E_{00} \ll kT$  the main current flow mechanism is thermionic emission, while at  $E_{00} \approx kT$  or  $E_{00} \gg kT$  these are thermal-field emission and tunnel emission, respectively,  $k$  is the Boltzmann constant,  $T$  is temperature. Knowing the flowing current, one can determine the resistivity  $R_c$  of metal–semiconductor contact:

$$R_c = \left( \frac{dI}{dV} \right)_{V=0}^{-1}, \quad (2)$$

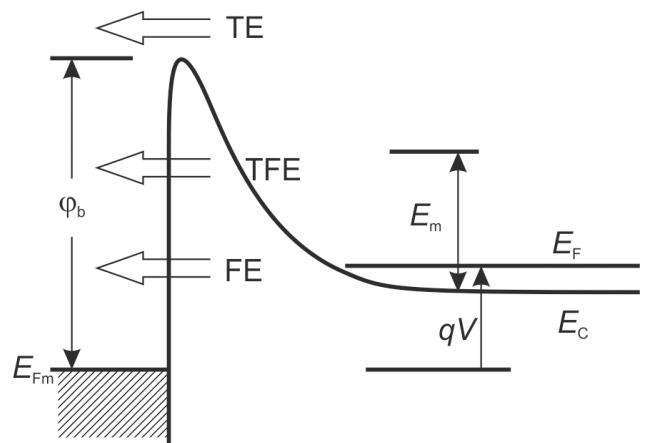


**Fig. 1.** The energy diagram of contact metal–semiconductor:  $E_c$  is the bottom of the conduction band and  $E_v$  is the top of the valence band in semiconductor;  $E_{Fm}$  is the Fermi level in metal;  $E_F$  is the quasi-Fermi level for electrons in semiconductor;  $\varphi_b$  is the barrier height, counted from the bottom of the conduction band;  $E_m$  is energy of thermal-field emission (TFE), and  $V$  is the applied voltage.

where  $I$  is flowing current density. The criterion for contact ohmicity is the inequality

$$R_c < R_b. \quad (3)$$

Here,  $R_b$  is the bulk semiconductor resistance. In the case of cylindrical geometry, it is equal to  $(q\mu_n N_d)^{-1} d/S$  ( $q$  is the elementary charge,  $\mu_n$  – mobility of majority charge carriers,  $d$  and  $S$  are thickness and cross-sectional area, respectively).

The temperature dependences of  $R_c$  for the above current flow mechanisms are as follows: 1) at the thermionic mechanism,  $R_c$  decreases with temperature according to the law  $\exp(q\phi_b/kT)$  ( $\phi_b$  is the barrier height); 2) at thermal-field mechanism,  $R_c$  also decreases with temperature but weaker than in the preceding case; 3) at tunnel mechanism,  $R_c$  does not depend on temperature.

In most practical applications, it is possible to use the following expression:

$$R_c \propto \exp\left(\frac{q\phi_b}{E_0}\right), \quad (4)$$

where  $E_0 = E_{00} \coth(E_{00}/kT)$ . In the case (1),  $\ln(R_c) = f_1(\phi_b/kT)$ , and its slope in coordinates  $1/T$  is proportional to the barrier height. In the case (2),  $\ln(R_c) = f_2(\phi_b/E_0)$ , and its slope in coordinates  $1/E_0$  is proportional to the barrier height. In the case (3),  $\ln(R_c) = f_3(\phi_b/E_{00})$ , and its slope in coordinates  $1/N_d^{1/2}$  makes it possible to determine the barrier height. More exact expressions of contact resistivity  $R_c$  for the above current flow mechanisms are presented, *e.g.*, in the monograph [19] and the review [10].

The case of the so-called doping step (when the semiconductor near-contact region is doped very heavily – up to degeneracy) is in fact a combination of the thermionic and tunnel mechanisms of current flow [27].

A special case of the step doping is  $\delta$ -doping that is used to obtain ohmic contacts in up-to-date microelectronic devices.

The barrier height can be reduced, if a semiconductor with narrower forbidden band is used in the near-contact region. In many cases, it promotes ohmic contact realization [10].

The case of current flow through metal shunts associated with extensive defects (*e.g.*, dislocations) in semiconductor near-contact region considered in [10] is a special case of more general one that will be considered below.

Practically in all reviews and monographs having chapters or sections dealing with ohmic contacts, it is stated that ohmic contacts can be realized in structures with high velocity of charge carrier recombination at the metal–semiconductor interface. This high velocity at the contact is obtained after previous lapping the semiconductor surface before formation of a metal–semiconductor contact. Indeed, it was shown in a number

of works (see [27]) that the contact becomes ohmic after pre-lapping the semiconductor surface. However, the physical reason for ohmic contact realization in this case is related to appearance of high density of dislocations (which ensure current flow through metal shunts) rather than to high surface recombination velocity. Moreover, as was shown in [27], the current of majority charge carriers flowing into ohmic contact does not depend on the surface recombination velocity value.

The results of analysis of the mentioned features of ohmic contact resistivity will be considered more comprehensively in the present review.

The results of analyzing the new ohmic contacts forming mechanisms are shown in [21-29].

It is shown that the case of conductivity through metal shunts, conjugated with prolonged defects in the semiconductor contact area (for example, dislocations) considered in [10] is a particular case of the general one analyzed in [21].

The case of a doping step is analyzed in details in the review. It is shown that for the weak and moderate semiconductor doping, the specific contact resistance is defined by the specific resistance of weakly doped area and increases with temperature. Special attention is paid to the analysis of contact ohmicity realization criteria, which allows correcting the inaccurate results given in literature. So, practically in all reviews and monographs having chapters or sections dealing with ohmic contacts, it is stated that ohmic contacts can be realized in structures with a high velocity of charge carrier recombination at the metal–semiconductor interface. This high velocity at the contact is obtained after previous lapping of semiconductor surface before formation of a metal–semiconductor contact. Indeed, it was shown in a number of works (see [27]) that the contact becomes ohmic after pre-lapping of semiconductor surface. However, the physical reason for ohmic contact realization in this case is related to appearance of high density of dislocations (which ensure current flow through metal shunts) rather than to high surface recombination velocity. Moreover, as was shown in [27], the current of majority charge carriers flowing into ohmic contact does not depend on the surface recombination velocity value.

And, at the end, the heavily doped semiconductor surface charge states reduction mechanism is analyzed. It is shown that this mechanism can promote contact ohmicity.

### 3. Mechanism of contact resistance formation in ohmic contacts with high dislocation density

#### 3.1 Introduction

In the recent years, a number of papers have appeared that reported on observation of anomalous behavior of contact resistance  $R_c$  in ohmic contacts to semiconductors with high dislocation density. The following anomaly was registered: in the temperature range starting from the room temperature, the contact resistance increases with

increasing temperature  $T$ . In particular, this temperature dependence of contact resistance was observed for In- $n$ -GaP and In- $n$ -GaN contacts [10, 31]. The increase of contact resistance with temperature was also observed for ohmic contacts fabricated to  $p$ - and  $n$ -InP [32]. The experimental  $R_c(T)$  curves obtained in the abovementioned papers are in contradiction with the thermionic mechanism of current flow, according to which  $R_c$  has to decrease with temperature. In fact, the situation is similar to realization of the thermal-field mechanism of current flow. In this case, one deals with Schottky contacts characterized by depletion in the near-contact semiconductor region. At the same time, the results obtained in Refs. [10, 31] were explained by assuming that current flow is limited by resistance of metal shunts on dislocations in semiconductor layers with a high dislocation density. Since metal resistance linearly increases with temperature at temperatures exceeding the Debye one, it should be expected appearance of linear behavior of  $R_c(T)$ . However, a number of experimental features in  $R_c$  behavior for metal-GaN contacts have not found their explanation. In particular, there was no justification done for specific region in the  $R_c(T)$  dependence just before the linear increase of contact resistance with temperature at low temperatures. In addition, it was observed that the contact resistance as a function of the doping level has a very weak dependence. To illustrate this, the authors studied the samples with the doping level changed by more than two orders of magnitude and demonstrated that the contact resistance at room temperature varied by no more than twice in a wide doping range.

A qualitative explanation for the observed increase of contact resistance with temperature [32] was as follows: in semiconductors with a stepped doping ( $n$ - $n^+$  junction), the flowing current may be restricted by diffusion mechanism supplying the electrons. For this case, it was supposed that  $R_c$  is proportional to  $T^2$ . However, a comprehensive analysis made earlier for Schottky contacts [33] with a stepped doping demonstrated that the current in Schottky contacts (except for weakly doped semiconductors with electron concentration  $\leq 10^{15} \text{ cm}^{-3}$ ) is defined by thermionic emission rather than the diffusion limitation. Thus, the diode theory of current flow through the contact was shown to be more appropriate than the diffusion theory. In this case, the temperature dependences of  $R_c$  in the framework of the thermionic mechanism of current flow have to be usual, *i.e.*, decreasing resistance with the temperature increase.

In this review, we propose a novel concept explaining the unusual behavior of ohmic contacts in the model considering the current flow through the metal shunts along the dislocations and current limiting by diffusion mechanism supplying electrons. An essential difference from the model developed in the work [21] is consideration of the current flow paths through the regions accumulating electrons rather than depleted ones. Being combined, the abovementioned two mechanisms allow us to explain the behavior of  $R_c(T)$  curves

(decreasing with temperature increase in the low temperature range and increase in  $R_c(T)$  curves in the higher temperature range) not only for the metal-GaP (GaN) ohmic contacts but also for contacts fabricated to other semiconductor layers containing a rather high dislocation density. A comparative analysis of the theoretical and experimental results demonstrates, as a rule, very good quantitative agreement.

### 3.2. Theoretical basis for the concept development

#### 3.2.1. Distribution of potentials

Let us assume that a potential well is formed near the end of each dislocation grown in a semiconductor. Generally speaking, the Schottky layer has to appear near the end of dislocation, nucleus of which is filled with metal. The reason for its appearance is related to the corresponding contact potentials difference and surface states. An extremely high electric field appears at the dislocation end as a result of considerable curvature as well as very small size of metal shunts. One can estimate the electrical field by assuming that the dislocation end is hemispherical, and their charge is defined by a small number  $Z$  of electrons (or ions). The electric field  $E_s$  in semiconductor near the end is obtained from the condition of equality of electric displacements in metal and semiconductor. Both the edge effect (that leads to considerable increase of the electric field strength) and the effect of mirror image forces lead to considerable reduction of the barrier height,  $\Delta\phi$ , near a shunt. Its value (in the above approximations) is:

$$\Delta\phi = \frac{q\sqrt{Z}}{4\pi\epsilon_0\epsilon_s r}, \quad (5)$$

where  $q$  is the elementary charge,  $\epsilon_s$  – semiconductor permittivity, and  $r$  – radius of the shunt.

Expression (5) is obtained in approximation that the mirror image forces in the metal-semiconductor contact vary according to the quasi-classical law  $1/z$ , where  $z$  is the normal drawn from the surface of the metal end to semiconductor. It is valid when the criterion  $z > a$  is satisfied, where  $a$  is the lattice parameter.

To estimate the  $r$  value, let us to use literature data on the effect of mirror image forces on lowering the barrier height in tip emitters, in which a high concentration of electric field also occurs. According to [34], in tip silicon emitters with the tip radius of  $r \approx 10^{-6} \text{ cm}$ , the initial height of the barrier  $\phi_s$  at  $10^7 \text{ V/cm}$  decreases to zero. Substituting this  $r$  value into formula (1), at  $\epsilon_s = 10$  and  $Z \approx 2.5 \cdot 10^3$ , we get  $\Delta\phi = 0.7 \text{ V}$ . *I.e.*, when  $\Delta\phi > \phi_s$ , we get at the end of the shunt not a barrier, but a potential well.

The size of the dislocation core, in which metal shunts can be placed, is of the order of  $10^{-6} \text{ cm}$  according to Matare [42].

In the case where the shunt diameter has atomic dimensions ( $\sim 2 \cdot 10^{-8} \text{ cm}$ ), the presence of surface states at its end can be neglected.

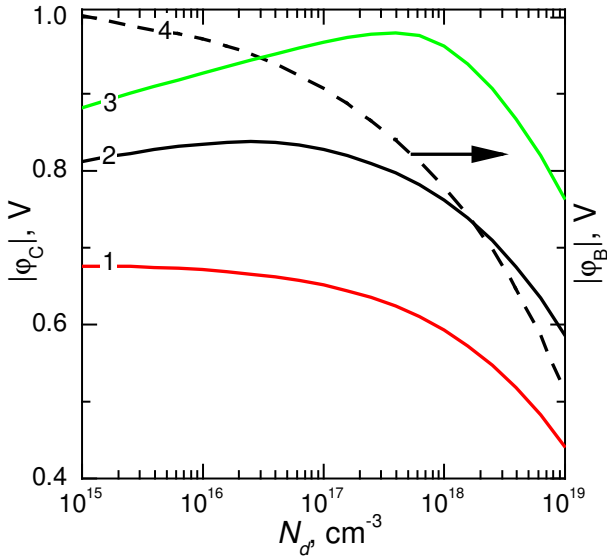


**Fig. 2.** The calculated dependences of the diffusion potential  $\phi_c$  and barrier height  $\phi_b$  of the contact to GaN as a function of the semiconductor doping level. The following parameters are used:  $\phi_{ms} = 0.5$  V,  $T = 300$  K, thickness of the dielectric gap  $d = 2 \cdot 10^{-8}$  cm, dielectric gap permittivity  $\epsilon_d = 1$ ,  $N_{sa}$ ,  $\text{cm}^{-2}$ : 1 –  $5 \cdot 10^{12}$ , 2 –  $10^{13}$ , 3 –  $1.6 \cdot 10^{13}$ , 4 –  $10^{13}$ .

Assuming (similar to that was made above) that the shunt end is hemispherical, with the radius of  $\sim 2 \cdot 10^{-8}$  cm, the volume of the hemisphere can be estimated as  $10^{-24}$   $\text{cm}^3$ . In terms of the concentration of surface centers, which have one surface level at each end, this corresponds to  $\sim 10^{16}$   $\text{cm}^{-2}$ . However, even for contacts to the GaAs-based materials having the largest concentration of surface centers of the order of  $10^{14}$   $\text{cm}^{-2}$ , the estimated value is by two orders of magnitude higher. It means that only one shunt of a hundred may be related with the surface state. Therefore, in the case when  $\phi_{ms} < 0$ , at the end of the shunt, enriching band bending should be realized.

The thermionic current flowing through the semiconductor regions accumulating electrons may decrease with temperature increase, taking into account current limitation by diffusion mechanism supplying electrons. It results in increasing the contact resistance. A sufficiently high density of scattering dislocation centers leads to decrease of electron mobility in favor for realization of the condition for current limitation by the diffusion mechanism.

Let us consider that the metal–semiconductor contact potential is nonuniform. In the places where dislocations come into a quasi-neutral region of semiconductor, a positive value of band bending  $\phi_{c1} = \phi_{c2}$  is realized, which forms a potential well for electrons. Between the dislocations, as usual, the contact potential  $\phi_{c2}$  is negative. It corresponds to realization of the Schottky barrier. The total current flowing through the contact interface is a sum of the current flowing through the dislocation short-circuits with metal shunts and current flowing between the dislocations. Current flowing through the dislocation shunts enables one to realize ohmic contacts, contact resistance of which will be calculated below.

When calculating the contact resistance, we take that the contribution from the current flowing between the dislocations can be neglected in the case of a high density of the latter. The reason for this is a high value (up to 1 V) of the contact potential related to high concentration of surface centers. The contact potential is the diffusion (built-in) potential  $\phi_c$  that is measured from the edge of the conduction band of semiconductor.

Shown in Fig. 2 are the theoretical dependences of diffusion potential  $\phi_c$  on the doping level for a metal–GaN contact with a tunnel-transparent dielectric gap calculated at different concentrations of acceptor surface centers  $N_{sa}$  located in the lower half of the bandgap. One can see that, at  $N_{sa} \geq 2 \cdot 10^{13}$   $\text{cm}^{-2}$ , the diffusion potential values exceed 0.7 V as the doping level varies up to about  $10^{19}$   $\text{cm}^{-3}$ .

Also shown in Fig. 2 are the dependences of  $\phi_b = \phi_c - E_F/q$  (i.e., the contact potential measured from the Fermi level in metal) as a function of the doping level; the concentration of surface centers is  $10^{13}$   $\text{cm}^{-2}$ . The Fermi level is not pinned at the surface (otherwise  $\phi_b$  would not depend on the doping level). The values of  $\phi_b$  ( $\geq 0.7$  V) are high over the whole doping level range, up to the concentrations over  $10^{18}$   $\text{cm}^{-3}$ . Thus, the abovementioned results demonstrate rather strong reason for neglecting the currents flowing between dislocations.

### 3.2.2. Calculation of currents

The problem of calculating the current flowing through one dislocation coupled with a shunt has a radial symmetry. The collection of current takes place on an area of the order of  $\pi L_D^2$ , and, taking this into account, it reduces to the one-dimensional one.

Here,

$$L_D = \left( \frac{\epsilon_0 \epsilon_s k T}{2 q^2 N_c} \right)^{0.5} (\Phi'_{1/2}(\epsilon))^{-1/2} \quad (6)$$

is the Debye screening length for the case of arbitrary degree of semiconductor degeneracy,  $N_c$  – effective density of states in the conduction band,

$$\Phi'_{1/2}(\epsilon) = \frac{2}{\sqrt{\pi}} \int_0^\infty \frac{\sqrt{\kappa} \exp(\kappa - \epsilon)}{(1 + \exp(\kappa - \epsilon))^2} d\kappa, \quad (7)$$

where  $\epsilon = E_F/kT$  is dimensionless Fermi energy in the semiconductor,  $\kappa = E/kT$  – dimensionless kinetic energy of electrons.

The surface density  $J_{nc}$  of the thermionic current flowing through the contact at the dislocation outcrop can be determined by solving the continuity equation for electrons. The relation between the electron concentration in the bulk  $n_w$ , and nonequilibrium electron concentration  $n(x)$  at a point  $x$  of the near-contact space-charge region (SCR) is obtained by double integration of the continuity equation over the coordinate  $x$  that is

perpendicular to the metal–semiconductor interface. For a nondegenerate semiconductor:

$$n(x) = e^{y(x)} \left( n_w - \frac{J_{nc}}{qD_n} \int_x^w e^{-y(x')} dx' \right), \quad (8)$$

where  $y(x) = q\phi(x)/kT$  is the dimensionless nonequilibrium potential at a point  $x$ ,  $D_n$  – electron diffusion coefficient, and  $w$  – width of near-contact SCR.

The amount  $J_{nc}$  is defined by the following expression:

$$J_{nc} = q \frac{V_T}{4} (n_c - n_{c0}). \quad (9)$$

Here,  $V_T$  means thermal velocity of electrons,  $n_c$  ( $n_{c0} = n_w \exp y_{c0}$ ) – nonequilibrium (equilibrium) electron concentration in the contact plane, and  $y_{c0} = q\phi_{c0}/kT$  – dimensionless equilibrium potential at the metal–semiconductor interface.

Taking  $x$  in Eq. (8) as being zero and using Eq. (9) for  $J_{nc}$ , it is possible to determine  $n_c$ . Then, substituting the expression for  $n_c$  to Eq. (9) and taking into account that the dimensionless nonequilibrium potential  $y_c = y_{c0} + \ln(qV/kT)$  (this is the condition for the contact to be ohmic), we obtain the following expression for the density of current flowing through the metal–semiconductor contact at the dislocation outcrop:

$$J_c = \frac{V}{\rho_{c0}}, \quad (10)$$

where

$$\rho_{c0} = \frac{kT}{q} \frac{\left( 1 + \frac{V_T}{4D_n} e^{y_{c0}} \int_0^w e^{-y(x)} dx \right)}{\frac{qV_T}{4} n_w e^{y_{c0}}}. \quad (11)$$

When calculating  $\rho_{c0}$ , we took into account that:

$$\int_0^w e^{-y} dx = L_D \int_{y_c}^{y_x} \frac{e^{-y}}{(e^y - y - 1)^{0.5}} dy. \quad (12)$$

The calculation shows that, at  $y_x = 0.5$ , the integral in Eq. (12) varies from 0.56 (for  $y_{c0} = 1.5$ ) up to 0.65 (for  $y_{c0} = 3.5$ ) and becomes practically constant at larger  $y_{c0}$ .

The contact resistance (determined by the diffusion input mechanism) for a contact of unit area was determined from the expression:

$$\rho_{diff} = \frac{\rho_{c0}}{\pi L_D^2 N_{D1}}, \quad (13)$$

where  $N_{D1}$  is the surface density of dislocations that take part in current flow. Generally speaking, the surface density of dislocations taking part in current flow ( $N_{D1}$ )

and surface density of dislocations taking part in scattering ( $N_{D2}$ ) are different. The first ones are mainly those normal to the interface, while the latter are dislocations parallel to the interface.

The amount  $\pi L_D^2 N_{D1} S$  ( $S$  is the contact area) is the total area of the current flowing through the dislocations. As a rule, the value of relative area,  $\pi L_D^2 N_{D1}$ , is rather less than unity, even at maximal dislocation densities ( $10^{10} \dots 10^{11} \text{ cm}^{-2}$ ). The exception is the case of weakly doped semiconductors with  $N_d \leq 10^{15} \text{ cm}^{-3}$ , where  $N_d$  is the concentration of shallow donor centers.

The electron diffusion coefficient, according to the Einstein relation, is  $D_n = kT\mu_n/q$ . We determined electron mobility  $\mu_n$  taking into account electron scattering by charged impurities ( $\mu_Z$ ), optical phonons ( $\mu_o$ ) and dislocations ( $\mu_D$ ):

$$\mu_n = \left( \mu_Z^{-1} + \mu_o^{-1} + \mu_D^{-1} \right)^{-1}. \quad (14)$$

In our calculations, we applied the expressions for  $\mu_Z$  and  $\mu_o$  from [35] and for  $\mu_D$  from [36]. These expressions can be described as follows:

$$\mu_Z(T) = \frac{3.68 \cdot 10^{20} \left( \frac{\epsilon_s}{16} \right)^2 \left( \frac{T}{100} \right)^{3/2}}{n_w \left( \frac{m}{m_0} \right)^{1/2} \log \left[ 1 + \left( \frac{\epsilon_s}{16} \right) \left( \frac{T}{100} \right) \left( \frac{2.35 \cdot 10^{19}}{n_w} \right)^{1/3} \right]^2}, \quad (15)$$

$$\mu_o(T) = \frac{31.8 \sinh \left( \frac{\theta}{2T} \right)}{\left( \frac{1}{\epsilon_{sh}} - \frac{1}{\epsilon_{sl}} \right) (\theta)^{0.5} \left( \frac{m}{m_0} \right)^{1.5} \left( \frac{\theta}{2T} \right)^{1/2} K_1 \left( \frac{\theta}{2T} \right)}, \quad (16)$$

where  $\theta$  is the temperature of longitudinal optical phonons,  $m$  – electron effective mass,  $m_0$  – electron mass,  $\epsilon_{sh}(\epsilon_{sl})$  – high- (low-)frequency permittivity of the semiconductor,  $K_1(\theta/2T)$  – modified Bessel function of the first order:

$$\mu_D = \frac{B \exp(\eta)}{T^{1/2} N_{D2} L_D^5} K_2(\eta), \quad (17)$$

where  $\eta = \frac{\hbar^2}{16m L_D^2 kT}$ ,  $K_2(\eta)$  is the modified Bessel

function of the second order,  $B = \frac{(\hbar^2 \epsilon_0 \epsilon_{sl} c)^2}{8\sqrt{2\pi k} q^3 \sigma^2 m^{5/2}}$  –

dimension factor,  $\sigma = \lambda/2qc$ ,  $\lambda$  – linear charge density of a dislocation line,  $c$  is lattice parameter in the [001] direction.

### 3.2.3. General relations and limit cases

The above expressions are valid for nondegenerate semiconductors. The quantity

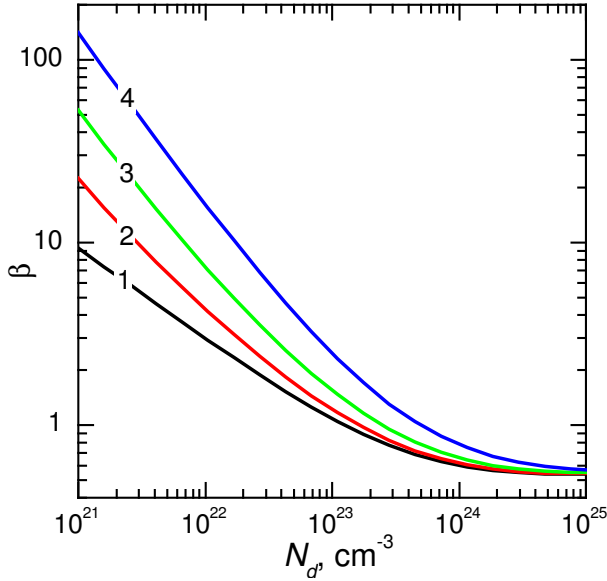


**Fig. 3.** The calculated dependences of  $\beta$  as a function of the GaN doping level for different density of scattering dislocations  $N_{D2}$  ( $\text{cm}^{-2}$ ): 1 –  $3 \cdot 10^9$ , 2 –  $10^9$ , 3 –  $3 \cdot 10^8$ , 4 –  $10^6$ . The following parameters are used for calculation:  $y_{c0} = 2$ ,  $E_d = -0.015$  eV,  $V_T = 2 \cdot 10^7$  cm/s.

$$\beta = \frac{V_T}{4D_n} e^{y_{c0}} \int_0^w e^{-y(x)} dx \quad (18)$$

defines the degree of diffusion limitation that is essential at  $\beta > 1$ .

In the simplest case, all the donors (concentration of which is  $N_d$ ) are ionized, and  $n_w = N_d$ . The theoretical  $\beta(N_d)$  curves for  $n$ -GaN at different density of scattering dislocations are shown in Fig. 3, taking the donor ionization energy to be 15 meV,  $y_{c0} = 2$ , and  $T = 300$  K. Thus, as a rule, contribution of diffusion limitation mechanism is rather high, when parameters vary over a wide range, if accumulation is realized in the band bending region at the dislocation end. However, one can see from Fig. 2 that, as the doping level increases, the value of  $\beta$  decreases from the value much exceeding unity to the value much less than unity. The reasons for this behavior are as follows: (i) decrease of the Debye screening length  $L_D$  and (ii) reduction of  $y_{c0}$  due to decrease of the electric field strength at the dislocation end. As a result, the diode theory of current flow in the metal–semiconductor contact will more appropriate in the case of degeneracy.

By applying the approach developed in [36], one can obtain the following expression for specific contact resistivity  $\rho_{te}$  in the case of degeneracy and realization of the thermionic mechanism of current flow:

$$\rho_{te} = \frac{k}{qA(m/m_0)T} \frac{1}{\ln[1 + \exp(\varepsilon + y_{c0})]}, \quad (19)$$

where  $A$  is the Richardson constant. The dimensionless Fermi energy  $\varepsilon$  can be determined from the equation of bulk neutrality:

$$\frac{N_d}{1 + \exp((E_F - E_d)/kT)} = \frac{2}{\sqrt{\pi}} N_{c0} \left( \frac{T}{300} \right)^{3/2} \int_0^\infty \frac{\kappa^{0.5}}{1 + \exp(\kappa - E_F/kT)} d\kappa, \quad (20)$$

where  $E_d$  is the energy level of shallow donors,  $N_{c0}$  – the effective density of states in the conduction band at  $T = 300$  K.

One should note that, for sufficiently shallow donors, Eq. (20) (written in the assumption that the donor level is discrete) does not hold at sufficiently low temperatures, because in that case it does not take into account broadening the donor levels and appearance of impurity band. If the inequality  $N_d \geq N_{c0}$  is true, then the electron concentration does not depend on temperature in all the temperature range down to the liquid helium one. In that case, the equation of semiconductor bulk neutrality is as follows:

$$N_d = n_w = \frac{2}{\sqrt{\pi}} N_{c0} \left( \frac{T}{300} \right)^{3/2} \int_0^\infty \frac{\kappa^{0.5}}{1 + \exp(\kappa - E_F/kT)} d\kappa. \quad (21)$$

At strong degeneracy, the Debye screening length in semiconductor,  $L_D$ , approaches  $r_0$  that does not depend on temperature and weakly depends on the doping level:

$$r_0 = \frac{1}{2} \left( \frac{\pi}{3} \right)^{1/6} \left( \frac{4\pi\epsilon_0\epsilon_s\hbar^2}{mq^2N_d^{1/3}} \right)^{1/2}. \quad (22)$$

According to the above consideration, the contact resistance  $\rho_{tw}$  in the case of strong degeneracy can be defined by the expression:

$$\rho_{tw} = \frac{\rho_{te}}{\pi r_0^2 N_{D1}}. \quad (23)$$

In this case, averaging the relaxation time  $\tau$  over the electron energy  $E$  for a specific scattering mechanism at  $\tau \sim E^r$  gives  $\langle E_{F\text{lim}}^r \rangle$ , where  $\langle E_{F\text{lim}} \rangle = \left( (3\pi^2)^{2/3} \hbar^2 N_d^{2/3} / 2m \right)$  is the Fermi energy for the case of full degeneracy. Since  $\langle E_{F\text{lim}} \rangle$  does not depend on temperature, the mobility for electron gas with strong degeneracy also does not depend on temperature. The exception of this rule is the polar optical scattering for which the relaxation time depends on the optical phonon energy rather than the electron energy.

Let us analyze how  $\rho_{diff}$  depends on the semiconductor doping level and dislocation density. For non-degenerate semiconductor:  $\rho_{diff} \sim L_D / (\mu_n N_d L_D^2 N_{D1})$ . In semiconductors with high dislocation density, electron scattering by dislocations is predominant at low doping [6, 7]. In this case:  $\mu_D \sim L_D^{-1}$  and  $\rho_{diff} \sim N_d^{-1}$ . At medium doping levels, the electron mobility is determined by scattering by optical phonons and

$\rho_{diff} \sim N_d^{-1/2}$ . At higher doping levels:  $\mu \approx \mu_z$  and  $\rho_{diff} \sim N_d^{1/2}$ . And in the case of strongly degenerate semiconductors the analog of  $\rho_{diff}$  is  $\rho_{tw} \sim N_d^{1/3}$ . Thus, the dependence of contact resistance (limited by diffusion input) on the semiconductor doping level is stronger than doping dependence in the case of the thermionic mechanism in Schottky contacts. As the doping level increases, the contact resistance may not only decrease but increase as well.

The  $\rho_{diff}$  dependence on dislocation density is non-trivial, too. It goes down as the density of dislocations taking part in current flow,  $N_{D1}$ , increases. At the same time, the  $\rho_{diff}$  dependence on the density of scattering dislocations is more complicated. At low doping levels,  $\rho_{diff}$  increases with the density of scattering dislocations due to decrease of electron mobility, while at high doping levels, it does not depend on  $N_{D2}$ .

The total resistance of the metal shunts is in series with resistance  $\rho_{diff}(\rho_{tw})$  in the case of nondegenerate (degenerate) semiconductor. Therefore, taking into account the results obtained in Ref. [10, 31], the total resistance of ohmic contact in a semiconductor with high dislocation density may be described as:

$$\rho_{cs} = \rho_{diff}(\rho_{te}) + \rho_{sh}(T), \quad (24)$$

where  $\rho_{sh}(T) = \frac{\rho_0(1 + \alpha T)}{\pi r^2 N_{D1}} d_D$ ,  $\rho_0$  is the metal resistivity at  $T = 0$  °C,  $\alpha$  – its temperature coefficient,  $d_D$  – distance traveled by electrons through dislocations from the bulk semiconductor to the contact metallization. It should be noted that all expressions of this section are obtained for contacts of unit area.

It should be noted that, at realization of current flow through dislocations associated with metal shunts, a contact remains ohmic down to helium temperatures [23]. At moderate levels of semiconductor doping, growth of contact resistivity  $\rho_c$  as temperature decreases is related to charge carrier freezing-out. At the same time, at doping levels comparable with the effective density of states in the conduction band, there is no strong growth of contact resistivity as temperature decreases. It is related to broadening the shallow donor levels into band and the Mott transition [29].

### 3.3. Discussion of results and comparison with experiment

If the current is limited by diffusion mechanism supplying electrons, then the contact resistance is inversely proportional to electron mobility. Therefore, one should expect rather strong reduction (increase) of  $\rho_{diff}$  as the electron mobility  $\mu$  increases (decreases) considerably with  $T$ . The electron mobility increases with temperature growth in the case of electron scattering by charged impurities and dislocations, while it decreases in polar semiconductors due to scattering by polar optical phonons. In sufficiently doped semiconductors,

**Table 1.** The semiconductor parameters used for calculation of the theoretical  $\mu_n(T)$  and  $\rho_c(T)$  curves.

Semiconductor	GaN	InP	GaAs	Si
$m/m_0$	0.2	0.08	0.063	1.08
$N_c / 10^{18} \text{ (cm}^{-3}\text{)}$	2.30	0.57	0.47	28.00
$\epsilon_{sl}$	9.0	12.5	12.8	12.7
$\epsilon_{sh}$	5.35	9.65	10.89	–
$\theta \text{ (K)}$	1056	494	419	–

scattering by charged impurities is predominant, while scattering by dislocations dominates at low doping levels. The efficiency of scattering by polar optical phonons is determined by the energy of a longitudinal optical phonon: the larger is this energy, the higher are the temperatures at which this scattering mechanism is dominant.

Table 1 presents the parameters of semiconductors: GaN, InP, GaAs and Si used to obtain the theoretical dependences  $\mu_n(T)$  and  $\rho_c(T)$ . Fig. 4 shows the calculated

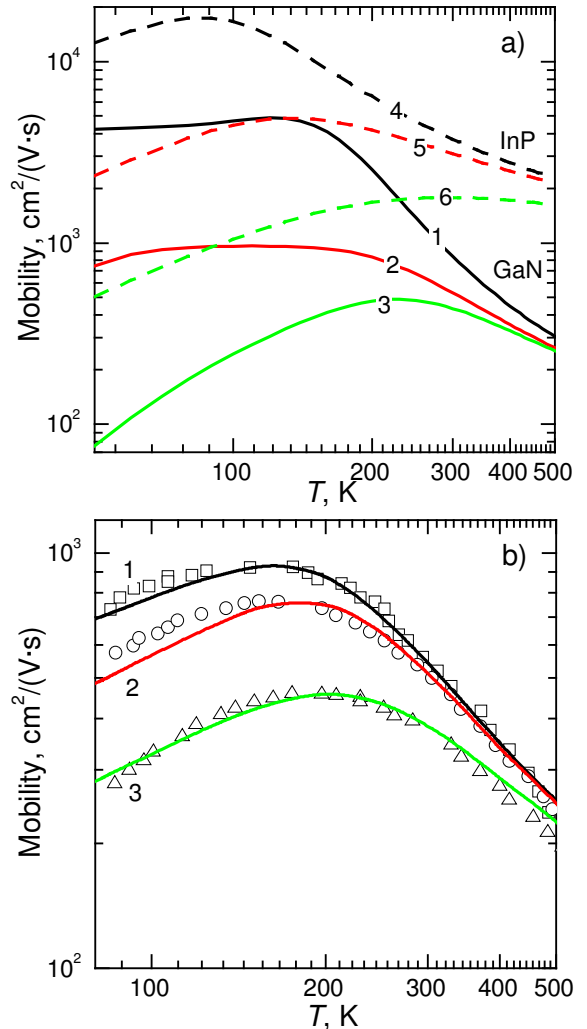


**Fig. 4.** The temperature dependences of electron mobility in GaN (curves 1–3) and InP (curves 4–6) calculated for different density of scattering dislocations. The following parameters are used for calculation:  $N_d \text{ (cm}^{-3}\text{)}$ : 1 –  $5 \cdot 10^{16}$ , 2 –  $10^{17}$ , 3 –  $10^{18}$ , 4–6 –  $9 \cdot 10^{15}$ .  $N_{D2} \text{ (cm}^{-2}\text{)}$ : 1 –  $10^7$ , 2 –  $3 \cdot 10^8$ , 3 –  $2 \cdot 10^9$ , 4 –  $10^6$ , 5 –  $10^7$ , 6 –  $5 \cdot 10^7$ .

temperature dependences  $\mu_n(T)$  for GaN and InP for several values of the density of scattering dislocations and semiconductor doping level. It should be noted that the values of scattering dislocation densities used for plotting the  $\mu_n(T)$  curves for GaN correspond to those used in fitting the theoretical and experimental dependences  $\rho_c(T)$ . Both the electron mobility obtained as well as its temperature dependence are in good agreement with the experimental results [37-39]. Indeed, for GaN, in particular, the temperature dependences of electron mobility calculated at different doping levels by fitting the scattering dislocation densities can match with an accuracy of 10% those measured in [37]. Similarly, the calculated  $\mu_n(T)$  curves are in good agreement with those obtained experimentally for InP [38, 39].

Let us analyze the dependences obtained taking into account the possibility for realization of an anomalous temperature dependence of contact resistance, *i.e.*, increasing  $\rho_c(T)$  with temperature increase. To this end, the electron mobility  $\mu(T)$  curve would have a decreasing portion in the high temperature range starting from room temperature. One can see from Fig. 4 that, for GaN, it occurs at a sufficiently large variation of the scattering dislocation density: from  $10^6$  up to  $2 \cdot 10^9 \text{ cm}^{-2}$ . For InP, this range is narrower: from  $10^6$  up to  $3 \cdot 10^7 \text{ cm}^{-2}$ . At scattering dislocation densities  $\geq 5 \cdot 10^7 \text{ cm}^{-2}$ , the electron mobility of InP in the usually studied temperature range increases with temperature. It corresponds to the case when the  $\rho_c(T)$  curves have to decrease at high dislocation densities. The reason for such a distinction is much stronger polar optical scattering in GaN that ensures a sufficiently larger reduction of electron mobility at medium and high temperatures. The situation in GaAs is similar to that in InP, because the optical phonon energy in GaAs is even lower than in InP.

Our analysis allows us to classify the main behavior of possible temperature dependences of contact resistance in the case of realization of the proposed mechanism of  $\rho_c$  formation in semiconductors with the high dislocation density. Generally, the final contact resistance value is defined by the diffusion input (*i.e.*,  $\rho_{diff}$  value) and total resistance of shunts (*i.e.*,  $\rho_{sh}$ ). Therefore, the relationship between  $\rho_{diff}$  and  $\rho_{sh}$  also may be crucial along with the character of dependence  $\mu(T)$  for realization of decreasing or increasing temperature dependence  $\rho_c(T)$ .

**III.A.** Let us consider the case when the peak in the  $\mu(T)$  dependence occurs and inequality  $\rho_{diff} > \rho_{sh}$  is realized. The clearly pronounced descending part of  $\mu(T)$  curve occurs in polar semiconductors with high energy of a longitudinal optical phonon. In particular, polar optical scattering in GaN (where the optical phonon temperature  $\theta$  is 1056 K) may reduce electron mobility at high temperatures down to  $10^2 \text{ cm}^2/\text{V}\cdot\text{s}$  (Fig. 4), while in InP (where  $\theta = 494 \text{ K}$ ) the electron mobility is reduced just to  $10^3 \text{ cm}^2/\text{V}\cdot\text{s}$  (see Fig. 4).

In *n*-Si, like to that in GaN, the electron mobility decreases rather strongly (in proportional to  $T^{-2.5}$ ) at high temperatures. It is related to contribution into carrier mobility of scattering by acoustic phonons and two

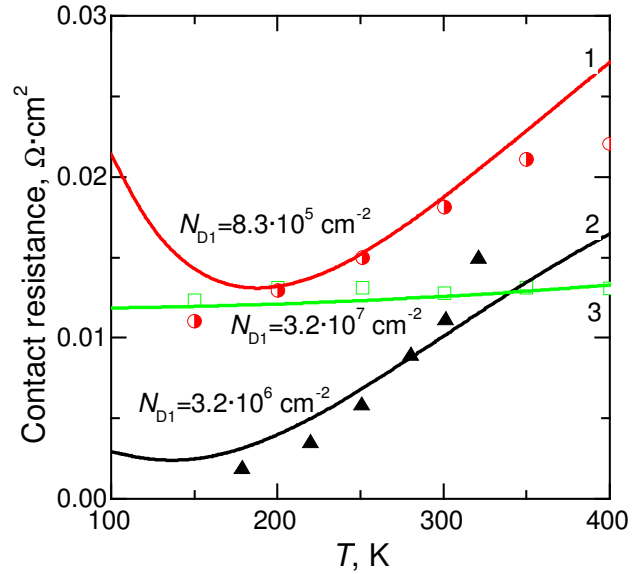


**Fig. 5.** The temperature dependences of In–GaN ohmic contact resistance for different densities of conducting dislocations. Circles and triangles – experimental data from [3], curves – theory. Experimental  $N_D$  ( $\text{cm}^{-3}$ ): open triangles –  $5 \cdot 10^{16}$ , filled triangles –  $3 \cdot 10^{18}$ , circles –  $10^{19}$ . The following parameters are used for calculation:  $E_d = -0.015 \text{ eV}$ ,  $V_T = 2 \cdot 10^7 \text{ cm/s}$ ,  $y_{c0} = 3$ ;  $N_D$  ( $\text{cm}^{-3}$ ): 1 –  $5 \cdot 10^{16}$ , 2 –  $10^{18}$ , 3 –  $10^{19}$ ;  $N_{D2}$  ( $\text{cm}^{-3}$ ): 1 –  $10^7$ , 2 –  $3 \cdot 10^8$ .

intervalley phonons (temperatures of which are 190 and 630 K) [40]. Thus, one should expect more strong increasing  $\rho_{diff}(T)$  in the region of mobility reduction in silicon than in InP. In both cases considered, an increased region has to be realized in the  $\rho_{diff}(T)$  curves (as well as a minimum appears under certain conditions).

Fig. 5 shows the experimental  $\rho_c(T)$  dependences for the In–GaN structures measured in [32] in the samples with the total dislocation density of about  $10^8 \text{ cm}^{-2}$  as well as the results of our calculations of  $\rho_{diff}(T)$  for three electron concentrations:  $5 \cdot 10^{16}$ ,  $10^{18}$  and  $10^{19} \text{ cm}^{-3}$ . In Fig. 5 (as well as in further Figures), the density of conducting dislocations  $N_{D1}$  was used as a parameter, when plotting the calculated curves. The data demonstrate that there is a rather good agreement between the theoretical and experimental results.

It should be noted a particular situation with semiconductor doping level of  $10^{19} \text{ cm}^{-3}$ . In this case, the thermionic mechanism of  $\rho_c(T)$  formation is valid. Therefore, we used in our calculations Eq. (19) in the approximation made for degenerated semiconductors. It was found that, at sufficiently strong semiconductor degeneracy and action of the thermionic mechanism, there is practically no temperature dependence of the parameters obtained. Similar situation occurs also for the Debye screening length at strong semiconductor degeneracy. A good agreement between the calculated and experimental contact resistance values in the degenerate semiconductor is obtained. It should be emphasized that both the calculated and experimental values of contact resistance weakly depend on the semiconductor doping level.

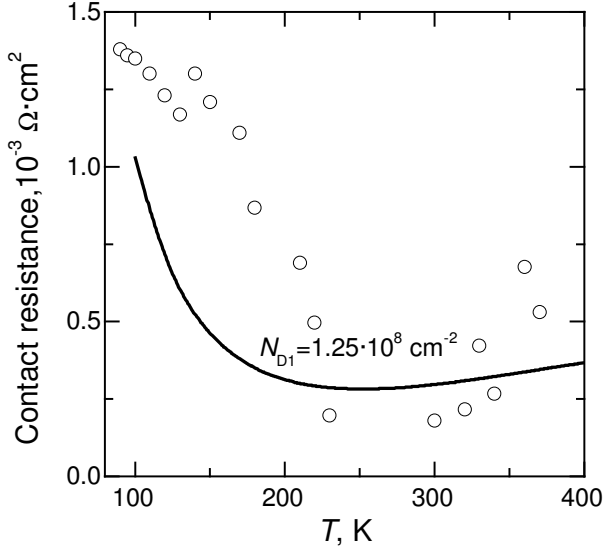


**Fig. 6.** The temperature dependences of GaN ohmic contact resistance (the doping level is  $10^{17} \text{ cm}^{-3}$ ). Circles – experiment, curves – theory. The following parameters are used for calculation:  $E_d = -0.015 \text{ eV}$ ,  $V_T = 2 \cdot 10^7 \text{ cm/s}$ ,  $y_{c0} = 3$ ,  $N_{D2} = 1.9 \cdot 10^9 \text{ cm}^{-2}$ .

Fig. 6 shows the experimental and calculated  $\rho_c(T)$  dependences for the Au–TiB<sub>x</sub>–Al–Ti–*n*–GaN structure. The GaN samples were prepared using MOCVD epitaxial growth on a sapphire substrate at  $T = 1050 \text{ }^\circ\text{C}$  with doping level of  $10^{17} \text{ cm}^{-3}$  and dislocation density of the order of  $10^8 \text{ cm}^{-2}$  [41]. The agreement between the theory and experiment in this case was not as good as in the previous case due to the structural parameters variation at the interfacial plane. We believe, however, that this agreement is rather good, because it enabled us to obtain correct values for both position of minimum of the  $\rho_c(T)$  curve and minimal  $\rho_c$  value. In particular, realization of  $\rho_c(T)$  minimum at the temperature close to 270 K indicates high density of scattering dislocations (of the order of  $10^9 \text{ cm}^{-2}$ ). The results are also supported by X-ray measurements. When summarizing the results obtained for GaN, it should be emphasized that presence of a well pronounced descending part in the  $\mu(T)$  dependences (see Fig. 3) is sufficient for explanation of the  $\rho_c(T)$  increasing.

**III.B.** Next, let us consider the cases when either the  $\mu(T)$  dependences contain a peak or they are increasing up to high temperatures at arbitrary interrelation between  $\rho_{diff}$  and  $\rho_{sh}$ . Such a situation is rather typical for the InP-based structures. To illustrate this, we present in Fig. 7 our experimental and calculated  $\rho_c(T)$  data obtained for the Au–TiB<sub>x</sub>–AuGe–*n*–*n*<sup>+</sup>–InP structures with high dislocation density and semiconductor doping level of  $9 \cdot 10^{15} \text{ cm}^{-3}$  (circles and triangles – experimental data, curves – the calculated dependences  $\rho_c(T)$  obtained using Eq. (24) for two samples with different alloying temperatures of ohmic contact). Since in this case the resistances  $\rho_{diff}(T)$  and  $\rho_{sh}(T)$  are in series, the total resistance is determined by the larger value of them. In the case of relation  $\rho_{sh}(T) > \rho_{diff}(T)$ , the mechanism proposed in [31] is valid.

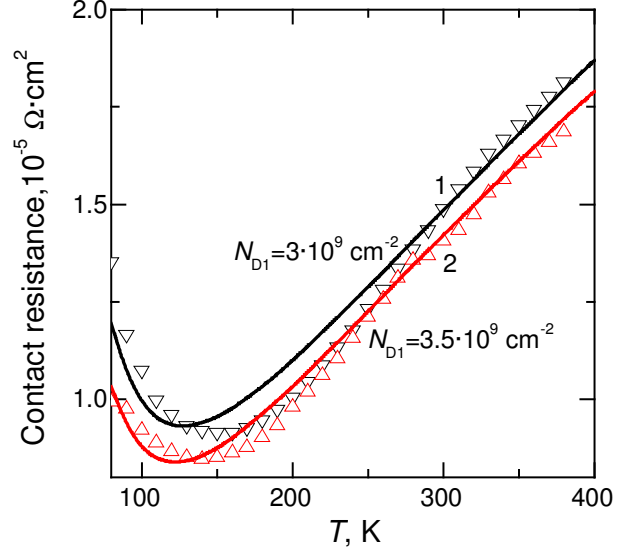


**Fig. 7.** The temperature dependences of Au(2000Å)–TiB<sub>2</sub>(1000Å)–Au(250Å)–Ge(250Å)–*n*–*n*<sup>+</sup>–*n*<sup>+</sup>–InP ohmic contact resistance. Triangles – experiment, curves – theory. The following parameters are used for calculation:  $N_d = 9 \cdot 10^{15} \text{ cm}^{-3}$ ,  $V_T = 4 \cdot 10^7 \text{ cm/s}$ ,  $E_d = -0.007 \text{ eV}$ ,  $y_{c0} = 2$ ,  $N_{D2} = 1 \cdot 10^{10} \text{ cm}^{-2}$ ,  $\alpha = 3.9 \cdot 10^{-3} \text{ K}^{-1}$ . Alloying temperature,  $T$  ( $^\circ\text{C}$ ): 1, triangles down – 420; 2, triangles up – 450.

To ensure the required increase in  $R_c(T)$  with temperature, the  $R_{sh}$  value has to be proportional to the distance  $d_D$  that electrons pass through a dislocation from bulk semiconductor to metal contact, and inversely proportional to  $r^2$ . In [10, 31], it was supposed that  $d_D = w$ . However, electrons can enter a shunt only at the dislocation end, where the required value of electrostatic potential is realized. Thus, they have to pass over the whole dislocation length. With assumption made for this case, one may ensure the required  $\rho_{sh}$  value by varying either the conducting dislocation density or metal shunt diameter.

According to [42], a diameter of dislocation nucleus may be sufficiently large ( $\geq 1 \text{ nm}$ ). Therefore, several needles composed of metal atoms can be located in it. Let it be gold that penetrates into a dislocation. For gold, the resistivity  $\rho \approx 2.25 \cdot 10^{-6} \text{ } \Omega \cdot \text{cm}^2$  and its temperature coefficient  $\alpha = 3.9 \cdot 10^{-3} \text{ K}^{-1}$ . Taking into account that the conducting dislocation density is  $\sim 10^{10} \text{ cm}^{-2}$ , one can obtain good fitting by setting  $d_D \approx 1 \text{ } \mu\text{m}$  and  $r \approx 2.8 \cdot 10^{-8} \text{ cm}$  (*i.e.*, two atomic radii of gold). Analysis of the obtained data (Fig. 6) demonstrates that the agreement between the theory and experiment for  $\rho_{sh}$  is rather good.

**III.C.** If there is no peak in the  $\mu(T)$  curve (the electron mobility increases with  $T$  up to the highest measured temperatures) and the inequality  $\rho_{diff} > \rho_{sh}$  holds, then in the case of realization of the proposed mechanism of diffusion limitation the temperature dependences of  $\rho_c$  will demonstrate the decrease, as in the case of the thermionic mechanism for Schottky contact. Shown in Fig. 8 are the experimental and calculated  $\rho_c(T)$  curves for the case of contact fabricated to GaAs-based material with the doping level of  $4 \cdot 10^{15} \text{ cm}^{-3}$ . The experimental curves were obtained for

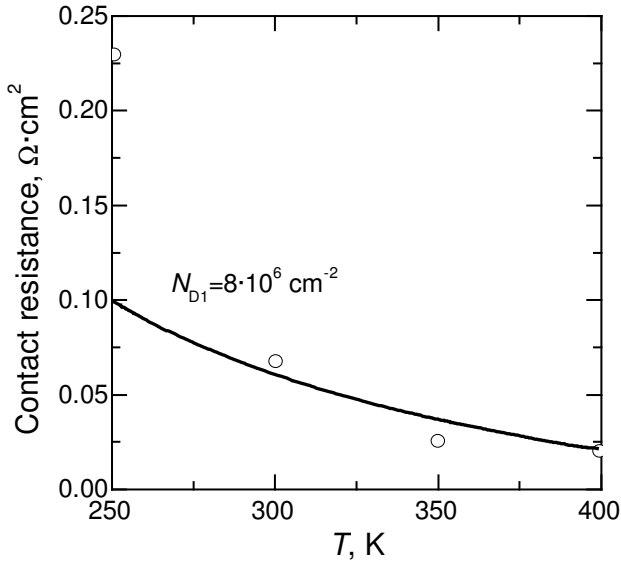


**Fig. 8.** Temperature dependences of In–GaAs ohmic contact resistance. Circles – experiment, curves – theory. The following parameters are used for calculation:  $N_d = 4 \cdot 10^{15} \text{ cm}^{-3}$ ,  $V_T = 4 \cdot 10^7 \text{ cm/s}$ ,  $y_{c0} = 0.8$ .

an In–GaAs alloyed contact [43]. The authors of Ref. [43] suggested that the presence of decreasing dependences  $\rho_c(T)$  proves that the thermionic mechanism of current flow is realized in that contact. They determined the barrier height (that turned out to be anomalously low) from the slope of the  $\rho_c(1/T)$  curve. It should be emphasized that we obtained the satisfactory agreement between the theory and experiment in the framework of the mechanism proposed by us in this work, assuming that the density of conducting dislocations is of the order of  $10^7 \text{ cm}^{-2}$ . In this case, both characteristics – the value of contact resistance and its temperature dependence – can be theoretically described. A large increase of contact resistance is caused by restriction of the current flow to relative small area. Our estimation shows that the relative area,  $\pi L_D^2 N_{D1}$ , is of the order of  $10^{-3}$  at the semiconductor doping level of  $4 \cdot 10^{15} \text{ cm}^{-3}$  and  $N_{D1} \sim 10^7 \text{ cm}^{-2}$ . The reduction of contact resistance at low temperatures in our model is correlated with comparatively weak freezing-out, because of the low donor energy and electron scattering by dislocations. Being combined, the above factors allow explaining the results obtained by us in this work. Estimation of resistance of indium shunts using the values  $d_D = 5 \cdot 10^{-5} \text{ cm}$ ,  $r = 5 \cdot 10^{-8} \text{ cm}$  and  $N_{D1} = 2.5 \cdot 10^7 \text{ cm}^{-2}$  gives a value that is smaller than the experimental  $R_c$  value by the factor of seven at  $T = 400 \text{ K}$ . Thus, the relation  $\rho_{sh}(T) < \rho_{diff}(T)$  that is required for realization of decreasing dependences  $\rho_c(T)$  is valid in this case.

The results allow determining the densities of scattering and conducting dislocations by comparing the theoretical and experimental dependences of contact resistance as a function of temperature. Thus, the proposed concept has a heuristic capability for determination of new parameters of metal–semiconductor contacts.

It should be noted that no averaging was applied when fitting the experimental dependences by using the calculated ones. It demonstrates that the scattering in parameters related to lateral nonuniformity of contact does not play a crucial role.

### 3.4. Conclusions

The mechanism of formation of metal–semiconductor contact resistance proposed in this work may take place, first of all, in wide band-gap semiconductors with high density of dislocations and surface centers in the contact. It seems paradoxical because, according to this mechanism, current flows through the depletion rather than accumulation regions.

At the same time, there are a number of facts counting definitely in favor of this mechanism. The theory developed is in good agreement with the experimental results, such as increasing the contact resistance  $R_c$  with increasing the temperature, weak dependence of contact resistance on the semiconductor doping level as well as strong dependence of  $\rho_c$  and position of minimum in the temperature dependence of  $\rho_c$  on the dislocation density. The above agreement was obtained for the contacts fabricated not only to III–V semiconductors but on heavily doped silicon as well.

Realization of the proposed mechanism does not still exclude the possibility of contact resistance decrease with temperature increase over the whole measurement range. It is more likely in the structures with low-energy optical phonons, and the mechanism has been demonstrated in weakly doped gallium arsenide [44, 45]. The characteristic features in this case are high contact resistance and extremely low contact barrier height obtained in assumption that the traditional thermionic mechanism of current flow is predominant.

## 4. Features of temperature dependence of contact resistivity in ohmic contacts on lapped *n*-Si

### 4.1. Introduction

No dependences  $\rho_c(T)$  growing with temperature were observed in dislocation-free silicon (with the exception of [32]). Moreover, metal–silicon contacts in dislocation-free silicon are rectifying [19].

At the same time, it is known that lapped silicon surface has a microrelief and contains a large number of structural defects, in particular, dislocations, which density may be  $10^7$ – $10^8 \text{ cm}^{-2}$  (see [46]). Such a surface also demonstrates pronounced adhesive and gettering characteristics, which ensure high quality of contact and *p*-*n* junctions. It also serves as efficient sink for defects, thus reducing their number. The authors [47–50] reported on the role of microrelief made with photolithography in reduction of dislocation density near the Si–Si interface formed at fabrication of *p*-*n* junctions for power electronics by direct silicon joining. The important role of structural factor in formation of *p*-*n* junction by using direct silicon joining was also stressed in [49]. In [49] it

was shown that, if a microrelief Si surface is joined with the smooth one, the dislocation density is by three orders of magnitude lower than that in the case of joining two smooth surfaces.

The lapped Si wafers are still used in manufacturing technology for  $p$ - $n$  junctions and ohmic contacts to high-power silicon isolators [51, 52]. However, the temperature dependence of  $\rho_c$  on lapped  $n$ -Si surfaces was not studied yet. Similar situation is also with investigation of power integrated circuits made using modern microelectronic technologies (including direct joining the epitaxial and other high-quality polished silicon structures [53, 54]). With consideration for the above, we believe that ohmic contacts to lapped  $n$ -Si wafers not only are a good model object for investigation of the effect of dislocations on  $\rho_c$  value but carry information about temperature dependence of  $\rho_c$  for structures used in power electronics.

Next, we show that making ohmic contacts on the lapped silicon wafers leads to realization of current flow through the metal shunts associated with dislocations. To prove that, we made contacts on lapped surface of initially dislocation-free silicon and investigated experimentally the dependence  $\rho_c(T)$  for the contacts obtained. It was shown that, at temperatures over 250 K, all the  $\rho_c(T)$  curves grow with temperature.

#### 4.2. Theoretical notions

Let us consider a theoretical approach to calculation of contact resistivity in ohmic contacts to  $n$ -Si with high dislocation density. One should note, first of all, that the above contacts are ohmic, no matter what the interrelation between the contact and semiconductor bulk resistivities. It is possible only if the current flows through the regions that accumulated electrons. In that case, the total applied voltage drops across the quasi-neutral bulk, thus providing contact ohmicity.

The contribution of thermionic current flowing through the regions that accumulated electrons may decrease as temperature grows (with allowance made for diffusion supply limitation). It results in growth of contact resistance. A sufficiently high density of scattering dislocations leads to reduction of charge carrier mobility, thus favoring realization of the condition of current limitation by diffusion supply of electrons.

In our case, the metal–semiconductor contact is nonuniform in contact potential value. For instance, the positive value of the contact potential  $\varphi_{c0}$  that corresponds to a potential well for electrons (see [55, 56]) is realized at the sites of the emergence of dislocations (associated with metal shunts) to the quasi-neutral region of semiconductor, while the negative contact potential  $\varphi_{c1}$  (corresponding to the Schottky barrier) is realized between the dislocations. (As the contact potential, we imply the diffusion (built-in) potential  $\varphi_c$  measured from the conduction band edge to the bottom of potential well or the barrier top.)

The total current flowing through the contact is a sum of the currents flowing through metal shunts

associated with dislocations (the so-called conducting dislocations) and those flowing between dislocations. Current flow through shunts makes it possible to realize ohmic contacts.

In the absence of degeneracy, the value of contact resistivity  $R_c$  is determined from Eqs. (6)–(17) presented in the previous subsection.

#### 4.3. The specimens and methods of measurement

We studied the Au–Ti–Pd<sub>2</sub>Si– $n$ -Si ohmic contacts made using layer-by-layer vacuum thermal deposition of metals onto  $n$ -Si (doped with phosphorus) wafers heated to 300 °C. The wafers were cut from the dislocation-free  $n$ -Si ingots obtained using crucibleless melting. The specimen parameters are given in Table 2.

The  $n$ -Si wafers (specimens 1–3) were lapped on both sides with abrasive powder M10. The dislocation density was estimated from the density of etch pits that appeared in Si after treatment in the selective etchant CrO<sub>3</sub> (100 g per 200 ml H<sub>2</sub>O):HF:H<sub>2</sub>O = 1:2:3 (Fig. 9). The concentration of near-surface structural defects (including dislocations) in the lapped specimens was  $10^6 \dots 7 \cdot 10^6 \text{ cm}^{-2}$ . The  $N_{D1}$  values calculated from the temperature dependence of  $\rho_c$  were in good agreement with those determined from the density of etch pits. The calculated values of both scattering and conducting dislocation densities are given in Table 3. The ohmic contact was formed by the palladium silicide phase Pd<sub>2</sub>Si that appeared in the course of metal deposition onto Si wafer heated to 300 °C.

**Table 2.** Resistivity  $\rho$ , impurity concentration  $N_d$ , dislocation density  $N_{D1}$  and thickness  $d$  of the  $n$ -Si wafers under investigation ( $T = 300 \text{ K}$ ).

Number of specimen	1	2	3
$\rho, \Omega \cdot \text{cm}$	0.12	0.045	0.024
$N_d, \text{cm}^{-3}$	$5 \cdot 10^{16}$	$3 \cdot 10^{17}$	$8 \cdot 10^{17}$
$N_{D1}, \text{cm}^{-2}$	$10^6$	$7 \cdot 10^6$	$1.2 \cdot 10^6$
$d, \mu\text{m}$	~350		

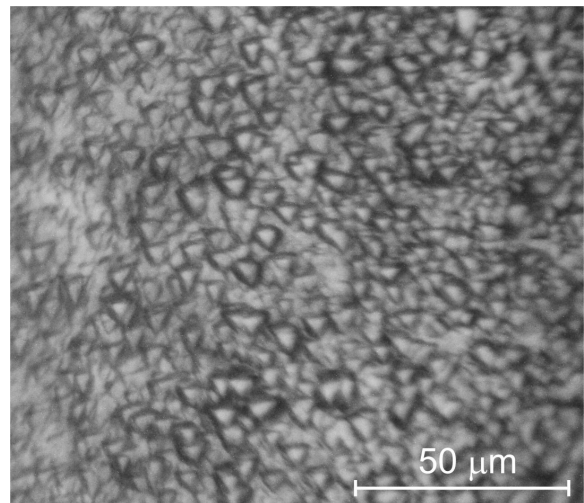


**Fig. 9.** Surface microstructure of lapped  $n$ -Si wafer after selective etching (a fragment); density of conducting dislocations  $N_{D1} = 7 \cdot 10^6 \text{ cm}^{-2}$ .

**Table 3.** Densities of scattering and conducting dislocations in contacts to the specimens 1–3.

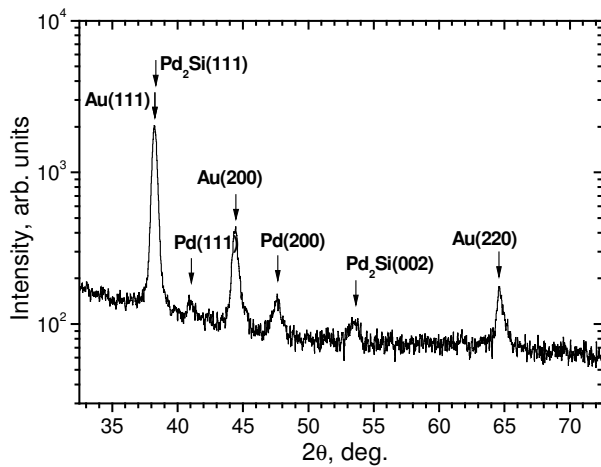
Number of specimen	1	2	3
Density of scattering dislocations, $\text{cm}^{-2}$ (calculation)	$2 \cdot 10^8$	$10^7$	$10^7$
Density of conducting dislocations, $\text{cm}^{-2}$ (calculation)	$1.05 \cdot 10^6$	$7 \cdot 10^6$	$1.45 \cdot 10^6$
Density of conducting dislocations, $\text{cm}^{-2}$ (experiment)	$10^6$	$7 \cdot 10^6$	$1.2 \cdot 10^6$

**Table 4.** Lattice parameters and coefficients of thermal expansion for Si, Pd and  $\text{Pd}_2\text{Si}$  ( $T = 300 \text{ K}$ ) [19, 20].

Material	Lattice parameters, nm		Coefficient of thermal expansion $\alpha$ , $\text{K}^{-1}$
	$a$	$c$	
Si	0.543		$2.54 \cdot 10^{-6}$
Pd	0.389		$11.75 \cdot 10^{-6}$
$\text{Pd}_2\text{Si}$	0.6497	0.3437	

Owing to mismatch of both the coefficients of thermal expansion and lattice parameters of materials (see Table 4), stresses appear in the Si near-contact region. Relaxation of those stresses leads to increase of the density of structural defects in the near-contact region of silicon as compared to the case of initial lapped surface. The calculated density of scattering dislocations grows and equals  $10^7$ – $2 \cdot 10^8 \text{ cm}^{-2}$ .

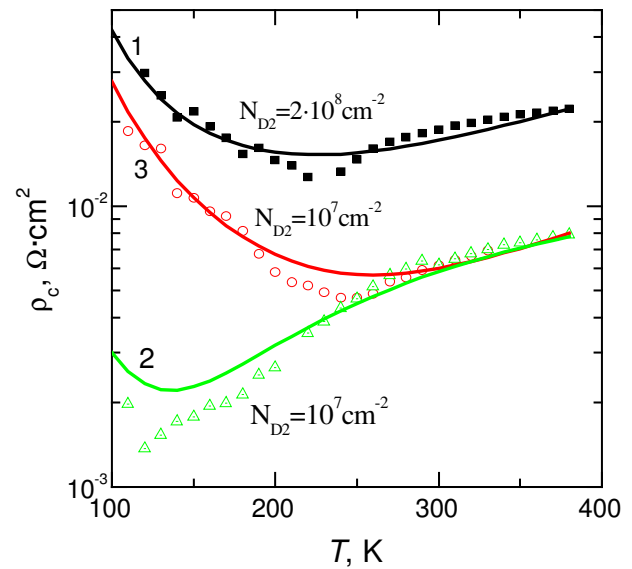
The contact resistivity was measured in the temperature range 100–380 K with the transmission line method [57]. The phase composition of contact metallization was studied with X-ray diffractometry technique in the Bragg–Brentano geometry using Philips X’Pert–MRD ( $\text{CuK}\alpha = 0.15418 \text{ nm}$ ). To separate phases of thin layers, the experimental diffraction patterns were taken at different angles of X-ray incidence. Fig. 10 shows the diffraction pattern obtained for the Au–Ti– $\text{Pd}_2\text{Si}$ – $n$ -Si contact metallization.


**Fig. 10.** X-ray diffraction pattern of the Au–Ti– $\text{Pd}_2\text{Si}$ – $n$ -Si contact metallization deposited onto a lapped  $n$ -Si wafer heated to 300 °C.

Phase analysis of the metallization layers showed that the following reflections were observed: Au (111, 200, 220), Pd (111, 200) and  $\text{Pd}_2\text{Si}$  (111, 002). Presence of the families of reflections from metallization indicates polycrystalline structure of single Au and Pd layers. Absence of reflections from the Ti film seems to be related to its X-ray amorphous state having metallic conductivity. The  $\text{Pd}_2\text{Si}$  phase is formed at Pd interaction with Si in the course of Pd deposition onto the wafer heated to 300 °C. This conclusion correlates with the data of X-ray diffraction and Auger electron spectrometry presented in [58].

#### 4.4. Experimental results and discussion

Shown in Fig. 11 are the  $\rho_c(T)$  dependences of the Au–Ti– $\text{Pd}_2\text{Si}$ – $n$ -Si ohmic contacts made on the lapped  $n$ -Si wafers with the impurity concentrations of  $5 \cdot 10^{16}$ ,  $3 \cdot 10^{17}$  and  $8 \cdot 10^{17} \text{ cm}^{-3}$  (curves 1–3, respectively). One can see that the resistivity  $\rho_c$  of the specimens under investigation is a nonmonotonic function of temperature. The calculated  $\rho_c(T)$  curves built using Eqs. (6)–(17) agree rather well with the experimental  $\rho_c(T)$  dependences (dots). The calculated density of conducting dislocations,  $N_{D1}$ , in the near-contact region varies within the range from  $10^6$  up to  $7 \cdot 10^6 \text{ cm}^{-2}$  and practically coincides with the results of metallographic analysis (see Table 3). The density of scattering dislocations,  $N_{D2}$ , is about  $10^7 \text{ cm}^{-2}$ , except the only case when it is about  $2 \cdot 10^8 \text{ cm}^{-2}$  (see curve 1 in Fig. 11). We believe that this increase of  $N_{D2}$  could result at contact alloying.


**Fig. 11.** Temperature dependence of contact resistivity  $\rho_c$  for three specimens (1–3) of Au–Ti– $\text{Pd}_2\text{Si}$ – $n$ -Si ohmic contact (full curves, theory; symbols, experiment). Impurity concentration  $N_d$ ,  $\text{cm}^{-3}$ : 1 –  $5 \cdot 10^{16}$ , 2 –  $3 \cdot 10^{17}$ , 3 –  $8 \cdot 10^{17}$ . The equilibrium dimensionless potential at the metal–semiconductor interface  $y_{c0}$ : 1 – 5, 2 – 2, 3 – 5. Densities of scattering dislocations  $N_{D2}$  are indicated.

The results obtained can be explained in the following way.

1. If  $\rho_c$  value is limited by diffusion supply of electrons, then nonmonotonic temperature dependence of  $\rho_c$  is typical for nondegenerate semiconductor (see [21]). One can see from Fig. 11 that, at low temperatures, the curve 3 for  $N_d = 8 \cdot 10^{17} \text{ cm}^{-3}$  passes above the curve 2 for  $N_d = 3 \cdot 10^{17} \text{ cm}^{-3}$ . It follows from the theoretical  $\rho_c(T)$  dependences described by Eqs. (11)–(13) that the contact resistivity  $\rho_c$  is a function of the density of conducting as well as scattering dislocations. As the density of conducting (scattering) dislocations grows, the  $\rho_c$  value decreases (increases). One can see from the data presented in Table 3 that the densities of scattering dislocations for the specimens 2 and 3 are the same, while the density of conducting dislocations for the specimen 2 is five times higher than that for the specimen 3. It leads to reduction of the  $\rho_c(T)$  value for the specimen 2 in comparison with that for the specimen 3, despite the fact that the higher doping level favors reduction of  $\rho_c$ . Besides, at low temperatures the value of accumulation band bending at the dislocation end,  $y_{c0}$ , essentially affects the  $\rho_c(T)$  curves. The larger band bending  $y_{c0}$ , the stronger growth of  $\rho_c(T)$  at low temperatures as the temperature decreases. To illustrate, the fitting value of  $y_{c0}$  for the curves 1 and 3 was five, while for the curve 2 it equalled two.

2. At further growth of measurement temperature (curves 1 and 3 after  $T > 240 \text{ K}$ , curve 2 after  $T > 125 \text{ K}$ ), the contact resistivity  $\rho_c$  increases. The reason for this is that the contribution from scattering dislocations and charged impurities to the temperature dependence of electron mobility  $\mu_n$  decreases, while that from scattering by phonons (leading to reduction of  $\mu_n$  with temperature) increases.

3. An analysis of the temperature dependences of  $\rho_c$  for ohmic contacts formed on lapped wafers of rather high-resistant nondegenerate silicon (curves 1–3) showed that a portion of the  $\rho_c(T)$  curve corresponding to anomalous temperature dependence of  $\rho_c$  was observed for all the specimens under investigation. This portion is due to current flowing through the regions of electron accumulation. Those regions appeared at the metal shunt ends under the condition of current limitation by diffusion supply of electrons.

The observed  $\rho_c(T)$  dependences corresponded to the mechanism of  $\rho_c$  formation proposed in Ref. [21]. It assumed existence of two types of dislocations in the near-contact region, namely, scattering dislocations (parallel to the metal–semiconductor interface) and conducting ones (crossing SCR). The origin of the latter dislocations is related to lapping the Si surface, while the scattering dislocations are related to stress relaxation in the contact. (The stresses were caused by mismatch of both the coefficients of thermal expansion and parameters of the  $\text{Pd}_2\text{Si}$  and Si lattices.)

It should be noted that the growth of contact resistivity with temperature may be also realized, in principle, if the near-contact region contains a large number of other extended defects, under the condition that they favor formation of metal shunts penetrating into semiconductor bulk.

## 4.5. Conclusions

The results of experimental measurement and theoretical analysis of the temperature dependence of contact resistivity,  $\rho_c(T)$ , of ohmic contacts to specimens made using lapped *n*-Si wafers indicated the mechanism of contact resistance formation, which is typical for contacts with a high dislocation density. It is supported by anomalous (growing with temperature)  $\rho_c(T)$  curves at sufficiently high temperatures as well as by the results of metallographic analysis indicating rather high dislocation density.

## 5. Some features of temperature dependence of contact resistivity for ohmic contacts to $n^+$ -InN

### 5.1. Introduction

It should be also noted that degenerate InN is practically always used. So, when calculating, one has to take into account degeneracy for correct comparison of the results of calculations with experiment. As will be shown later, resistivity  $\rho_c$  of InN-based contacts in the temperature range of device operation is defined by the mechanism of current flow through metal shunts. Calculation of contact resistivity for this mechanism of current flow was performed in [10]. In this subsection, a theoretical approach to calculate temperature dependence of InN-based nanowire resistance is proposed, and comparison of the developed theory with experiment is performed [24].

In recent years, indium nitride and InN-based solid solutions are one of the most intensely studied materials among the III–N compounds. The interest in them is aroused, in particular, by the prospects for their application when developing a number of active elements for optoelectronics, spintronics and microwave electronics [59–61]. The parameters of these materials are largely defined by their manufacturing technology.

At present, there is no native substrate material for the III–N compounds, so InN and InN-based solid solutions are grown as heterostructures, and  $\text{Al}_2\text{O}_3$ , GaAs, Si and fianites serve as substrates. Because of lattice mismatch and distinctions between thermal expansion coefficients of InN film and substrate (e.g.,  $\text{Al}_2\text{O}_3$ ), intrinsic stresses appear in heterostructures. Relaxation of those stresses leads to generation of dislocations (with the density from  $10^8$  up to  $3 \cdot 10^{11} \text{ cm}^{-2}$ ) [62]. It has an impact on parameters of the corresponding devices, primarily ohmic contacts to them.

It was shown in Refs. [10, 21, 22] that both the value of contact resistivity  $\rho_c$  of ohmic contacts to semiconductors with high dislocation density and temperature dependence  $\rho_c(T)$  may depend essentially on dislocation density. The dislocations serve for penetration of a contact-forming metal (alloy) into a thin near-contact semiconductor layer in the course of ohmic contact formation. As a result, metal shunts associated with dislocations appear in that layer. In that case, it was found that the dependence  $\rho_c(T)$  may be growing at sufficiently high temperatures.

Gol'dberg *et al.* (see, *e.g.* [10]) ascribed the growing  $\rho_c(T)$  curves to temperature dependence of metal shunt resistance. Their explanation, however, does not describe behavior of the  $\rho_c(T)$  curves over a rather wide temperature range. To illustrate, at sufficiently low temperatures, either decreasing or independent of temperature  $\rho_c(T)$  curves are realized.

For nondegenerate semiconductors with high dislocation density, the behavior of experimental dependences  $\rho_c(T)$  over sufficiently wide temperature range obtained complete explanation in [21, 22], where shunt resistance as well as that appearing at electrons passage from semiconductor to the shunt ends were taken into account. It was shown that, owing to high electric fields at the shunt end–semiconductor interfaces, there are accumulation band bendings in the semiconductor near-contact region. The diffusion theory of current flow is realized in a nondegenerate semiconductor in that case, with current directly proportional (and resistivity inversely proportional) to electron mobility. It explains the behavior of  $\rho_c(T)$  curves over a rather wide temperature range. It was also shown in [21, 22] that, at sufficiently strong semiconductor degeneracy, the contact resistivity  $\rho_c$  practically does not depend on temperature. In that case, however, the current flow mechanism is thermionic rather than the tunneling one.

There are two groups of researchers [62–65], who studied the properties of such ohmic contacts to *n*-InN in the temperature range 223–398 K [63, 65] as well as at the temperature 300 K [64] and in the temperature range 4.2–400 K [66]. They observed growing temperature dependences of resistance in ohmic contacts to highly degenerate *n*-InN with the doping level over  $10^{20} \text{ cm}^{-3}$ . The dependences  $\rho_c(T)$  were determined using the transmission line method [63, 65]. First in [66], a nanosized wire was made of highly degenerate *n*-InN, then temperature dependences of the total resistance of nanowire and two identical contacts were measured. (No contact resistivity was determined separately in that case.) The results obtained in Refs. [63, 65, 66] will be discussed later.

Next, we studied experimentally the  $\rho_c(T)$  dependence of ohmic contacts to *n*-InN layers in the temperature range 4.2–300 K. The structures under investigation were grown on  $\text{Al}_2\text{O}_3$  substrates with a gallium nitride buffer layer; the dislocation density was over  $10^8 \text{ cm}^{-2}$ . The results obtained were explained within the framework of approach developed in [21, 22].

### 5.2. The specimens and methods of investigation

The ohmic contacts were made using successive deposition of palladium, titanium and gold onto the InN(0.6  $\mu\text{m}$ )–GaN(0.9  $\mu\text{m}$ )– $\text{Al}_2\text{O}_3$ (400  $\mu\text{m}$ ) heterostructure heated to 350 °C. The Au(500 nm)–Ti(60 nm)–Pd(30 nm)–*n*<sup>+</sup>-InN ohmic contact was formed in the course of metal deposition and was not subjected to additional annealing. The InN–GaN– $\text{Al}_2\text{O}_3$  heterostructures were MBE-grown with plasma activation. Their parameters were similar to those of the structures

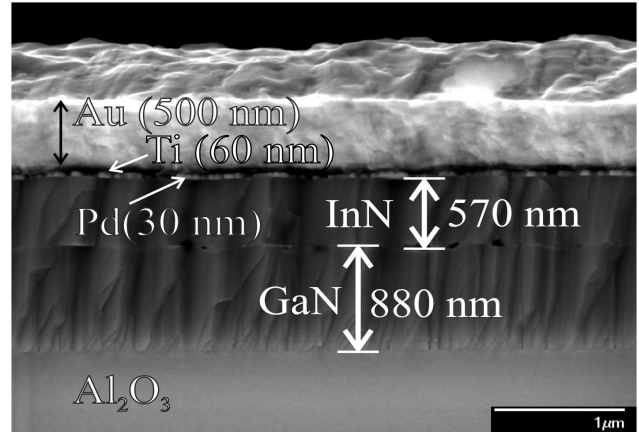


Fig. 12. Surface morphology of Au–Ti–Pd–InN–GaN– $\text{Al}_2\text{O}_3$  contact structure cleavage.

studied in [65]. InN (0001) was grown on a GaN buffer layer preliminary formed on an  $\text{Al}_2\text{O}_3$  substrate at  $T = 300 \text{ K}$ . The electron concentration (mobility) in *n*-InN was  $\sim 2 \cdot 10^{18} \text{ cm}^{-3}$  ( $\sim 1300 \text{ cm}^2/\text{V}\cdot\text{s}$ ).

For specimens with continuous metallization, we measured the dislocation density in the heterostructure, phase composition of contact metallization (using X-ray diffractometry) and concentration depth profiles of contact metallization components (using Auger electron spectrometry). It was determined that the density of screw (edge) dislocations in *n*-InN was  $\sim 2.3 \cdot 10^8 \text{ cm}^{-2}$  ( $\sim 3.4 \cdot 10^{10} \text{ cm}^{-2}$ ). Titanium, gold and  $\text{Au}_{0.919}\text{Ti}_{0.081}$  compound were detected in the contact metallization. Palladium and its compounds were not detected because of their amorphous state. Presence of palladium was confirmed by the results of Auger electron spectrometry.

Measurements of  $\rho_c(T)$  were performed for planar test structures in the temperature range 4.2–300 K by using the transmission line method. The contact width (length) was 75  $\mu\text{m}$  (400  $\mu\text{m}$ ); the spacings between contact pads  $l_i$  were 150, 100, 80, 60, 40 and 20  $\mu\text{m}$ . The test structures were mounted in a case to obtain the dependences  $\rho_c(T)$ .

The cleavages of Au–Ti–Pd–InN–GaN– $\text{Al}_2\text{O}_3$  contact structures were studied with electron microscopy. A photomicrograph (Fig. 12) shows a columnar structure of both GaN buffer layer and InN film, with characteristic defects at the InN–GaN interface. The linear density of vertical defects in InN (GaN) was about  $10^4 \text{ cm}^{-1}$  ( $\sim 7 \cdot 10^4 \text{ cm}^{-1}$ ).

### 5.3. The results of measurements and discussion

The *I*–*V* curves of the contacts under investigation were linear and symmetric over the whole temperature range measured. It indicated ohmicity of the contacts.

The experimental temperature dependence  $\rho_c(T)$  is presented in Fig. 13 (open circles). Its behavior differs considerably from  $\rho_c(T)$  curves typical for ohmic Schottky contacts. In the latter ones,  $\rho_c$  either does not depend on temperature (tunneling mechanism of current flow) or decreases with temperature (thermal-field mechanism of current flow). In our case,  $\rho_c$  grows with

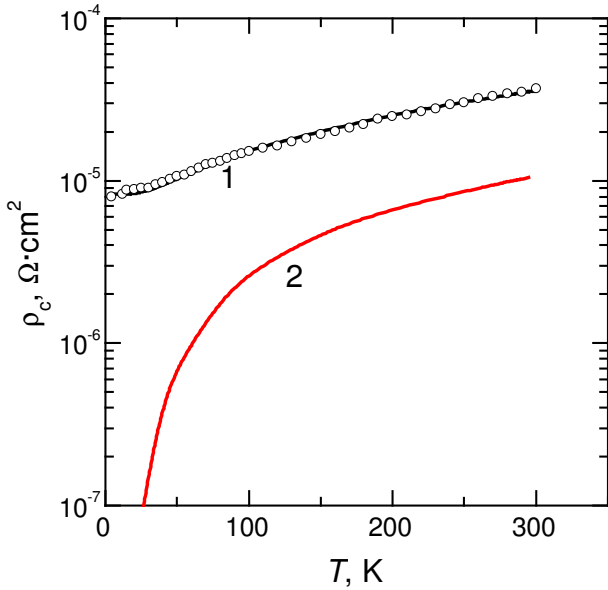


**Fig. 13.** 1 – experimental (open circles) and theoretical (full curve) dependences  $\rho_c(T)$  of Au–Ti–Pd– $n^+$ –InN ohmic contact, 2 – temperature dependence of shunt resistivity  $\rho_{sh}(T)$ .

temperature over the whole temperature range measured: at low temperatures (from 4.2 up to 30 K)  $\rho_c$  increases very slow, while  $\rho_c \sim T$  at temperatures over 150 K.

When performing theoretical modeling of the experimental dependence  $\rho_c(T)$  for an ohmic contact to  $n^+$ –InN presented in Fig. 13, we take into account semiconductor degeneracy. Let us suppose that current flows through metal shunts associated with the so-called conducting dislocations. To calculate  $\rho_c(T)$ , we apply the expressions from Ref. [21] that are valid for degenerate semiconductor.

In a general case, the expressions for  $\rho_{te}$  are described by formulae (6)–(13).

In the case of degenerate semiconductor, the resistance of all metal shunts is connected in series with  $\rho_{nw}$ . So, the total resistivity of ohmic contact in the semiconductor with a high dislocation density is

$$\rho_c = \rho_{nw} + \rho_{sh}, \quad (25)$$

where  $\rho_{sh} = R_{sh}(T)/N_{D1}$ ,  $R_{sh}(T) = \rho_0(T) d_D / \pi r^2$  is a metal shunt resistance,  $\rho_0$  – metal resistivity,  $d_D$  – dislocation length, and  $r$  – shunt radius (in calculation, all shunts were considered to be identical). It is assumed that the current flowing between dislocations can be neglected in comparison with the current flowing through the metal shunts associated with conducting dislocations. It is provided by high potential barriers between dislocations [21].

According to [67, 68] the temperature dependence  $\rho_{sh}(T)$ , with allowance made for temperature dependence of the contact forming metal (palladium), behaves in the following way. At  $T = 0$  K, the resistance of normal metal is equal to the residual resistance  $R_s$ . As the temperature grows, the resistance increases like to  $T^5$  (see Fig. 13, curve 2) because of electron scattering by

phonons [15]. Then a transition region with growth  $\sim T^n$  is realized, with  $n$  decreasing rapidly. And, at last, at  $T \geq T_D$  ( $T_D$  is the Debye temperature),  $n = 1$ , i.e., metal resistance grows linearly with temperature.

The theoretical dependence  $\rho_c(T)$  (Fig. 13, curve 1) was calculated using Eq. (5). When calculating, the data on InN parameters given in [58, 69, 70] were used. One can see from Fig. 13 that there is good agreement between the calculated contact resistivity  $\rho_c$  and the experimental data. It was achieved by using the following parameters:  $N_D \approx 5 \cdot 10^9 \text{ cm}^{-2}$ ,  $r = 5 \cdot 10^{-8} \text{ cm}$ ,  $d_D \sim 0.1 \mu\text{m}$ . One should note that, since  $R_{sh} \propto d_D / r^2$ , there exists some ambiguity in determination of  $d_D$  and  $r$  values (as  $d_D$  grows,  $r$  grows, too).

The total density of screw and edge dislocation found by us is quite enough for realization of the mechanism considered. One can see from Fig. 13 that in our case the value of contact resistivity  $\rho_c$  at  $T = 300$  K is about  $3 \cdot 10^{-5} \Omega \cdot \text{cm}^2$ .

Let us return to discussion of the results obtained in Refs. [62, 64, 65]. In the works [62, 64], the value  $\rho_c \sim 2 \cdot 10^{-7} \Omega \cdot \text{cm}^2$  was obtained for InN with doping level  $> 10^{20} \text{ cm}^{-3}$ , and the  $\rho_c(T)$  curves were growing. The estimations show that, taking into account the high effective density of conducting dislocations, the results obtained in [62, 64] could be explained by the mechanism considered in the present work. However, a narrow temperature range for measuring  $\rho_c$  in the cited works made it impossible to determine  $\rho_c$  values in the region where  $\rho_c$  dependence on temperature is weak or is absent at all. Therefore, by using the results obtained in [62, 64] one cannot distinguish exactly a contribution related to semiconductor resistance from that related to the total shunt resistance.

In [71] nanowires with the diameter of about 100 nm were made on the basis of highly degenerate InN (doping level of  $5 \cdot 10^{20} \text{ cm}^{-3}$ ). The temperature dependences of total resistances of contacts and nanowire were measured. An attempt was made to explain the growing (linear) character of the dependences under investigation of metallic behavior inherent to highly degenerate InN.

It should be noted that physics of conduction formation in metal and highly degenerate semiconductor related to scattering of charge carriers by optical phonons at sufficiently high temperatures is different. In metals (as was noted before), the resistivity grows with temperature:  $\sim T^5$  at very low temperatures and linearly at temperatures over the Debye one. For degenerate III–V semiconductors, at low temperatures, the electron mobility  $\mu_n$  does not depend on temperature and is determined mainly by scattering on impurities, [72] (at high dislocation density, by scattering on dislocations, too). At sufficiently high temperatures,  $\mu_n$  decreases (in general, nonlinearly) because of electron scattering by optical phonons. In this case, resistance of a degenerate semiconductor grows nonlinearly.

To solve finally the problem of a close to linear decrease of electron mobility in highly degenerate

electron gas at sufficiently high temperatures, let us calculate the electron mobility  $\mu_n$  for the above case. For a degenerate semiconductor in the temperature region where the Fermi energy  $E_F$  is much higher than the thermal energy  $kT$ , the equilibrium distribution function can be approximated by the Heaviside unit function  $\theta(E_F - E)$ . If the doping level is sufficiently high, then the Mott transition in the impurity band has occurred and all donors are ionized, no matter what is the temperature. In other words, the impurity band and conduction band overlap. It means that the electron and donor concentrations are determined by the Fermi momentum  $p_F$ :  $n = N_d = p_F^3 / (3\pi^2 \hbar^3)$ . It is convenient to describe nonparabolicity of the conduction band with a model [73]:

$$E(p) = \frac{p_s^2}{m} \left[ \sqrt{1 + (p/p_s)^2} - 1 \right], \quad (26)$$

where  $p_s$  is the characteristic momentum:  $p_s^2 = mE_s/2$ . In this case,  $E_s \approx E_g$ , where  $E_g$  is the bandgap width. To avoid confusion, we note that the relation between the Fermi momentum and Fermi energy is  $E(p_F) = E_F$ .

By applying kinetic equation in the low-field approximation for calculation of conduction  $\sigma$  and presenting electron mobility as  $\mu_n = \sigma / qn$ , we obtain the following expression for mobility of degenerate electron gas:

$$\mu_n = q\tau_m(E_F) / m\sqrt{1 + (p_F/p_s)^2}, \quad (27)$$

where  $\tau_m(E_F)$  is the momentum relaxation time calculated for the Fermi energy. The partial contributions of different mechanisms of electron momentum relaxation  $\tau_m^{-1}(E_F) = \sum_j \tau_{jm}^{-1}(E_F)$  are summated in the

same way as the partial contributions of mobilities:  $\mu^{-1}(E_F) = \sum_j \mu_j^{-1}(E_F)$ . For the methods for calculating

the corresponded relaxation times  $\tau_i(E)$ ,  $\tau_D(E)$ , and  $\tau_{opt}(E)$  see, e.g. [35, 74].

In what follows, there are the expressions for corresponding electron mobilities. At relaxation due to electron interaction with charged impurities,

$$\mu_i = \left\{ \frac{2m^2 q^3}{3\pi \hbar^3} \left( \frac{1}{4\pi \epsilon_s \epsilon_0} \right)^2 \left[ 1 + \left( \frac{p_F}{p_s} \right)^2 \right] \times \left[ \ln \left| 1 + \frac{4p_F^2}{\hbar^2 \lambda_{TF}^2} \right| - \frac{4p_F^2}{4p_F^2 + \hbar^2 \lambda_{TF}^2} \right] \right\}^{-1}, \quad (28)$$

where  $\lambda_{TF} = \left[ q^2 m p_F \sqrt{1 + (p_F/p_s)^2} / (\epsilon_s \epsilon_0 \pi^2 \hbar^3) \right]^{-1/2}$  is the Thomas–Fermi screening length. At relaxation due to electron interaction with dislocations,

$$\mu_{Dc,s} = \left\{ \frac{2m^2 q^3}{3\hbar^3} \left( \frac{\lambda_{TF}^2}{\epsilon_s \epsilon_0 a} \right)^2 \left[ 1 + \left( \frac{p_F}{p_s} \right)^2 \right] \right\}^{-1} \frac{\Phi_{c,s}}{N_{Dc,s}}. \quad (29)$$

Here,  $a$  is the lattice parameter,  $N_{Dc}$  – effective density of the so-called conducting dislocations (those normal to the contact–semiconductor interface),  $N_{Ds}$  – effective density of the so-called scattering dislocations (those parallel to the contact–semiconductor interface).  $\Phi_{c,s}$  – corresponding angular factor:

$$\Phi_c = \left[ \sinh^3(2A)/3 + \sinh(4A)/4 - A \right] / 8a^3, \quad \text{where} \\ a = 2p_F \lambda_{TF} / \hbar \quad \text{and} \quad \sinh(A) = a; \\ \Phi_s = \left[ \sin^3(2B)/3 - \sin(4B)/4 + B \right] a^3 / 8b^6, \quad \text{where} \\ b = a / \sqrt{1 + a^2} \quad \text{and} \quad \sin(B) = b.$$

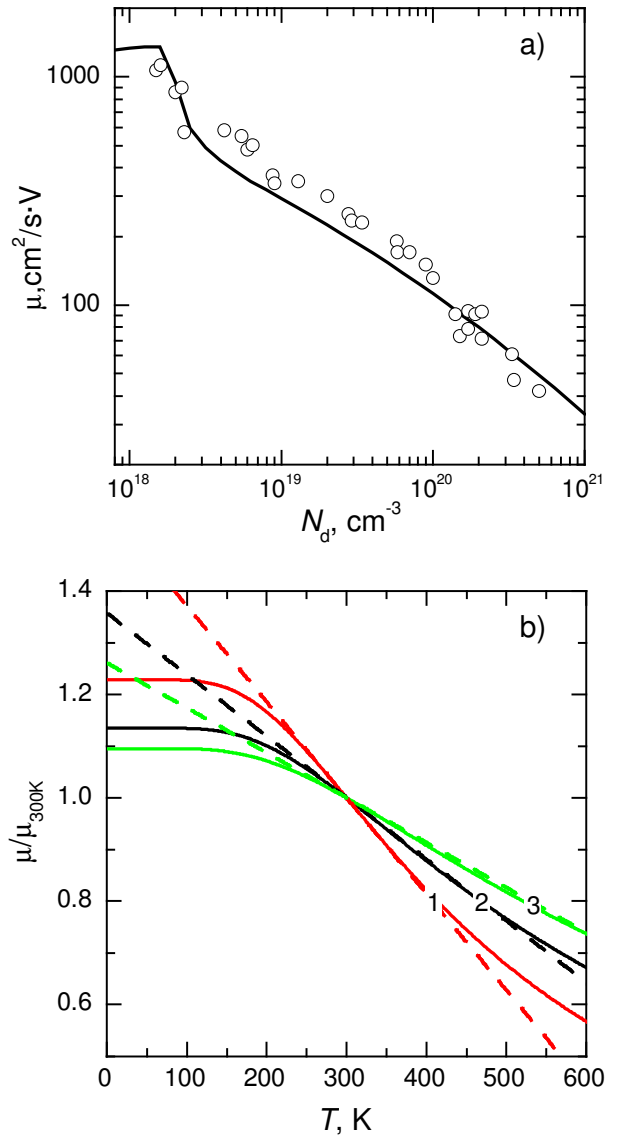


**Fig. 14.** Electron mobility in degenerate InN as a function of: (a) doping level at room temperature (the experimental data are taken from Ref. [22]); (b) temperature at different doping levels: 1 –  $2 \cdot 10^{18} \text{ cm}^{-3}$ , 2 –  $5 \cdot 10^{18}$ , 3 –  $5 \cdot 10^{20}$  (the mobility values are normalized to that at  $T = 300 \text{ K}$ ).

Optical phonon (as perturbation) leads to local variation of the electric polarization vector. With allowance made for electron scattering by optical phonons, the mobility is [34]:

$$\mu_{opt} = \left\{ \frac{qm^2 \hbar \omega_o (\epsilon_d^{-1} - \epsilon_s^{-1})}{4\pi \epsilon_o \hbar^2} \sqrt{1 + \left(\frac{p_F}{p_s}\right)^2} N\left(\frac{\hbar \omega_j}{kT}\right) \times \left[ \xi_{jF}^+ \ln \left| \frac{p_F + p_s \sqrt{\xi_{jF}^{+2} - 1}}{p_F - p_s \sqrt{\xi_{jF}^{+2} - 1}} \right| + \exp\left(\frac{\hbar \omega_j}{kT}\right) \xi_{jF}^- \ln \left| \frac{p_F + p_s \sqrt{\xi_{jF}^{-2} - 1}}{p_F - p_s \sqrt{\xi_{jF}^{-2} - 1}} \right| \theta(\xi_{jF}^- - 1) \right] \right\}^{-1}, \quad (30)$$

where  $\xi_{jF}^{\pm} = \sqrt{1 + (p_F / p_s)^2 \pm m \hbar \omega_j / p_s^2}$ ,  $\hbar \omega_{opt}$  is the optical phonon energy,  $\epsilon_d(\epsilon_s)$  – dynamic (static) semiconductor permittivity and  $N(x)$  – Planck blackbody radiation distribution function.

Shown in Fig. 14 are the dependences of electron mobility  $\mu_n$  in degenerate InN calculated (a) for absolute values  $\mu_n(N_d)$ , (b) for relative values  $\mu_n(T)/\mu_n(300\text{ K})$  using the expression

$$\mu_n = (\mu_i^{-1} + \mu_D^{-1} + \mu_{opt}^{-1})^{-1}. \quad (31)$$

The following values of material parameters were used: the effective electron mass  $m = 0.07m_0$ , static permittivity  $\epsilon_s = 15.3$ , dynamic permittivity  $\epsilon_d = 7.5$ , optical phonon energy  $\hbar \omega_{opt} = 73\text{ meV}$ , nonparabolicity parameter of the conduction band  $E_s = 0.5\text{ eV}$ . One can see from Fig. 14 that the higher is doping level, the closer is the law of mobility decrease at sufficiently high temperatures to the linear one.

When using the parameters of highly degenerate InN, the above equations for mobility of degenerate electron gas give for doping levels (up to  $10^{21}\text{ cm}^{-3}$ ) the values that are very close to the experimental ones (see Fig. 15). At the doping level  $5 \cdot 10^{20}\text{ cm}^{-3}$ , the calculated electron mobility is sufficiently close to the maximum possible value of  $50\text{ cm}^2/\text{V}\cdot\text{s}$  obtained by using  $\rho_s = 2.5 \cdot 10^{-4}\ \Omega\cdot\text{cm}$  and presented in [71] (with allowance made for error in  $\rho_s$ ).

The doping level is a parameter of the calculated curves in Fig. 14b. One can see from Fig. 14b that, at the doping level of  $5 \cdot 10^{18}\text{ cm}^{-3}$ , a decrease of mobility dependences (normalized to  $\mu_n(300\text{ K})$ ) at  $T > 100\text{ K}$  is closer to linear than in the case of doping level  $2 \cdot 10^{18}\text{ cm}^{-3}$ . And at  $T > 150\text{ K}$ , the linear approximation of electron mobility decrease for the case of doping level of  $5 \cdot 10^{20}\text{ cm}^{-3}$  is sufficiently good. It is natural that close to linear mobility decrease corresponds to close to linear growth of resistance of a highly degenerate semiconductor:  $R(T) = R_0(1 + \alpha_{eff}(T - T_0))$ . However, linearity of the quantities considered occurs, at best, with a graphical accuracy only, while accurately calculated slope of mobility curve still remains weakly dependent on temperature.

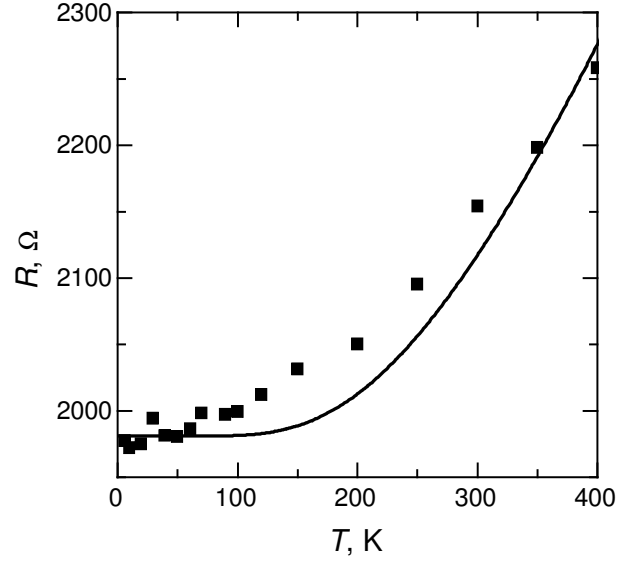


**Fig. 15.** Temperature dependence of nanocontact resistance: full squares – experimental data from Ref. [71], curve – calculation.

Thus, one should not assert that for highly degenerate semiconductors dependence  $R(T)$  is of metallic character. Besides, the temperature resistance coefficient  $\alpha_{eff}(T)$  for highly degenerate semiconductor (contrary to the case of metals, where the typical  $\alpha$  value is close to  $1/273\text{ K}^{-1}$ ) goes down as the electron mobility value  $\mu(T=0)$  decreases, and the effective electron mass  $m$  increases. As a result, at high degeneration  $\alpha_{eff}$  value for semiconductors is about an order below that for metals.

It should be noted that for the case considered in [71] (where only total  $R$  value was measured)

$$R = 2R_c + \frac{\rho_s L_s}{\pi r_s^2}. \quad (32)$$

Here,  $R_c$  is the contact resistance,  $\rho_s = (nq\mu_n)^{-1}$  – resistivity of a degenerate nanowire and  $r_s(L_s)$  – its radius (length). Some additional information on the  $R_c$  and  $R_s = \rho_s L_s / \pi r_s^2$  values may be obtained when taking into account that, at  $T \geq 300\text{ K}$ , the following interrelations are valid:

$$R_c = R_{c0} + R_{m0} [1 + \alpha(T - T_0)], \quad (33)$$

$$R_s = R_{s0} [1 + \alpha_{eff}(T - T_0)], \quad (34)$$

where  $R_{c0} = \rho_{tw} / \pi r_s^2$ ,  $R_{m0}$  is the total resistance of all metal shunts associated with dislocations at  $T = T_0$ , and  $R_{s0}$  – nanowire resistance at  $T = T_0$ .

For  $T > 150\text{ K}$  and considering that  $T_0 = 300\text{ K}$ , one can write down

$$2(R_{c0} + R_{m0}) + R_{s0} = 2150\ \Omega, \quad (35)$$

$$\alpha_{eff} + \alpha(2R_{m0}/R_{s0}) = 4.7 \cdot 10^{-4}\text{ K}^{-1}. \quad (36)$$

As a result, we have two equations with three unknowns:  $R_{c0}$ ,  $R_{m0}$  and  $R_{s0}$ . Bearing in mind that  $R_{s0} = \rho_{s0}L_s/\pi r_s^2$  (where  $\rho_{s0}$  is the nanowire resistivity), only two unknowns remain in Eqs. (33), (34). The preliminary estimations show that  $R_{m0} \ll R_{c0}$  and  $R_{m0} \ll R_{s0}$ , so it is possible to neglect  $R_{m0}$  value to a first approximation.

After substitution of nanowire parameters and the lower value of  $\rho_{s0}$  (according to Ref. [71], it is  $2.5 \cdot 10^{-4} \Omega \cdot \text{cm}$ ) into the expression for  $R_{s0}$ , we obtain  $R_{s0} = 1548 \Omega$ . Then, by substituting  $R_{s0}$  into Eqs. (35) and (36), we get  $2R_{c0} \approx 600 \Omega$ . On the other hand, the  $R_c$  value can be determined from the expression  $R_{c0} = \rho_{tw}/\pi r_s^2$ . By using the values of  $5 \cdot 10^{20} \text{ cm}^{-3}$  and  $5 \cdot 10^{11} \text{ cm}^{-2}$  for the doping level and density of metal shunts, respectively, when calculating  $\rho_{tw}$  from Eq. (25), we obtain that  $2R_{c0} \approx 600 \Omega$ , this corresponds to the above value. At the doping level of  $5 \cdot 10^{20} \text{ cm}^{-3}$ , the calculated slope of  $\mu_n(T)$  curve is very close to the value of  $4.7 \cdot 10^{-4} \text{ K}^{-1}$  given in Ref. [11].

Shown in Fig. 15 are the experimental dependence  $R(T)$  taken from Ref. [71] (full squares) and theoretical curve built from Eqs. (27)-(35), with allowance made for the abovementioned. The base of nanocontact is a nanowire made of  $n$ -InN ( $N_d = 5 \cdot 10^{20} \text{ cm}^{-3}$ ),  $7 \mu\text{m}$  in length and  $120 \text{ nm}$  in diameter. One can see sufficiently good agreement between the theoretical and experimental results. In this case, the contribution from contact resistance  $R_c$  of both contacts to the total resistance  $R$  is about 28%, so the  $R$  value is determined mainly by the nanowire resistance. Recalculation of resistance  $R_c(300 \Omega)$  to contact resistivity gives about  $3 \cdot 10^{-8} \Omega \cdot \text{cm}^2$ . It should be noted that the contact resistivity value of  $1.09 \cdot 10^{-7} \Omega \cdot \text{cm}^2$  given in Ref. [71] corresponds, as a matter of fact, to the product of the total resistance of nanowire and two contacts by the contact area.

#### 5.4. Conclusions

1. We obtained experimentally (as in Refs. [8, 10, 11]) growing temperature dependences  $\rho_c(T)$  of contact resistivity  $\rho_c$  in degenerate ohmic contacts to InN. It is shown that they are explained by current flow through metal shunts associated with dislocations.

2. Based on the estimations made, it is shown that the above mechanism can also explain the growing  $\rho_c(T)$  curves in ohmic contacts to InN with the doping level over  $10^{20} \text{ cm}^{-3}$  that were observed in Refs. [62, 64].

3. It has been confirmed that linear character of temperature dependence of total resistance of a nanowire and two contacts to highly degenerate InN (obtained in [71] is practically related to the linear temperature dependence of nanowire resistance). We explained this dependence within the framework of the mechanism of electron scattering by optical phonons. It is also shown that the value of contact resistivity  $\rho_c$  estimated using the data from [71], taking into account that contact resistance  $R_c$  is much lower than the nanowire resistance  $R_{s0}$  [76] is close to  $3 \cdot 10^{-8} \Omega \cdot \text{cm}^2$ .

## 6. The temperature dependence of contact resistivity for ohmic contacts to $n$ -Si with an $n^+$ - $n$ doping step

### 6.1. Introduction

At present, there exists a fixed notion of the mechanisms of current flow in ohmic metal–semiconductor contacts as well as the processes of minimization of contact resistivity and their contribution to the parameters of semiconductor devices and integrated circuits [19]. This notion asserts that contact resistivity  $\rho_c$  should be minimal and demonstrate thermal and electrical stability, and  $I$ – $V$  curves of ohmic contacts must be linear and symmetric. As a rule,  $\rho_c$  of such contacts is described within either field emission ( $\rho_c$  does not depend on temperature) or thermal-field emission ( $\rho_c$  decreases with temperature).

However, recent investigations [10, 21, 22, 77, 78] showed that in some cases  $\rho_c$  does not demonstrate the above behavior. To illustrate, for ohmic contacts to wide-gap semiconductors with high dislocation density it was shown in [10, 21, 76, 77] that  $\rho_c$  increases with temperature. Such growing dependences  $\rho_c(T)$  were obtained in [22, 78] for ohmic contacts to lapped as well as polished  $n$ -Si, at presence of high density of structural defects in the Si near-contact region. In that case, calculation of the number of defects from etching pits made for lapped silicon gave  $\sim 10^7 \text{ cm}^{-2}$ . According to the model proposed in [21, 22], this value turned out to be sufficient for description of growing dependence  $\rho_c(T)$ .

Along with the above-mentioned, some other conditions of ohmic contact formation may lead to  $\rho_c$  growth with temperature. For instance, usually used as an ohmic contact is an isotype  $n^+$ - $n$  junction ( $n^+$ - $n$  doping step) or  $p^+$ - $p$  junction – analog of metal–semiconductor contact, in which degenerate  $n^+$ -semiconductor (or  $p^+$ -semiconductor) acts as a metal. In this case, we deal practically with a Schottky diode without a potential barrier [35]. In what follows, we consider the model of this ohmic contact and its experimental testing.

### 6.2. Model of the ohmic contact with a doping step

Let us consider a model of ohmic contact with an  $n^+$ - $n$  doping step in the near-contact region, with electrons in the heavily doped  $n^+$ -layer being degenerate. This situation is realized in the manufacturing technology for silicon devices, in particular, IMPATT diodes. In that case, the thickness  $W_{n^+}$  of the heavily doped region with electron concentration  $n_1^+$  exceeds the Schottky layer thickness  $W_{sh}$ , and the doping level is over the effective density of states  $N_c$  in the conduction band. Just this situation means that electrons in the heavily doped region are degenerate.

In this work, we made an analytical calculation of the  $\rho_c(T)$  curve for Si-based ohmic contacts with an  $n^+$ - $n$  doping step in the limiting case, when the contact band diagram is of the form shown in Fig. 16. One can see that

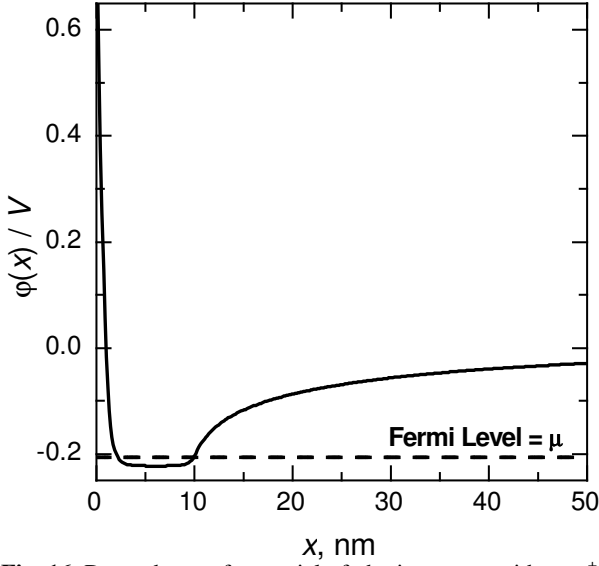


**Fig. 16.** Dependence of potential of ohmic contact with an  $n^+-n$  doping step,  $n^+ \sim 5 \cdot 10^{20} \text{ cm}^{-3}$ ,  $n \sim 10^{16} \text{ cm}^{-3}$ ,  $W_{n^+} \sim 0.01 \mu\text{m}$ .

the thickness  $W_{n^+}$  of the heavily doped region with electron concentration  $n_1^+$  exceeds the Schottky layer thickness  $W_{sh}$  ( $W_{n^+} > W_{sh}$ ), and the doping level exceeds the effective electron density of states in the conduction band  $N_c$  ( $n_1^+ > N_c$ ). It means that electrons in the heavily doped region are degenerate.

Figs 17a and 17b present band diagrams for contacts to Si with a doping step, at two values of heavily doped layer thickness  $W_{n^+}$ : 5 and 10 nm. In our calculations, we used the following values:  $n_2 = 10^{16} \text{ cm}^{-3}$ ,  $n_1^+ = 2 \cdot 10^{18}, 5 \cdot 10^{18}, 10^{19}, 2 \cdot 10^{19}$  and  $5 \cdot 10^{19} \text{ cm}^{-3}$ . To obtain the band diagrams, we solved the Poisson equations for the heavily doped and lightly doped regions (both with allowance made for electron degeneracy) of the form

$$\frac{d^2\phi}{dx^2} = \frac{1}{\epsilon_0\epsilon_s} \rho(x), \quad (37)$$

where

$$\rho(x) = q \left[ \frac{8\pi(m_p T)^{3/2}}{(2\pi\hbar)^3} \int_0^\infty dz \frac{z^{1/2}}{\exp\left(z - \frac{E_F - q\Phi}{kT}\right) + 1} - \frac{n_1^+ \theta(W_{n^+} - x) + n_2 \theta(x - W_{n^+})}{\exp\left(\frac{E_a + E_F - q\Phi}{kT}\right)} \right]. \quad (38)$$

Here,  $E_a \approx 0.005 \text{ eV}$ ,  $\theta(x)$  is the Heaviside function.

The barrier height at the contact (or, more exactly, the diffusion potential  $\phi_c$ ) was preset as 0.4 V. The electrostatic potential was considered to vanish for  $x \rightarrow \infty$ . The solutions of the Poisson equation in the heavily and lightly doped regions were matched at the boundary  $x = W_{n^+}$ , that is to say, the values of potentials, as well as their derivatives (*i.e.*, the electric fields), were matched, respectively.

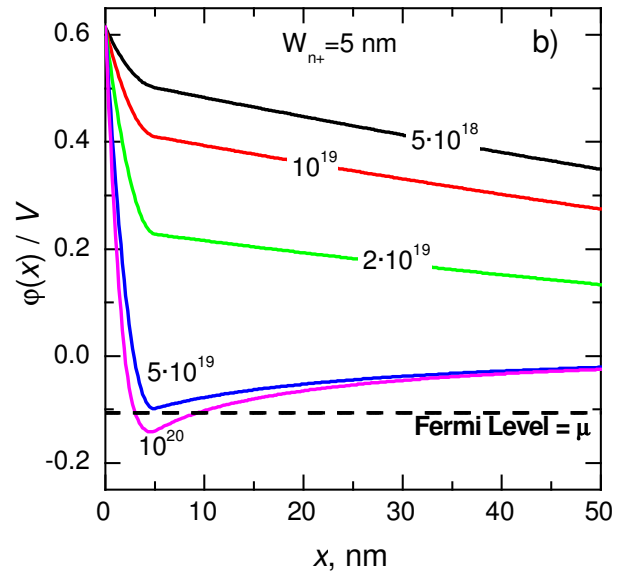
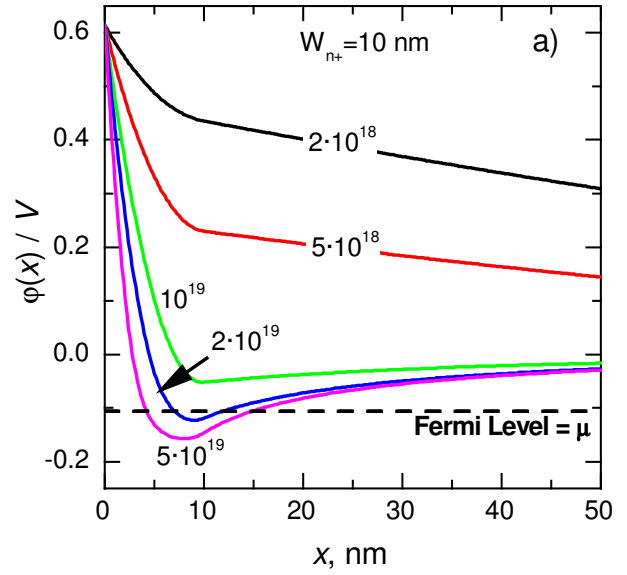


**Fig. 17.** Dependences of potential of contacts with a doping step for Si at two thickness values of heavily doped layer  $W_{n^+}$ : 5 nm (a) and 10 nm (b);  $n^+$ :  $5 \cdot 10^{18}, 10^{19}, 2 \cdot 10^{19}$  and  $5 \cdot 10^{19} \text{ cm}^{-3}$  at  $n_2 = 10^{16} \text{ cm}^{-3}$ .

Naturally, all the  $n_1^+$  values taken for calculation obeyed the inequality  $n_1^+ > N_c$ . However, since the Schottky layer thicknesses in the heavily doped region met the condition  $W_{n^+} < W_{sh}$  at all doping levels, there was no portion of  $\phi(x)$  independent of the coordinate  $x$  shown in Fig. 16.

One should note that, depending on the behavior of potential  $\phi(x)$  in the near-contact region, the contact will be either rectifying (in the case of monotonic dependence of  $\phi$  on the coordinate  $x$ ) or ohmic (in the case of a strongly pronounced non-monotony of  $\phi(x)$ ). In the latter case, the contact resistivity may be presented as a sum of two terms (corresponding to series resistances):

$$\rho_c = \rho_{c1} + \rho_{c2}. \quad (39)$$

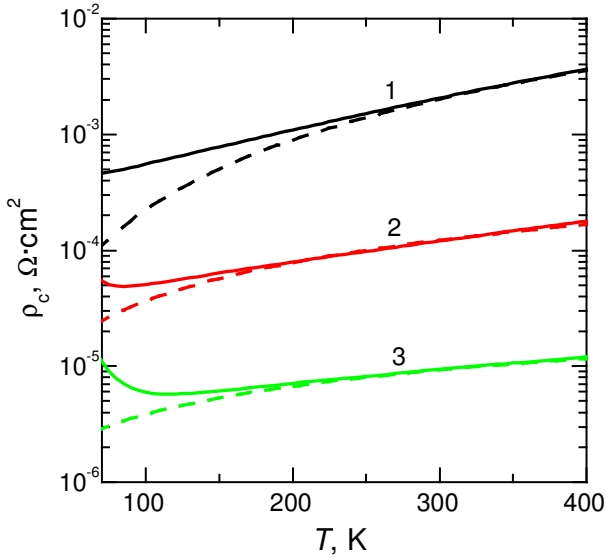


**Fig. 18.** Theoretical  $\rho_{c2}(T)$  curves built using Eq. (4) (solid curves) and with allowance made for low-temperature freezing-out of electrons (dashed curves;  $n_2$ ,  $\text{cm}^{-3}$ : 1 –  $10^{14}$ , 2 –  $10^{15}$ , 3 –  $10^{16}$ ).

Here,  $\rho_{c1}$  is the contact resistivity related to thermal-field passage of electrons through the barrier at the interface between a heavily doped semiconductor and metal, and

$$\rho_{c2} = \frac{kN_c}{qA^*Tn_2} \left( 1 + \frac{L_D A^* T}{k\mu_n N_c} \right) \quad (40)$$

is the effective contact resistance of the lightly doped region in the limiting case of contact energy band being of the form shown in Fig. 16. Here,  $k$  is the Boltzmann constant,  $A^*$  – effective Richardson constant,  $\mu_n$  – electron mobility in the lightly doped region,  $L_D = (\epsilon_0 \epsilon_s kT / 2q^2 n_2)^{0.5}$  – Debye screening length for the lightly doped region. It should be noted that Eq. (39) was obtained with allowance made for the results of [34] and [79, 80]: it takes into account both the diffusion and emission terms in the current flowing through the lightly doped region.

Thus, if the inequality  $\rho_{c2} > \rho_{c1}$  holds, then contact is purely ohmic. In that case, band bending in the lightly doped region is accumulation rather than depletion, so the total voltage applied to the contact drops across the neutral bulk, thus ensuring contact ohmicity. The electron mobility  $\mu_n$  in the region of light doping was calculated with allowance made for electron scattering by charged impurities as well as by intervalley and acoustic phonons [39]. It was assumed that dislocation density in the lightly doped region is sufficiently low and does not affect electron mobility. The expressions for  $\mu_n$  calculation are given in [21].

Now let us dwell on an analysis of temperature dependence of contact resistivity  $\rho_{c2}$ . If the role of diffusion current is insignificant (that is to say, the

inequality  $\left( \frac{L_D A^* T}{k\mu_n N_c} \right) < 1$  holds), then one obtains (with

allowance made for  $N_c(T) = N_{c0}(T/300\text{K})^{3/2}$ ) that  $\rho_{c2} \sim \sqrt{T}$ , i.e., the contact resistivity grows with temperature as  $\sqrt{T}$ . It was shown in [10] that the above inequality is valid at the doping levels  $n_2 \gg 10^{15} \text{ cm}^{-3}$ .

At lower and intermediate doping levels,  $\left( \frac{L_D A^* T}{k\mu_n N_c} \right) \geq 1$ , and (as analysis shows) the degree of  $\rho_{c2}$  growth with temperature increases as compared with the law  $\sqrt{T}$ .

Fig. 18 presents the theoretical  $\rho_{c2}(T)$  curves built using Eq. (39) as well as low-temperature freezing-out of electrons. The doping level serves as a parameter of curves. At temperatures over 125 K, all the curves grow with temperature (see curves 1–3). For the curve 1 (that corresponds to the lowest doping level of  $10^{14} \text{ cm}^{-3}$ ), the exponent of the power dependence  $\rho_{c2}(T)$  at room and elevated temperatures is maximal (equal to 2). When the doping level increases, that exponent goes down: it equals 1.1 at  $n_2 = 10^{15} \text{ cm}^{-3}$  and 0.8 at  $n_2 = 10^{16} \text{ cm}^{-3}$ .

It should be noted that the above current mechanism (as well as that related to current flow through the metal shunts associated with dislocations – see [21, 22]) ensures purely ohmic contact behavior.

Shown in Fig. 19 are experimental  $\rho_c(T)$  dependences for Si samples with the doping step. The step was created by diffusion of phosphorus to the depth 0.2  $\mu\text{m}$ . The dependences were measured in two intervals: from helium temperatures 10 up to 300 K and from nitrogen temperatures 170 up to 300 K. The figure shows good consistence of experimental curves in  $T \geq 170$  K range. The theoretical curve is calculated by (40) taking into account freezing the carriers. There is a good coincidence of the theory with experiment. However, it should be noted that coincidence was achieved with  $1.6 \cdot 10^{13} \text{ cm}^{-3}$  bulk concentration, while initial doping was  $\sim 10^{15} \text{ cm}^{-3}$ . As we assume, almost 2 orders  $n_2$  decrease is due to silicon compensation in about micrometer layer by deep acceptors diffusion from the contact due to 450 °C heating.

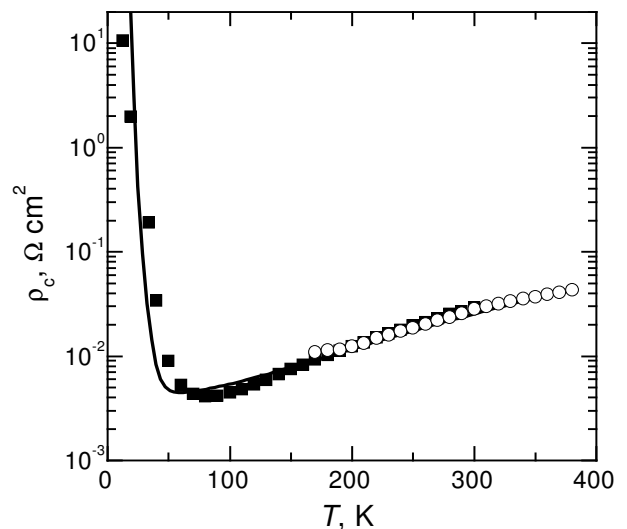


**Fig. 19.** Experimental (dots) and theoretical (solid lines)  $\rho_c(T)$  dependences for silicon with the doping step.

### 6.3. Conclusions

Thus, it has been shown (both theoretically and experimentally) for ohmic contacts formed to an  $n^+$ - $n$  doping step of silicon that, in the case of electron degeneracy in the  $n^+$ -layer and high-resistance  $n$ -Si bulk, the contact resistivity  $\rho_c$  increases with temperature ( $\sim T^2$ ) within the range 70–375 K.

## 7. On the ohmicity of Schottky contacts

### 7.1. Introduction

From the content of the fourth and fifth subsections of the present review it follows that a contact will be ohmic at current flow through metal shunts associated with dislocations as well as in the case of a doping step presence because there is an accumulation band bending at the metal–semiconductor interface or at the boundary between heavily and moderately doped semiconductors. And to realize ohmic contact in the case of Schottky contacts (with a depletion band bending at the metal–semiconductor interface), the criterion  $R_c < R_b$  has to be met ( $R_b$  is the resistance of semiconductor bulk). Therefore, it is necessary to specially study the problem of ohmic contact realization for Schottky contacts in which thermionic and thermal-field mechanisms of current flow take place. The results of this analysis for the case of silicon are given in the present subsection.

Until recently, three characteristic mechanisms of current flow through metal–semiconductor ohmic contacts were known: thermionic [81, 82], thermally-assisted field, and tunnel [19]. Gol'dberg *et al.* proposed another mechanism, which implies current flow through metal shunts matched with dislocations (see, *e.g.*, [10]). In [21, 22, 83], this mechanism was supplemented by considering the supply of the current flowing in the near-contact semiconductor region adjacent to the shunt ends. It was shown that, due to very small diameters of metal shunts, a very high electric field arises at their ends, due to which mirror-image forces change the sign of band bending at the semiconductor–shunt-end interface from depleting to enriching. This contact is ohmic at any temperatures, including those of liquid helium. General relations for the specific contact resistance of these contacts were derived in [21]. In the limiting case, where the current is restricted by the shunt resistance, the expressions reported in [19] are valid, whereas in another limiting case, where the current supply to the shunt ends is restricted, the relations given in [22, 83] hold true.

A model experiment for silicon–metal contacts with a previously ground surface was performed in [22, 83]. These contacts were shown to be ohmic, in contrast to silicon–metal contacts with a polished semiconductor surface. They are characterized by a high dislocation density, sufficient for implementing current flow through dislocations matched with metal shunts. The theoretical and experimental results were found to be in good agreement.

The question regarding the type of metal–semiconductor contact with a ground semiconductor surface has been analyzed for a fairly long time. For example, ohmic contacts were formed both on a ground silicon surface [84] and on the ground surface of other semiconductors [85–87]. Moreover, it is well known that a necessary component of the technology of forming ohmic contacts in structures for Si-based power electronic devices is preliminary grinding of the silicon surface [88, 89].

Attempts were made [11, 90, 91] to explain the obtained results by a high carrier-recombination rate at the metal–semiconductor interface. It was stated that the carrier concentration at the metal–semiconductor interface in these contacts is close to equilibrium, and near-contact SCR is lacking.

The influence of the surface recombination rate at the antibarrier rear contact of a  $p$ - $n$  junction on its current–voltage ( $I$ - $V$ ) characteristic was analyzed in [92–94], where the behavior of the contacts in structures with a  $p$ - $n$  junction rather than in Schottky contacts was considered.

In this paper, we report the following results. First, we derive general relations for the currents through a Schottky contact with a dielectric gap. Second, the criteria for Schottky-contact ohmicity are given. Third, we analyze the current flow through Schottky contacts within a generalized model and show that a small injection level, when the excess concentration of minority carriers (holes),  $\Delta p$ , is low in comparison with the equilibrium electron concentration ( $n_0$ ) in semiconductor, does not ensure (in contrast to a  $p$ - $n$  junction) ohmicity of Schottky contacts.

It is assumed that the criterion of the absence of current-induced heating the main charge carriers (electrons) is satisfied:  $E_b < kT / ql_p$ , where  $E_b$  is the electric field in the semiconductor bulk, and  $l_p$  – electron mean free path.

Hence, one can use Boltzmann statistics for electrons and holes with a temperature equal to the lattice temperature.

### 7.2. General expressions for the current of majority and minority carriers through the Schottky contact with a dielectric gap

Simulation of properties inherent to the antibarrier contact to a  $p$ - $n$  junction in [92–94] was performed using the following drain boundary condition for the minority-carrier (hole) current density in a lightly doped  $n$ -type region:

$$J_p = qS_k \Delta p(x = d), \quad (41)$$

where  $d$  is the thickness of this region. Moreover, it was supposed that  $S_k$ , which is the surface recombination rate in the contact plane  $x = d$ , can be arbitrarily high.

It should be noted that the relation (41) cannot be used to find the hole current density, because bands undergo bending in the  $x = d$  plane, whereas the drain boundary condition is valid only in the absence of band

bending, *i.e.*, in a plane spaced from the  $x = d$  plane at a distance equal to the SCR thickness  $w$  [95].

Then, instead of (41), one must use the following relation as a boundary condition:

$$J_p = qS_{eff}\Delta p(x = d - w), \quad (42)$$

where  $\Delta p(x = d - w)$  is the excess hole concentration in the  $x = d - w$  plane and  $S_{eff}$  – effective surface recombination rate in the  $x = d - w$  plane, which is limited by the minority carrier supply to the  $x = d$  plane and cannot be arbitrarily high [95].

The energy-band diagram of a forward-biased Schottky contact with a dielectric gap is shown in Fig. 20.

We will derive an expression for the minority-carrier current density through the Schottky contact with a dielectric gap proceeding from a more general boundary condition, assuming that the hole current flows through the semiconductor–insulator interface ( $x = 0$ ) with nonzero band bending (see Fig. 20). In this case, according to [95], the boundary condition for the minority-carrier current density can be written as

$$J_p = -q\vartheta_p \frac{V_p}{4}(p_c - p_{c0}), \quad (43)$$

where  $\vartheta_p$  is the transmission coefficient of the dielectric gap for holes,  $V_p$  – mean thermal hole velocity,  $m_p$  – hole effective mass, and  $p_c$  and  $p_{c0}$  are, respectively, the nonequilibrium and equilibrium hole concentrations at the semiconductor–insulator interface in the metal–semiconductor contact.

Double integration of the hole current continuity equations over the  $x$  coordinate (*i.e.*, in the direction perpendicular to the metal–semiconductor contact plane) in the nondegenerate case yields the following expression for the nonequilibrium hole concentration in near-contact SCR:

$$p(x) = e^{-y(x)} \left( p_w - \frac{J_{pc}}{qD_p} \int_w^x e^{y(x')} dx' \right), \quad (44)$$

where  $y(x) = q\varphi(x)/kT$  is the dimensionless electrostatic potential (band bending),  $p_w$  – nonequilibrium hole concentration at the boundary between SCR and quasi-neutral volume in the plane  $x = w$ , and  $D_p$  – hole diffusion coefficient.

The excess hole concentration at the SCR boundary  $x = w$   $\Delta p_w = p_w - p_0$ , can be found from the generation-recombination balance equation, which has the following form for thick (as compared with the diffusion length  $L_d$ ) semiconductor:

$$\frac{J_p}{q} = \left( S + \frac{D_p}{L_d} \right) \Delta p_w, \quad (45)$$

where  $S$  is the effective surface recombination rate in semiconductor in the plane  $x = w$ .

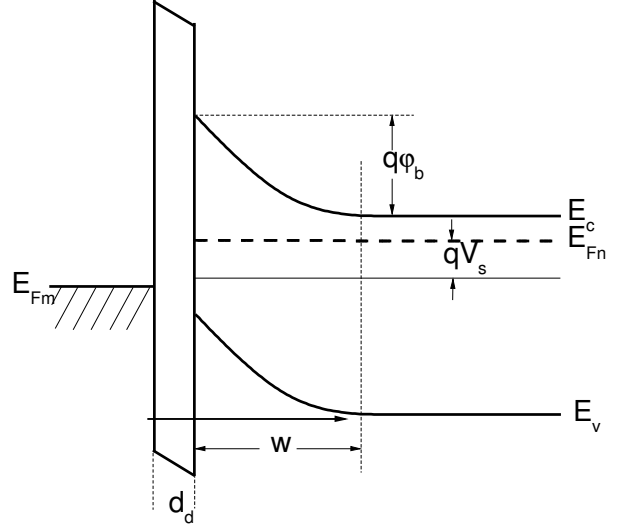


**Fig. 20.** Energy-band diagram of a Schottky contact with a dielectric gap:  $E_c$  is the bottom of the conduction band and  $E_v$  is the top of the valence band in semiconductor;  $E_{Fm}$  is the Fermi level in metal;  $E_{Fn}$  is the quasi-Fermi level for electrons in semiconductor;  $\varphi_b$  is the barrier height, counted from the bottom of the conduction band;  $d_d$  is the dielectric-gap thickness;  $w$  is the SCR thickness; and  $V_s$  the voltage drop in semiconductor.

Using Eq. (43), provided that the criterion  $L_d \gg L_D$  holds true ( $L_D$  is the Debye screening length), one arrives at the following expression for the hole current density:

$$J_p = \frac{qV_{pe}p_0(e^{qV_s/kT} - 1)}{1 + \frac{V_{pe}}{S + D_p/L_d}}. \quad (46)$$

Here,  $V_{pe} = \vartheta_p V_p$  is the effective hole emission rate from semiconductor to metal,  $p_0$  – equilibrium hole concentration in the neutral bulk,  $y_c$  – dimensionless nonequilibrium band bending at the interface  $x = 0$ , and  $V_s$  – part of the voltage  $V$  across the diode structure that drops in the semiconductor.

If the criterion

$$V_{pe} \gg S + \frac{D_p}{L_d} \quad (47)$$

is satisfied, the hole current density is

$$J_p = qp_0 \left( S + \frac{D_p}{L_d} \right) (e^{qV_s/kT} - 1). \quad (48)$$

This value corresponds to the current density through an asymmetric  $p$ - $n$  junction.

Similarly, one can calculate the electron current density  $J_n$ . If the electron current has a thermionic nature, and semiconductor is not degenerate, then, according to [95],

$$J_n = \frac{q}{4} \vartheta_n V_n (n_c - n_{c0}), \quad (49)$$

where  $\vartheta_n$  is the transmission coefficient of the dielectric gap for electrons,  $V_n$  – mean thermal electron velocity; and  $n_c$  and  $n_{c0}$  are, respectively, the nonequilibrium and equilibrium electron concentrations at the boundary  $x = 0$ .

Double integration of the electron-current continuity equations over coordinate  $x$  (*i.e.*, in the direction perpendicular to the metal–semiconductor contact plane) yields the following expression for the electron concentration in SCR:

$$n(x) = e^{y(x)} \left[ n_0 + \int_w^x \frac{e^{-y(x')}}{D_n} \frac{J_{nc}}{q} dx' \right]. \quad (50)$$

Here,  $D_n$  is the electron diffusion coefficient.

Let us introduce the value

$$V_{nr} = D_n e^{-y_c} \left/ \int_0^w e^{-y(x)} dx \right., \quad (51)$$

the physical meaning of which is the velocity of electrons passing through SCR of semiconductor.

When the electrostatic potential changes according to the Schottky law throughout the entire SCR,  $V_{nr}$  is equal to the electron drift velocity:  $V_{nr} = \mu_n E_c$ , where  $\mu_n$  is the electron mobility and  $E_c$  is the electric field in the contact plane.

Substituting (50) into (49) (at  $x = 0$ ), one obtains a relationship between the electron concentrations in the neutral bulk and at  $x = 0$ . The final expression for the electron current density through the contact, with allowance for (49), has the form

$$J_n = \frac{q}{4} \vartheta_n V_n n_0 \left( \frac{e^{y_c} - e^{y_{c0}}}{1 + \vartheta_n V_n / 4V_{nr}} \right), \quad (52)$$

where  $y_c = y_{c0} + \frac{qV_s}{kT}$ .

If the criterion  $\frac{1}{4} \vartheta_n V_n \ll V_{nr}$  is satisfied, electrons obey diode theory, and the expression for the electron current density is simplified and takes the form

$$J_n = \frac{q}{4} \vartheta_n V_n n_0 e^{y_{c0}} \left( e^{qV_s / kT} - 1 \right). \quad (53)$$

The  $\vartheta_p$  and  $\vartheta_n$  values will be considered below as parameters of the problem. When drawing plots, we will also assume that  $\vartheta_p = \vartheta_n$  and  $V_s \cong V$ . The latter condition means that the variation in the voltage drop across the insulator (under voltage  $V$  across the entire structure) can be neglected in comparison with a change in the voltage drop in the near-contact semiconductor region.

It was stated in [11, 90, 91], irrespectively of the structure type ( $p$ - $n$  junction or Schottky diode), that “recombination” ohmic contacts are contacts with a high carrier-recombination rate at the metal–semiconductor

interface. There are no objections that the so-called recombination contact to a  $p$ - $n$  junction at  $x = d$  can be antibarrier (*i.e.*, ohmic) [92, 93]. At the same time, we cannot agree that the “recombination” contact to a Schottky diode is also ohmic in the case of sufficiently high effective surface recombination rates  $S$ . The effective surface recombination rate  $S$  (see the expression (48)) may be rather high; however, it is limited, from above, by hole thermal velocity  $V_p$ . For the same reason, the condition  $p_c \cong p_{c0}$  cannot be implemented either when the nonequilibrium concentration of minority carriers is equal to the equilibrium concentration.

In other words, the conditions for Schottky-contact ohmicity do not correspond to those for the ohmicity of contacts to a  $p$ - $n$  junction. Therefore, we will analyze below the criteria for ohmicity to Schottky contacts.

### 7.3. Criteria for Schottky-contact ohmicity

Let us consider the case where the Schottky contact is based on a nondegenerate  $n$ -type semiconductor. First, we assume that the inequality  $J_n \gg J_p$  is satisfied. Then, the current through the contact is determined by the expression similar to (46), which can be written as

$$I_n = I_{ns} \left( \exp\left(\frac{qV}{kT}\right) - 1 \right), \quad (54)$$

where  $I_{ns} = \frac{q}{4} A \vartheta_n V_n n_0 \left/ \left( 1 + \vartheta_n V_n / 4V_{nr} \right) \right.$ ,  $A$  is the contact area,  $n_{c0} = n_0 \exp\left(-\frac{q\Phi_b}{kT}\right)$ , and  $\Phi_b$  – electrostatic potential at the semiconductor–insulator interface, counted from the bottom of the conduction band of semiconductor.

According to [19], the contact resistance is

$$R_c = \left( \frac{dI_n}{dV} \right)_{V=0}^{-1}. \quad (55)$$

Substitution of (48) into (49) yields

$$R_c = \frac{kT}{q} \frac{1}{I_s}. \quad (56)$$

Let us now derive a criterion for Schottky-contact ohmicity in the case under consideration. To this end, we will write an expression for the current taking into account the bulk resistance  $R_b = \rho d / A$  ( $\rho$  and  $d$  are, respectively, the semiconductor resistivity and thickness):

$$I_n = I_s \left( \exp\left(\frac{q(V - IR_b)}{kT}\right) - 1 \right) \quad (57)$$

Expression (57) can be rewritten in the form

$$I = \frac{V}{R_b} - \frac{kT}{qR_b} \ln \left( 1 + \frac{I}{I_s} \right). \quad (58)$$

At  $III_s \ll 1$ , Eq. (58) can be reduced (taking into account (54)) to the form

$$I = \frac{V}{R_b} - I \frac{R_c}{R_b}. \quad (59)$$

Thus, as follows from (59), the criterion for Schottky-contact ohmicity is the inequality  $R_c \ll R_b$ ; i.e., in this case the contact resistance must be much lower than the bulk one. This criterion, in particular, coincides with the criterion reported in the monograph [3].

The same criterion for Schottky-contact ohmicity was obtained in [96] for the case where the main carrier current through a Schottky contact is defined by the thermally-assisted field current. The aforementioned situation can be implemented at sufficiently large  $\phi_b$  values and (or) at fairly low temperatures.

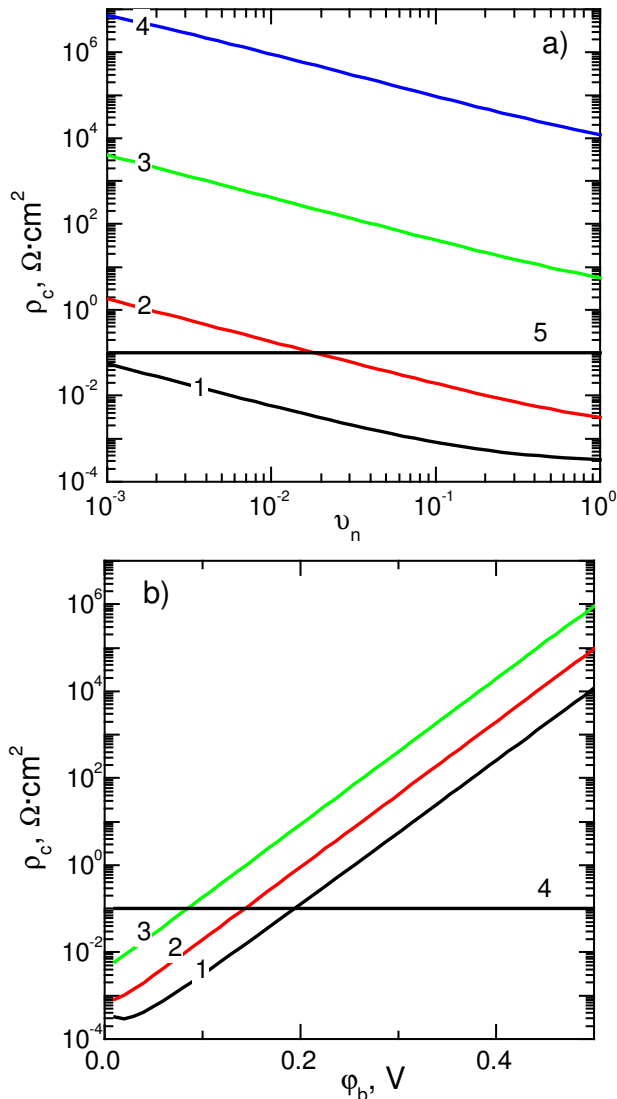


**Fig. 21.** Dependences of the specific contact resistance  $\rho_c$  on (a) the transmission coefficient  $\Delta n$  of the dielectric gap for electrons ( $\phi_b = 0.01$  (1), 0.1 (2), 0.3 (3), and 0.5 V (4)) and (b) barrier height  $\phi_b$  ( $v_n = 1$  (1),  $10^{-1}$  (2), and  $10^{-2}$  (3)). The horizontal lines (5 in panel (a) and 4 in panel (b)) indicate the  $AR_b$  value.

Fig. 21a shows the dependences of  $\rho_c = AR_c$  on the dielectric-gap transmission coefficient  $\vartheta_n$  (for the parameters of silicon). The curve parameter is the barrier height  $\phi_b$ . The plots in Fig. 21 were constructed using the assumption that  $A = 1 \text{ cm}^2$ .

We note that the specific contact resistance  $\rho_c$  and contact resistance  $R_c$  are numerically equal for this  $A$  value. The currents and current densities are also numerically equal. The figure shows that the criterion for Schottky-contact ohmicity with the parameters of silicon in use can be satisfied only at  $\phi \leq 0.1 \text{ V}$  for a sufficiently large electron transmission coefficient  $\vartheta_n$  of the dielectric gap. When constructing plots in this and subsequent figures, it was also assumed that  $n_0 = 10^{15} \text{ cm}^{-3}$ ,  $S = 10^5 \text{ cm/s}$ ,  $d = 220 \text{ }\mu\text{m}$ , and  $T = 300 \text{ K}$ .

Fig. 20b shows the dependences of  $\rho_c$  on  $\phi_b$ . The curve parameter is the  $\vartheta_n$  value. It can be seen that the  $\phi_b$  values, at which the criterion for Schottky-contact ohmicity is satisfied, decrease with a decrease in the  $\vartheta_n$  value. It should be noted that the decrease in the gap transmission coefficient  $\vartheta_n$  is equivalent to an increase in barrier height  $\phi_b$ . The criterion for contact ohmicity may be invalid even at small  $\phi_b$  values (Fig. 21a, curve 2). This circumstance must be taken into account when analyzing experimental  $I$ - $V$  characteristics.

#### 7.4. Analysis of currents through the Schottky contacts with allowance for the minority-carrier current

It was stated in [92-94] that a contact is ohmic, when a low injection level is implemented; i.e., when the criterion  $\Delta p \ll n_0$  is satisfied. Below, we will show that this statement is invalid for Schottky contacts.

When a voltage drop in the insulator can be neglected, the expression for the excess hole concentration  $\Delta p$  takes the form

$$\Delta p = \frac{p_0 V_{pe}}{V_{pe} + S + D_p / L_d} \left[ \exp\left(\frac{q(V - IR_b)}{kT}\right) - 1 \right]. \quad (60)$$

In this case,  $\Delta p = \Delta p_w$ , which follows from the condition of constancy of the quasi-Fermi level for holes in near-contact SCR.

Let us now consider the case where the total current  $I$  through the Schottky contact is the sum of electron and hole currents; i.e.,  $I = I_n + I_p$ , where  $I_n = AJ_n$  and  $I_p = AJ_p$ , and the  $J_n$  and  $J_p$  values are determined by the expressions (51) and (45), respectively. As previously, we assume that the voltage drop in insulator can be neglected in comparison with the voltage drop in semiconductor. Then, the total current through the Schottky contact can be written as

$$I = (I_{ns} + qAp_0(S + D_p / L)) \left( \exp\left(\frac{q(V - IR_b)}{kT}\right) - 1 \right). \quad (61)$$

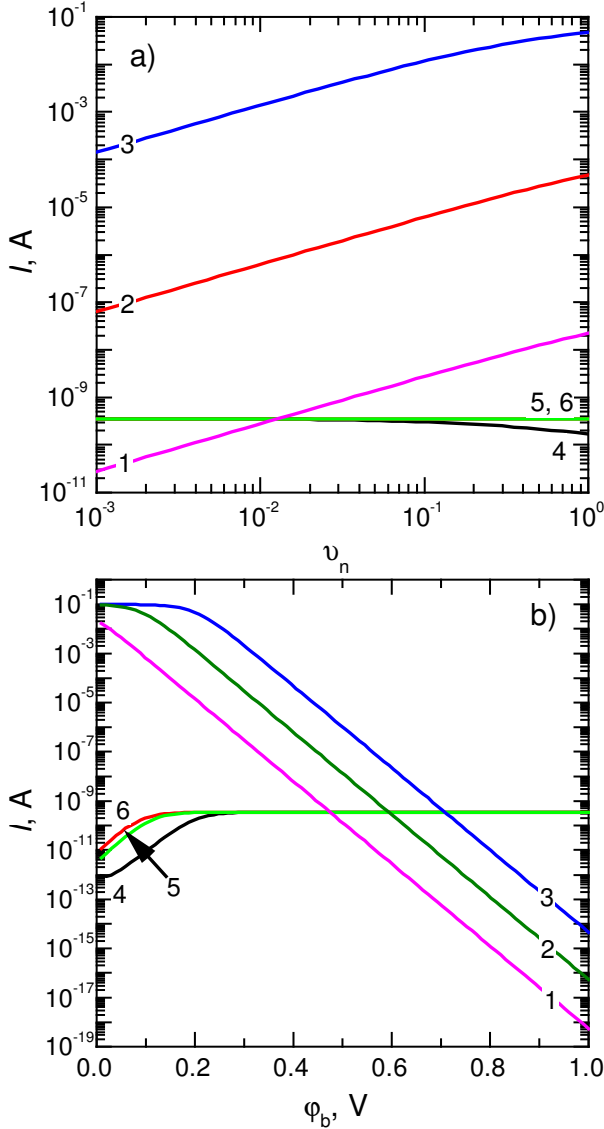


**Fig. 22.** Dependences of the (1–3) electron and (4–6) hole currents on (a) the dielectric-gap transmission coefficient  $\Delta n$  ( $\varphi_b = 0.2$  (1, 4), 0.4 (2, 5), and 0.6 V (3, 6)) and (b) barrier height ( $\Delta n = 10^{-4}$  (1, 4),  $10^{-2}$  (2, 5), and 1 (3, 6)).

Fig. 22a shows the dependences of electron current  $I_n$  and hole current  $I_p$  (which are proportional, respectively, to the first and second additives in round parentheses in (61)) on the dielectric-gap transmission coefficient for electrons,  $\vartheta_n$ , and (equal to it) gap transmission coefficient for holes,  $\vartheta_p$ . The plots in this and subsequent figures were constructed using the assumption that the diffusion length  $L_d$  is 100  $\mu\text{m}$ . This a typical value for silicon in terms of the order of magnitude [97]. The curve parameter is  $\varphi_b$ . It can be seen that for all  $\varphi_b$  values used to construct these plots (except for  $\varphi_b = 0.2$  V), the hole current density is constant and depends neither on the gap transmission coefficient nor on the  $\varphi_b$  value. However, a decrease in  $\vartheta_n$  leads to a significant decrease in  $I_n$ . As a result, the hole current may exceed the electron current at small  $\vartheta_n$  values. When  $I_p > I_n$ , the Schottky contact behaves as a  $p$ - $n$

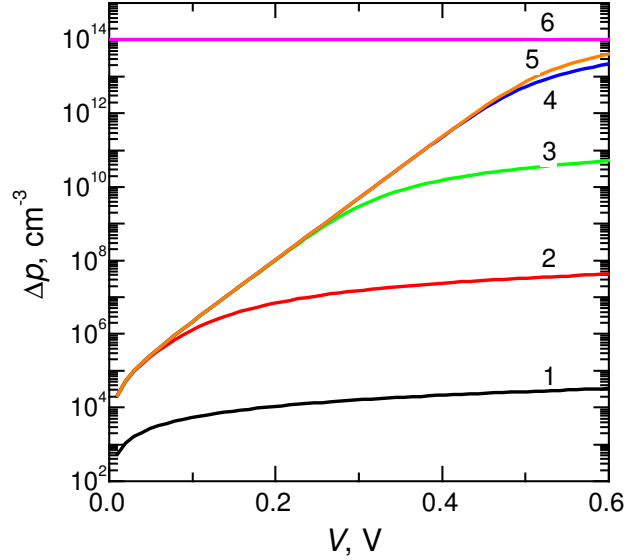


**Fig. 23.** Dependences of the excess hole concentration on the applied voltage for  $\varphi_b = 0.1$  (1), 0.3 (2), 0.5 (3), 0.7 (4), and 0.9 V (5). The horizontal line (6) indicates  $\Delta n$ .

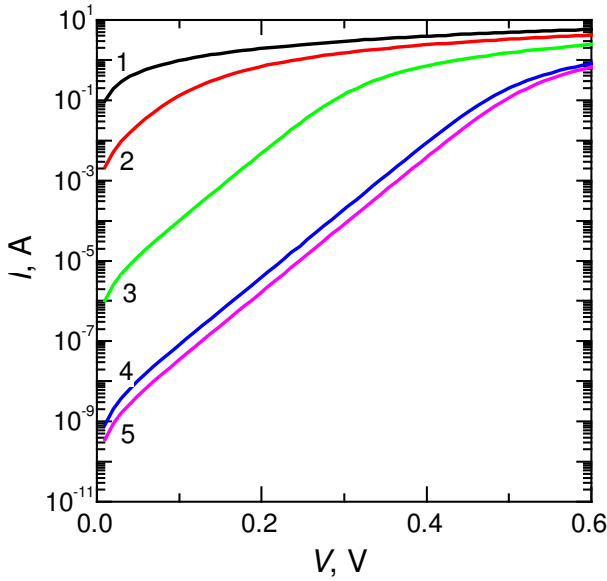
junction, whereas at  $I_p < I_n$  its behavior is classical. A decrease in  $\vartheta_n$  leads to a decrease in the  $\varphi_b$  values, at which the condition  $I_p > I_n$  is satisfied. We note that, when  $\vartheta_n = 1$ , the condition  $I_p \geq I_n$  (for the parameter values in use) is implemented if  $\varphi_b \geq 0.71$  V.

Fig. 22b shows the dependences of the electron current  $I_n$  and hole current  $I_p$  on  $\varphi_b$ . The curve parameters for  $I_n$  and  $I_p$  are, respectively, the  $\vartheta_n$  and  $\vartheta_p$  values, which were assumed to be equal when constructing the plots. For the  $\vartheta_p$  values in use, the hole current  $I_p$  is independent of  $\vartheta_p$  and  $\varphi_b$ , beginning with  $\varphi_b > 0.2$  V. At  $\varphi_b \leq 0.2$  V, the  $I_p$  value decreases with a reduction in  $\varphi_b$ . This decrease is related to the violation of criterion (47), due to which the Schottky contact does not transmit entirely the injected hole current.

Fig. 23 presents the dependences of the excess hole concentration  $\Delta p$  on applied voltage  $V$ , which were calculated using the formula (60). The curve parameter is  $\varphi_b$ .

Finally, Fig. 24 shows the dependences of the total current through the Schottky contact on the applied voltage, calculated using the formula (61). As in Fig. 23, the curve parameter is  $\varphi_b$ .

We note that the curves in both Figs. 23 and 24 were plotted for the case where  $\vartheta_p = \vartheta_n = 1$ . As can be seen in Fig. 24, for the parameter values in use, the condition  $\Delta p < n_0$  is satisfied for all  $\varphi_b$  values; *i.e.*, the injection level is low. At the same time, as it follows from Fig. 24, all curves exhibit a pronounced portion of exponential dependence of the current on applied voltage at  $\varphi_b \geq 0.3$  V. This fact indicates that, in the case of Schottky contacts, implementation of a low injection level, in contrast to the cases considered in [92–94], is not sufficient to provide contact ohmicity. The choice of  $n_0$  value equal to  $10^{15}$   $\text{cm}^{-3}$  is due, on the one hand, to the



**Fig. 24.** Dependences of the current through the contact on the applied voltage at  $\phi_b = 0.1$  (1), 0.3 (2), 0.5 (3), 0.7 (4), and 0.9 V (5).

fact that in this case the inequality  $I_p > I_n$  is satisfied at attainable  $\phi_b$  values for silicon, whereas at  $n_0 \geq 10^{16} \text{ cm}^{-3}$  the electron current dominates at all attainable  $\phi_b$  values. On the other hand, the value  $n_0 = 10^{15} \text{ cm}^{-3}$  is typical (on the order of magnitude) for silicon solar cells and some Si-based transistor structures [97, 98]. It should be also noted that, despite the fact that a highly degenerate near-contact layer provides contact ohmicity in the majority of cases, the specific contact resistance is generally determined by the high-resistivity region and can be fairly high [26].

### 7.5. Results and discussion

The current through a metal–semiconductor contact depends on the effective surface recombination rate only when the minority-carrier current exceeds the majority-carrier current; to this end, the Schottky contact should behave as a  $p$ - $n$  junction. This may occur only at large barrier heights. However, the contact resistance also becomes high in this case, and the condition for contact ohmicity,  $R_c \ll R_b$ , is not satisfied. Correspondingly, the contact is non-ohmic.

Although the nonequilibrium carrier concentration at the contact is close to equilibrium in this case, the band bending at the semiconductor–insulator interface is nonzero (which contradicts the statements of [11, 90, 91]). Analysis shows that, under a forward bias  $V$ , the applied voltage first drops at near-contact SCR. The  $I$ - $V$  characteristic of the contact is rectifying. Obviously, SCR will exist at  $V \leq \phi_b$ .

Concerning the strong effect of the surface recombination rate  $S$ , which leads to a decrease in  $\Delta p$ , it is not so strong in reality. With allowance for the fact that  $S \leq V_p \approx 10^7 \text{ cm/s}$  [98], estimates show that, even at  $S \approx 10^7 \text{ cm/s}$ ,  $\Delta p$  is about  $10^{12} \text{ cm}^{-3}$ , provided that  $J_p = J_n$  and  $V = 0.6 \text{ V}$ , whereas  $p_0 \approx 10^5 \text{ cm}^{-3}$ . Thus, the excess hole concentration in the  $x = w$  plane exceeds the equilibrium

concentration by several orders of magnitude in this case. Recalculation of the hole recombination rate in the  $x = w$  plane, equal to  $S$ , to the value in the contact plane yields a value of  $V_p/4$  (at  $\vartheta_p = 1$ ). Therefore, the  $S_{eff}$  value, determined using the relation of the (1b) type, cannot be let to run to infinity.

We note that the thermionic current of majority carriers is independent of the recombination characteristics, in particular, surface recombination. A similar dependence is also lacking for the thermally-assisted field and tunnel currents. This dependence exists for only  $p$ - $n$  junctions.

Our analysis was limited to the consideration of only the thermionic current of majority carriers in the Schottky contacts. It should be noted that the situation will not change radically when passing to the thermally-assisted field mechanism of majority-carrier current in the Schottky contacts. A radical change occurs when the tunnel mechanism of current transport dominates in the Schottky contact. In this case, the semiconductor bulk is degenerate (the degree of degeneracy increases with an increase in the doping level). Therefore, the effective barrier height, counted from the Fermi level in semiconductor, decreases with an increase in the doping level. The barrier thickness also decreases under these conditions, due to which barrier transparency increases. Correspondingly, the contact resistance decreases as well, and the contact behaves as the ohmic one.

As follows from the results obtained, the larger the dielectric-gap transmission coefficient for electrons,  $\vartheta_n$ , the better the condition for Schottky-contact ohmicity ( $R_c \ll R_b$ ) is satisfied. Since  $\vartheta_n \propto \exp(-\alpha d_d)$  [98], where  $\alpha$  is a constant and  $d_d$  is the dielectric-gap thickness, minimum possible  $d_d$  values must be implemented to increase  $\vartheta_n$ . The  $\alpha$  value, in turn, depends on the insulator band gap  $E_d$ : it increases with an increase in  $E_d$  and decreases when  $E_d$  decreases. In the case of Si-based Schottky contacts, the  $E_d$  value is determined by the degree of stoichiometry of the  $\text{SiO}_x$  oxide. The smaller the  $x$  value in comparison with 2, the smaller the  $E_d$  value is and, correspondingly, the smaller the  $\alpha$  value is.

Let us now discuss the approximation  $\vartheta_n = \vartheta_p$ , which was used in our analysis. In general, this equality is invalid. However, when the barrier height  $\phi_b$  is sufficiently large ( $>0.3 \text{ V}$ ), the hole current, at parameter values used in the calculation, is defined by the expression (48) and is independent of the dielectric-gap transmission coefficient for holes,  $\vartheta_p$ , when the latter changes by several orders of magnitude. It, all the more, occurs when the inequality  $I_p > I_n$  is satisfied; *i.e.*, when a  $p$ - $n$  junction is implemented, because in this case the  $\phi_b$  value is even larger. However, if the criterion (47) is violated, the hole current is proportional to  $\vartheta_p$ .

A Schottky contact is implemented at smaller  $\phi_b$  values, because  $I_n \gg I_p$ . In this case, the electron current  $I_p$  is proportional to  $\Delta n$ . The error introduced by the

replacement of  $\vartheta_p$  with  $\Delta n$  in the calculation of  $I_p$ , although leading to an incorrect  $I_p$  value, will barely affect the value of the total current  $I$ .

## 7.6. Conclusions

Thus, based on the results of our analysis and taking into account the data of [10, 21-23], we can draw the following conclusions.

(i) A Schottky contact is ohmic when the inequality  $R_c \ll R_b$  holds true. The smaller the transmission coefficient  $\vartheta_n$  for majority carriers in the Schottky contact, the worse the condition for contact ohmicity is satisfied. Calculations showed that Si-based Schottky contacts are ohmic at temperatures of  $\geq 300$  K, if the barrier height (counted from the bottom of the conduction band) is  $\leq 0.1$  V and the  $\vartheta_n$  value is close to unity.

(ii) The condition of injection-level smallness ( $\Delta p < n_0$ ) does not provide Schottky-contact ohmicity.

(iii) The “recombination” Schottky contacts (*i.e.*, the contacts in which the minority-carrier current dominates) are rectifying at any attainable values of the recombination rate  $S$ .

(iv) The explanation of formation of an ohmic contact after grinding the semiconductor surface is beyond the scope of the model under consideration. This effect can be understood only within the concepts developed in [10, 21-23].

## 8. A new mechanism for realization of ohmic contacts

### 8.1. Introduction

Fabrication of ohmic contacts was for a long time associated with great difficulties, and the mechanisms of their formation are being refined even now. In this study, the analysis of one mechanism promoting realization of ohmic contacts is performed. This mechanism includes incomplete charge screening by surface states at a high doping level. We speak about a metal–semiconductor contact with a dielectric gap. To date, the analysis of current-flow mechanisms in this contact has been performed only under the assumption that the distribution law of surface states along the coordinate perpendicular to the surface is described by the  $\delta$ -function [19]. At the same time, it is known that the concentration of surface states lowers when moving into the semiconductor depth according to an exponential law with the characteristic damping parameter  $l_s$  [7, 99]. According to the data [100, 101], a typical value of  $l_s$  for such semiconductors as Si and GaAs is  $10^{-7}$  cm. Therefore, when the SCR thickness  $w$  becomes by the order or smaller than  $l_s$ , it should be noted that approximation of the  $\delta$ -function will be invalid, and the Poisson equation should be solved taking into account the distribution of surface states along the coordinate  $x$ . We solved the problem in this study precisely in this approximation.

### 8.2. Problem statement

In the case when inequality  $\varphi_c > E_F/q$ , where  $\varphi_c$  is the barrier height and  $E_F$  – Fermi energy, is fulfilled at high semiconductor doping levels, in the presence of an insulating interlayer, the magnitude of the contact barrier is determined by solving the integral neutrality equation taking into account charges accumulated in metal, at surface states, and in semiconductor, which has the form

$$\frac{\varepsilon_0 \varepsilon_d kT}{q^2 d} \left( \frac{\varphi_{ms}}{kT} - y_c \right) - N_{sd} (1 - f_d(E)) + N_{sa} f_a(E) - \frac{\varepsilon_0 \varepsilon_s kT}{q^2 L_D} (y_c)^{0.5} = 0. \quad (62)$$

Here,  $\varepsilon_d$  is the dielectric constant of the insulator,  $d$  – thickness,  $\varphi_{ms}$  – contact potential difference between metal and semiconductor,  $y_c = q\varphi_c/kT$ ,  $f(E_i) = [1 + \exp(E_i/kT - y_c - N_d/n_i(E_g))]^{-1}$  – Fermi distribution in the equilibrium case for a surface level with the energy  $E_i$ . This energy is counted from the band gap middle of semiconductor at the interface with insulator,  $N_d$  – donor concentration,  $n_i(E_g)$  – charge-carrier concentration in the intrinsic semiconductor, the magnitude of  $\varphi_c$  is counted from the conduction-band bottom in the neutral bulk, and other notations are generally accepted. It is assumed in expression (1) that discrete surface levels are arranged at the interface between the semiconductor and insulator; it is also assumed that the distribution of charges localized at surface states can be described by the  $\delta$ -function. It means that the thickness of the localization region of surface states  $l_s$  is considerably smaller than the SCR thickness  $w$ , where  $w = 2L_D(y_c)^{0.5}$ . This condition is

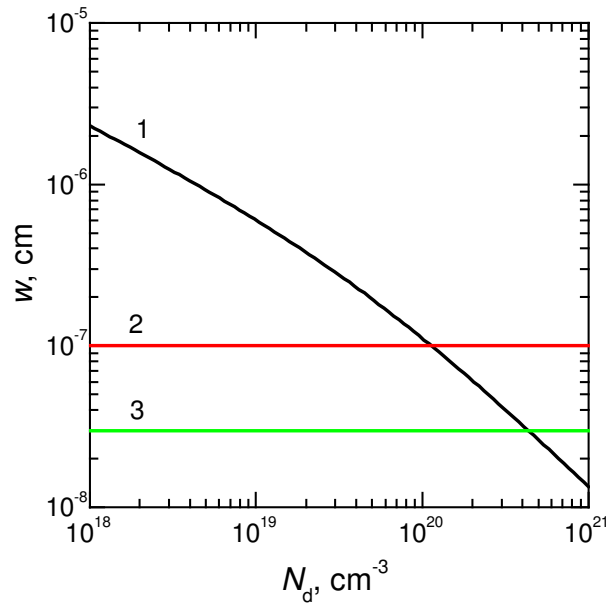


Fig. 25. Dependence of the thickness of space charge region in Si on the doping level  $N_d$ .

fulfilled in the region of low doping levels. However, the calculation shows that this inequality is violated at high doping levels. Fig. 25 shows the dependences of  $w$  on the doping level plotted for parameters of Si, when the effective density of states in the conduction band  $N_c = 2.8 \cdot 10^{19} \text{ cm}^{-3}$ ,  $\varphi_{ms} = 0.5 \text{ V}$ ,  $\varepsilon_s = 11.7$ ,  $d = 4 \cdot 10^{-8} \text{ cm}$ , and  $\varepsilon_d = 2$  [19]. Herewith, we considered for simplicity that only acceptor surface states with the concentration  $N_{sa} = 2.7 \cdot 10^{13} \text{ cm}^{-2}$  are present in semiconductor. We note that according to the data [19], a high peak of the density of states with an energy higher than the valence-band edge by 1/3 of the bandgap width is present in most covalent semiconductors.

According to this fact, we accepted that  $E_a = -0.23 \text{ eV}$  in the case of Si. We note that this approach can be used in the case of not only discrete surface levels but surface zones as well. The authors of [102] showed that the energy characteristics of surface states, which comprise the surface zones, could be described by efficient surface levels in most cases. It is seen from Fig. 25 (curve 1) that inequality  $w \ll l_s$  is fulfilled in a region of moderate doping levels, and we can assume in the calculations that the distribution of surface states is described well by the  $\delta$ -function. However, the SCR thickness becomes smaller than  $l_s$  at  $N_d > 1.42 \cdot 10^{20} \text{ cm}^{-3}$ . It is noteworthy that the curves 2 and 3 in Fig. 25 correspond to the characteristic thicknesses of the localization regions of surface states, which equal  $10^{-7}$  and  $3 \cdot 10^{-8} \text{ cm}$ . In this case, the distribution of charges localized at surface states cannot be described by the  $\delta$ -function but should be determined from solution of the Poisson equation. According to the data [103], surface states on the actual surfaces of semiconductor appear because of the presence of defects or foreign atoms. According to [99], the wave function of the ground state of an electron center localized on a semiconductor surface can be written in the form  $\psi(x) = Ax \exp(-x/l_{s1})$ . Taking into account normalization of the wave function, the distribution of surface states along the coordinate  $x$  and their filling with electrons is described by the law

$$\begin{aligned} N_s(x) &= \frac{4N_{sa}}{l_{s1}^3} f(E_a, x) x^2 \exp\left(-\frac{2x}{l_{s1}}\right) = \\ &= \frac{N_{sa}}{2l_s^3} f(E_a, x) x^2 \exp\left(-\frac{x}{l_s}\right), \end{aligned} \quad (63)$$

where

$$\begin{aligned} f(E_a, x) &= \left[1 + \exp\left(E_a/kT - y(x) - N_d/n_i(E_g)\right)\right]^{-1}, \\ y(x) &= q\varphi(x)/kT, \text{ and } \varphi(x) \text{ is the dependence of the} \\ &\text{dimensionless electrostatic potential on the coordinate } x. \end{aligned}$$

The authors of [100, 101] assumed that the spatial dependence of the distribution of surface states along the coordinate  $x$  has the form  $\exp\left(-\frac{x}{l_s}\right)$ . Taking into account the function of surface state population with electrons,

$$N_s(x) = \frac{N_{sa}}{l_s} f(E_a, x) \exp\left(-\frac{x}{l_s}\right). \quad (64)$$

In the cases under consideration, we can derive an expression for  $\varphi_c$  by solving the Poisson equation for semiconductor, taking into account the charge of surface states. Using the conditions: (a) equality of electric biases at the surface of semiconductor and insulator, (b) continuity of the potentials, and (c) reducing the electric field and electrostatic potential to zero, we derive a set of two equations for finding quantities  $w$  and  $\varphi_c$ . Let us limit ourselves by consideration of the case of absence of charge-carrier degeneracy in semiconductor. Herewith, the following equations are valid for the SCR thickness  $w$  and barrier height  $\varphi_c$ .

$$\begin{aligned} \varphi_{ms} - \frac{q}{\varepsilon_0 \varepsilon_s} N_d w \left( \frac{w}{2} + \frac{\varepsilon_s d}{\varepsilon_d} \right) + \frac{q}{\varepsilon_0 \varepsilon_s} \left( w + \frac{\varepsilon_s d}{\varepsilon_d} \right) \times \\ \times \int_0^w N_s(x) dx - \frac{q}{\varepsilon_0 \varepsilon_s} \int_0^w \int_0^x N_s(x') dx' dx = 0, \end{aligned} \quad (65)$$

$$\varphi_c = \varphi_{ms} - \frac{qd}{\varepsilon_0 \varepsilon_d} \left( N_d w - \int_0^w N_s(x) dx \right). \quad (66)$$

### 8.3. Analysis of results

It is seen from expressions (63)–(65) that, in general, when solving the Poisson equation, it is necessary to take into account not only the spatial distribution of the density of surface states, but the dependence of their degree of population on the coordinate  $x$  as well. The analysis shows that the contact potential  $\varphi$  initially increases with increasing  $N_d$ , then passes through a

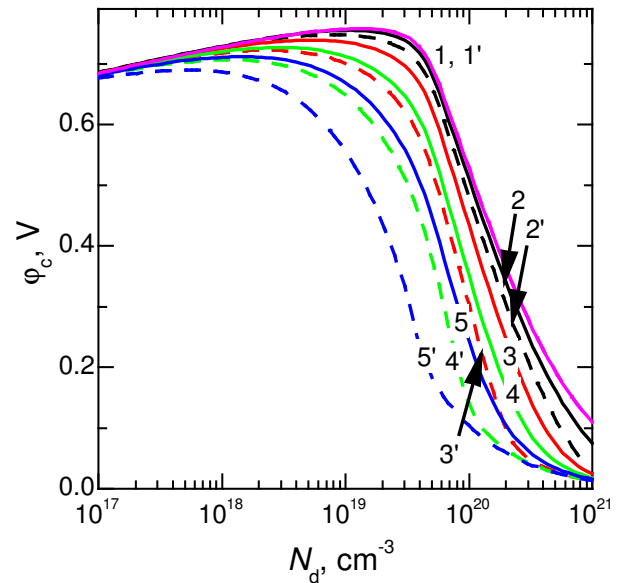


**Fig. 26.** Dependence of the barrier height  $\varphi_c$  on the doping level  $N_d$  at  $\varphi_{ms} = 0.5 \text{ V}$ . The used parameter  $l_s$ , cm:  $10^{-8}$  (2, 2'),  $5 \cdot 10^{-8}$  (3, 3'),  $1 \cdot 10^{-7}$  (4, 4') and  $2 \cdot 10^{-7}$  (5, 5'). Curve 1 is found when realizing Eq. (62).

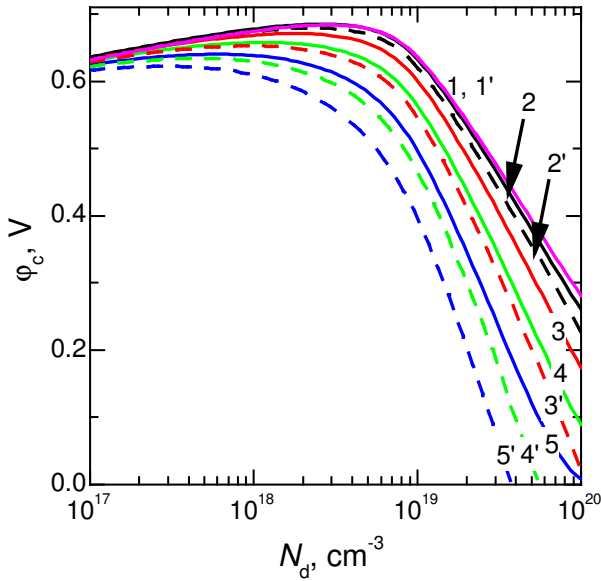


**Fig. 27.** Dependence of the barrier height  $\phi_c$  on the doping level  $N_d$  at  $\phi_{ms} = 0$  V. The used parameter  $l_s$ , cm:  $10^{-8}$  (2, 2'),  $5 \cdot 10^{-8}$  (3, 3'),  $1 \cdot 10^{-7}$  (4, 4') and  $2 \cdot 10^{-7}$  (5, 5'). Curve 1 is found when realizing Eq. (62).

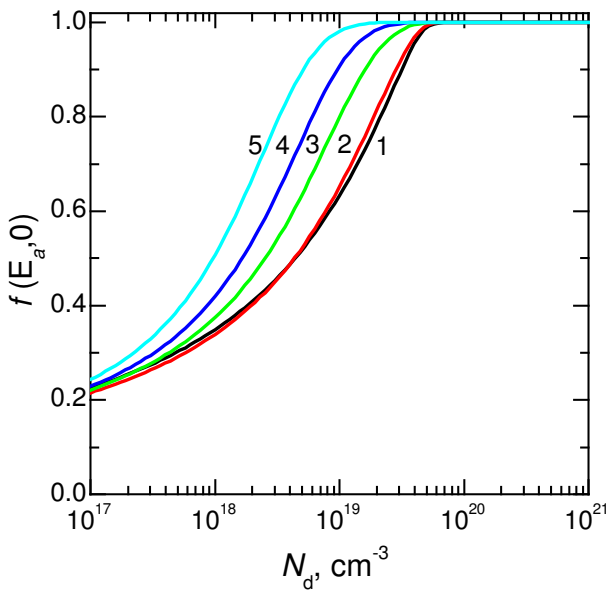


**Fig. 28.** Dependence of the degree of filling of the surface level  $f(E_a, 0)$  with an energy of  $-0.23$  eV on the doping level  $N_d$  at  $\phi_{ms} = 0.5$  V. The used parameter  $l_s$ , cm:  $10^{-8}$  (2, 2'),  $5 \cdot 10^{-8}$  (3, 3'),  $1 \cdot 10^{-7}$  (4, 4') and  $2 \cdot 10^{-7}$  (5, 5'). Curve 1 is found when Eq. (62) is valid.

maximum, and then decreases (Figs. 26 and 27). If the following criteria are fulfilled: (i)  $w \ll l_s$  and (ii)  $f(E_a, 0) \cong 1$  at  $w \leq l_s$ , when solving Eqs. (65) and (66), we can neglect the dependence of  $f(E_a, x)$  on the coordinate  $x$ . Fulfillment of the criterion (i) means that approximation of the  $\delta$ -function is valid for the distribution of surface states, while fulfillment of the criterion (ii) evidences that if the surface layer is completely filled at  $x = 0$ , it will also be completely filled at  $x \neq 0$ .

Estimations show that, at the parameters used for calculation, the criterion (i) is fulfilled at  $2 \cdot 10^{18} \text{ cm}^{-3}$ , while the criterion (ii) is fulfilled in the  $N_d$  range from  $1 \cdot 10^{19}$  up to  $5 \cdot 10^{19} \text{ cm}^{-3}$  depending on the magnitude of  $l_s$ . It is seen from Fig. 28, in which the dependences of the degree of filling of the surface layer with the energy  $-0.23$  eV on the doping level  $N_d$  are presented. At intermediate values of  $N_d$ , we should take into account both the dispersion of the density of surface states and the dependence of filling the density of surface states on the coordinate  $x$ . However, taking into account the spread of the density of surface states turns out to be more substantial in calculation. Figs. 26 and 27 show the dependences of the contact potential  $\phi_c$  on the doping level of semiconductor for Si, which were found using Eq. (62) (curve 1), and the dependences derived including the charge of surface states into the Poisson equation, when using relationships (63)–(66). When plotting Fig. 26, we assumed that the contact potential difference was  $\phi_{ms} = 0.5$  V, while when plotting Fig. 27, we assumed  $\phi_{ms}$  was equal to zero. When calculating Figs. 26 and 27 as well as subsequent ones, we assumed that the values of  $l_s$  were equal to  $10^{-8}$ ,  $5 \cdot 10^{-8}$ ,  $10^{-7}$ , and  $2 \cdot 10^{-7}$  cm, respectively. Curves 2 to 5 that were plotted when using the law (64), are solid, while the curves 2' to 5' that are valid for realization of (63), are dashed. It is seen from Figs. 26 and 27 that the dependences  $\phi_c(N_d)$ , which are presented by the curves 3–5 and 3'–5', descend with increasing  $N_d$  from  $10^{17}$  to  $10^{21} \text{ cm}^{-3}$  more rapidly than the dependence presented in curve 1. At the same time, the dependences presented by the curves 2 and 2' for the case when  $l_s = 10^{-8}$  cm are rather close or coincide with the dependences presented by the curve 1. It is seen from Fig. 26 that the value of  $\phi_c$  for the curve 5 is 0.1 V at  $N_d = 10^{20} \text{ cm}^{-3}$ , while the value of  $\phi_c$  found in the  $\delta$ -function approximation is 0.53 V. The difference between the values of  $\phi_c$  found in the  $\delta$ -function approximation and when using the expression (63) is even larger in the case when  $\phi_{ms} = 0$  V, *i.e.*, the work functions for metal and Si are equal to one another (Fig. 27). It should be noted that the largest decrease in the barrier height  $\phi_c$ , as compared with the case when the  $\delta$ -function approximation is used, occurs in the region  $N_d > 10^{19} \text{ cm}^{-3}$ , when the degree of filling of surface states with electrons is close or equal to unity.

We note that a larger decrease in the contact potential for the curves 3–5 and 3'–5' presented in Figs. 26 and 27 in fact means that the efficient density of surface states participating in charge screening decreases. It is illustrated by Figs. 29 and 30 that represent the dependences

$$N_s^* = \int_0^w N_s(x) dx. \quad (67)$$

When plotting Figs. 29 and 30, we used the same values of  $l_s$  as when plotting Figs. 26 and 27. It is seen from Figs. 29 and 30 that the efficient density of surface states participating in charge screening can significantly decrease in the region of rather high doping levels (more than by an order of magnitude).

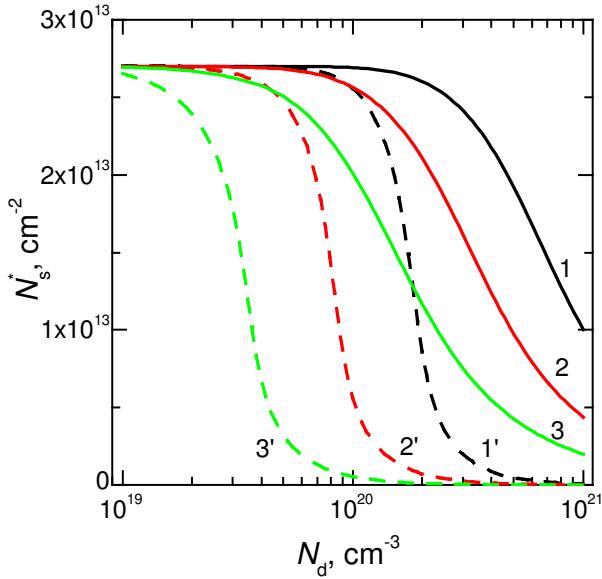


**Fig. 29.** Dependences of the efficient density of surface states  $N_s^*$  on the doping level  $N_d$  at  $\varphi_{ms} = 0.5$  V. The used parameter  $l_s$ , cm:  $10^{-8}$  (2, 2'),  $5 \cdot 10^{-8}$  (3, 3'),  $1 \cdot 10^{-7}$  (4, 4') and  $2 \cdot 10^{-7}$  (5, 5').

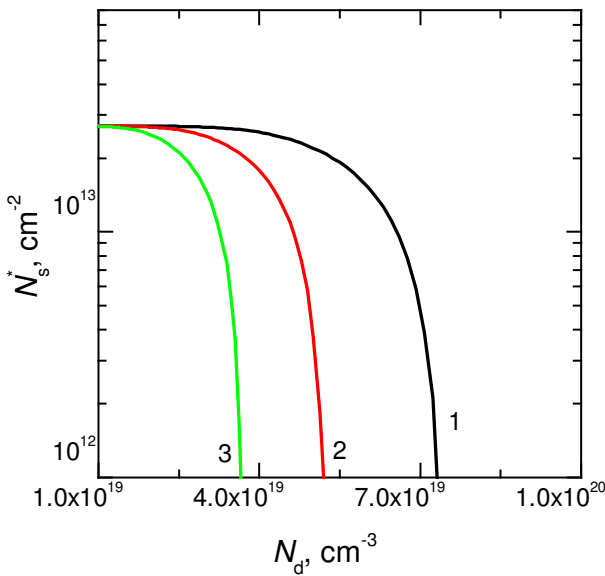


**Fig. 30.** Dependences of the efficient density of surface states  $N_s^*$  on the doping level  $N_d$  at  $\varphi_{ms} = 0$ . The used parameter  $l_s$ , cm:  $10^{-8}$  (2, 2'),  $5 \cdot 10^{-8}$  (3, 3'),  $1 \cdot 10^{-7}$  (4, 4') and  $2 \cdot 10^{-7}$  (5, 5').

Estimations in a more general approximation, which emerges from the limits of realization of the Schottky contact show that the sign reversal of the contact potential is possible at  $\varphi_{ms} < 0$ . The higher the modulus quantity  $\varphi_{ms}$ , the lower the values of  $N_d$ , at which the transition from the case of the Schottky contact to the case of realization of enriching band bending occurs. This situation resembles the case of Mott theory for a dense contact [1] when inequality  $\varphi_{ms} < 0$  automatically means realization of enriching band bending. The difference lies in the fact that the sign reversal of the contact potential occurs in this case when the efficient density of surface states decreases rather strongly. It is

also noteworthy that the smaller the value of  $\varphi_{ms}$ , the smaller the value of  $l_s$ , at which a rather large decrease in  $\varphi_c$  associated with the mechanism under consideration occurs (Fig. 27, curves 5, 5').

It should be noted that the difference when using relationships (63) and (643) for the distribution of surface states along the coordinate  $x$  is nonessential, although when using (63), the decrease in the values of  $\varphi_c$  and with increasing  $N_d$  is larger than when using (64).

The most substantial result following from the analysis is the possibility of sign reversal of the contact potential, *i.e.*, the realization of enriching band bending instead of the depletion type. In our opinion, this mechanism was implemented in [104] for contacts of Si with W in the region  $N_d \sim 10^{20} \text{ cm}^{-3}$ . Proof of this fact is the contact resistivity increase with increasing the temperature, which is possible only in the case of enriching band bending. According to [28], the criterion of contact ohmicity is the condition  $R_c < R_b$ , where  $R_c$  is the contact resistance and  $R_b$  is the semiconductor resistance. The magnitude of  $R_b$  in the actual region of doping levels decreases like to the case of increasing  $N_d$ . At the same time, with the used values of parameters  $\varphi_{ms} = 0$  and  $l_s = 10^{-7} \text{ cm}$  it decreases probably more rapidly. Therefore, the contact is ohmic in the case under consideration at  $N_d \geq 1 \cdot 10^{19} \text{ cm}^{-3}$  and  $d_s = 10 \mu\text{m}$ , where  $d_s$  is the semiconductor thickness.

Estimations show that a dielectric gap of  $(4 \dots 5) \cdot 10^{-8} \text{ cm}$  in thickness for the Si–SiO<sub>2</sub> system has a tunneling transparency coefficient substantially smaller than unity. Herewith, the mechanism of formation of negative charge in semiconductor via tunneling from metal, which is considered in [105], becomes impossible. Taking this mechanism into account is not required because the required value of negative charges provided by the intrinsic surface states of semiconductor.

To date, the effect of decreasing the contact potential due to incomplete charge screening by surface states at rather high doping levels has not been analyzed. At the same time, it can provide the realization of ohmic contacts, which is usually prescribed to the manifestation of a tunneling mechanism of current passage in the presence of the doping step [19]. It is for this reason that it requires the most careful theoretical and experimental investigation.

#### 8.4. Conclusions

The dependences of the contact resistance and efficient density of screening surface states on the doping level of semiconductor for the metal–semiconductor contact with a dielectric gap, if taking into account the spatial distribution of surface states, are found and analyzed. It has been shown that it leads to a stronger decrease in the contact potential with increasing the doping level, which in the  $\delta$ -function approximation provides a decrease in the density of surface states screening the charge. The larger the characteristic damping parameter of surface states  $l_s$  and the smaller the contact potential difference  $\varphi_{ms}$ , the larger the effect is. This effect promotes

realization of ohmic contacts under conditions of low degeneracy of the semiconductor bulk, *i.e.*, is a competitor for the tunneling mechanism of current passage, which is realized in the presence of a doping step.

## 9. General conclusions

Ohmic contacts may be separated into two groups according to the features related to temperature dependences of contact resistivity. The first group includes ohmic contacts based on the Schottky structures with a depletion layer in the space charge region. They are characterized by decreasing the contact resistivity with temperature (at thermionic and thermal-field mechanisms of current flow) and temperature independence of tunnel mechanism of current flow.

The second group includes ohmic contacts based on the structures with an accumulation layer in SCR. There are several ways to realize accumulation layers in the contact region. One of them is analyzed in detail for the case of contacts with high dislocation density. As a rule, in that case dislocations are associated with metal shunts, sizes of which are close to atomic ones. As it takes place, the image force potential is so high that it ensures the charge sign change at the shunt ends in semiconductor (from depletion to accumulation).

Another case is presence of a doping step. In this case, contact resistivity is determined by series connection of two resistances. One of them is contact resistance related to potential barrier penetration by electrons (in accord with the thermal-field or field mechanisms) at the boundary of heavily doped semiconductor and metal, while another is efficient contact resistance of weakly doped region at the boundary with the heavily doped one. Usually the first contact resistance is much lower than the second one (realized in the semiconductor region accumulating the majority charge carriers) that just determines value of the resulting contact resistance.

The third case is related to realization of accumulation band bending in SCR of semiconductor on condition that the metal work function is less than the semiconductor work function. This case (unlike the Mott theory) may be realized in contacts with high density of surface states at high levels of semiconductor doping due to reduction of surface states charge. The latter is related to its incomplete screening at SCR thicknesses less than the characteristic attenuation length of surface state concentration.

It is very important that ohmic contacts of the second type remain ohmic down to helium temperatures. At the same time, contacts of the first type (except tunnel contacts) inevitably become non-ohmic at helium temperatures. It should be noted, however, that contacts of the second type may become non-optimal. It takes place, because operating temperature of many semiconductor devices may be much over the room temperature.

To avoid undesired influence on the characteristics of semiconductor devices, the ohmic contact resistance has to be sufficiently low. Now the achieved values of ohmic contact resistivity  $R_c$  are about  $(10^{-6}-10^{-8}) \Omega/\text{cm}^2$  [10]. As the doping level grows,  $R_c$  value decreases as  $N_d^{-1}$  for ohmic contacts of the first type only. As to ohmic contacts of the second type, decrease of  $R_c$  in them is achieved by varying other factors. For example, in the case of current flow through shunts associated with dislocations, the higher is the dislocation density, the lower is  $R_c$ . In the case of doping step,  $R_c$  value, as a rule, does not depend on the concentration of majority charge carriers in heavily doped region; it is defined by the doping level in weakly doped region. In the case of mechanism related to reduction of surface states charge,  $R_c$  value is defined primarily by relation between the metal and semiconductor work functions. At realization of the above mechanism,  $\Phi_{ms}$  value is negative; the higher is its magnitude, the lower will be  $R_c$  value.

The results of theoretical analysis of formation mechanism for ohmic contacts (with the allowance made for reduction of surface states charge at high doping levels) presented in this review expand essentially the notion of possibilities to obtain ohmic contacts. They may be used for practical realization of ohmic contacts as well as for optimization of their properties.

## References

1. Mott N.F. Note on the contact between a metal and an insulator or semi-conductor. *Math. Proc. Cambridge Philos. Soc.* 1938. **34**. P. 568–572.
2. Schottky W. Halbleitertheorie der Sperrschicht. *Naturwissenschaft.* 1938. **26**, N 52. S. 843.
3. Spenke W.E. Zur quantitativen Durchführung der Raumladungs- und Schottky Randschichttheorie der Kristallgleichrichter. *Wissenschaftliche Veröffentlichungen aus den Siemens-Werken* 1939. **18**. S. 225–291.
4. Davydov B.I. About contact resistance of semi-conductors. *Zhurnal Eksperiment. Teor. Fiziki.* 1939. **9**. P. 451 (in Russian).
5. Davydov B.I. Junction resistances in semi-conductors. *Zhurnal Eksperiment. Teor. Fiziki.* 1940. **10**. P. 1342 (in Russian).
6. Pekar S.I. Theory of contact with dielectric and semiconductor. *Zhurnal Eksperiment. Teor. Fiziki.* 1940. **10**. P. 1210 (in Russian).
7. Pekar S.I. Contact of semiconductor with metal and near-electrode jumps of potential. *Izv. AN SSSR, ser. fiz.* 1941. **5**, No 4-5. P. 422–433 (in Russian); Lifshits I.M. *Tamm bounded states of electrons on the crystal surface and surface oscillations of lattice atoms.* *Uspekhi fizich. nauk.* 1955. **56**, No 4. P. 531 (in Russian).
8. Bardeen J. Surface states and rectification at a metal semiconductor contact. *Phys. Rev.* 1947. **71**, No 10. P. 717–727.

9. Spicer W.E., Kendelewicz T., Newman N., Cao R., McCants C., Miyano K., Lindau I., Liliental-Weber Z., Weber E.R. The advanced unified defect model and its applications. *Appl. Surf. Sci.* 1988. **33/34**. P. 1009–1029.
10. Blank T.V. and Gol'dberg Yu.A. Mechanisms of current flow in metal-semiconductor ohmic contacts. *Semiconductors*. 2007. **41**, No 11. P. 1263–1292.
11. Roderick E.H. *Metal-Semiconductor Contacts*. Clarendon, Oxford, 1978.
12. Strikha V.I. *Theoretical Basics of the Operation of Metal-Semiconductor Contact*. Naukova Dumka, Kiev, 1974 (in Russian).
13. Morkoç H. *Handbook of Nitride Semiconductors and Devices*, Vol. 2. WILEY-VCH Verlag GmbH & Co, KGaA, Weinheim, 2008.
14. *Contacts to Semiconductors. Fundamentals and Technology*. Ed. by L.J. Brillson. Noyes Publication, Park Ridge, New Jersey, 1993. Chapter 1. Marshall E.D., Murakami M. Ohmic contacts to GaAs and other III-V compounds: Correlation of microstructures with electrical properties. P. 1–59; Chapter 4. Tung R.T. Schottky barriers and ohmic contacts to silicon. P. 176–276.
15. *Processing of Wide Band Gap Semiconductors*. Ed. by S.J. Pearton. Norwich, NY, William Andrew Publishing – Noyes Publications, 2000.
16. *Handbook of compound semiconductors: growth, processing, characterization, and devices*. Ed. by P.H. Holloway, G.E. McGuire. Park Ridge, N.J., U.S.A.: Noyes Publications, 1995. Chapter 4. Katz A. Physical and chemical deposition of metals as ohmic contacts to InP and related materials, P. 170–250; Chapter 3. Kim T.J., Hollovey P.H. Ohmic contacts to II-VI and III-V compounds semiconductors. P. 80–150.
17. *SiC Materials and Devices*. Ed. by M. Shur, S. Rumyantsev, M. Levinstein. Vol. 1. World Scientific, London, 2007. Chapter 3. Roccaforte F., La Via F., Raineri V. Ohmic contacts to SiC. P. 77–116.
18. Marshall E.D. *Ohmic Contacts to n-Type Aluminum Gallium Arsenide Utilizing Limited Solid-Phase Reactions*. Ph.D. dissertation, University of California, San Diego, 1989.
19. Sze S.M., Ng K.K. *Physics of Semiconductor Devices*. 3<sup>rd</sup> ed. John Wiley & Sons, Inc., Hoboken, NJ, USA, 2007.
20. Henish A.K. *Rectifying Semiconductor Contacts*. Clarendon, Oxford, 1957.
21. Sachenko A.V., Belyaev A.E., Boltovets N.S., Konakova R.V., Kudryk Ya.Ya., Novitskii S.V., Sheremet V.N., Li J., and Vitusevich S.A. Mechanism of contact resistance formation in ohmic contacts with high dislocation density. *J. Appl. Phys.* 2012. **111**, No 8. P. 083701.
22. Sachenko A.V., Belyaev A.E., Boltovets N.S., Vinogradov A.O., Kladko V.P., Konakova R.V., Kudryk Ya.Ya., Kuchuk A.V., Sheremet V.N., Vitusevich S.A. Features of temperature dependence of contact resistivity in ohmic contacts on lapped *n*-Si. *J. Appl. Phys.* 2012. **112**, No 6. P. 063703.
23. Sachenko A.V., Belyaev A.E., Boltovets N.S., Konakova R.V., Vitusevich S.A., Novitskii S.V., Sheremet V.N., Pilipchuk A.S. The temperature dependence of the resistivity of ohmic contacts based on gallium arsenide and indium phosphide in the 4.2–300 K range. *Techn. Phys. Lett.* 2016. **42**, No 6. P. 649–651.
24. Sachenko A.V., Belyaev A.E., Boltovets N.S., Brunkov P.N., Jmerik V.N., Ivanov S.V., Kapitanchuk L.M., Konakova R.V., Klad'ko V.P., Romanets P.N., Saja P.O., Safryuk N.V., Sheremet V.N. Temperature dependences of the contact resistivity in ohmic contacts to  $n^+$ -InN. *Semiconductors*. 2015. **49**, No 4. P. 461–471.
25. Sachenko A.V., Belyaev A.E., Boltovets N.S., Konakova R.V., Kapitanchuk L.M., Sheremet V.N., Sveshnikov Yu.N., Pilipchuk A.S. Mechanism of current flow in a Au-Ti-Al-Ti- $n^+$ -GaN ohmic contact in the temperature range of 4.2–300 K. *Semiconductors*. 2014. **48**, No 10. P. 1308–1311.
26. Sachenko A.V., Belyaev A.E., Boltovets N.S., Vinogradov A.O., Pilipenko V.A., Petlitskaya T.V., Anischik V.M., Konakova R.V., Korostinskaya T.V., Kostilyov V.P., Kudryk Ya.Ya., Lyapin V.G., Romanets P.N., Sheremet V.N. On a feature of temperature dependence of contact resistivity for ohmic contacts to *n*-Si with an  $n^+$ -*n* doping step. *SPQEO*. 2014. **17**, No 1. P. 1–6.
27. Sachenko A.V., Belyaev A.E., Konakova R.V. On the ohmicity of Schottky contacts. *Semiconductors*. 2016. **50**, No. 6. P. 761–768.
28. Sachenko A.V., Belyaev A.E., Konakova R.V. On a new mechanism for the realization of ohmic contacts. *Semiconductors*. 2018. **52**, No 1. P. 138–142.
29. Romanets P.N., Sachenko A.V. Electron transport near the Mott transition in *n*-GaAs and *n*-GaN. *Phase Transitions*. 2016. **89**, No 1. P. 52–59.
30. Padovani F.A. and Stratton R. Field and thermionic-field emission in Schottky barriers. *Solid State Electronics*. 1966. **9**, No 7. P. 695–707.
31. Bessolov V.N., Blank T.V., Gol'dberg Yu.A., Konstantinov O.V., Posse E.A. Dependence of the mechanism of current flow in the In-*n*-GaN alloyed ohmic contact on the majority carrier concentration. *Semiconductors*. 2008. **42**, No 11. P. 1315–1317.
32. Clausen T., Leistiko O., Chorkendorff I., and Larsen J. Transport properties of low-resistance ohmic contacts to InP. *Thin Solid Films*. 1993. **232**, No 2. P. 215–227.
33. Kupka R.K. and Anderson W.A. Minimal ohmic contact resistance limits to *n*-type semiconductors. *J. Appl. Phys.* 1991. **69**, No 6. P. 3623.
34. Svechnikov G.S., Morozovskaya A.N. *Nanotubes and Graphene – Materials of Electronics of the Future*. Kiev, Logos, 2009 (in Russian).

35. Seeger K. *Semiconductor Physics*. Springer-Verlag, Wien–New York, 1973.
36. You J.H. and Johnson H.T. Chapter 3. Effect of dislocations on electrical and optical properties in GaAs and GaN. *Solid State Physics*. 2009. **61**. P. 143–261.
37. Götz W., Johnson N.M., Chen C., Liu H., Kuo C., Imler W. Activation energies of Si donors in GaN. *Appl. Phys. Lett.* 1996. **68**, No 22. P. 3144.
38. Walukiewicz W., Lagowski J., Jastrzebski L., Pava P., Lichtensteiger M., Gatos G.H. Electron mobility and free-carrier absorption in InP; determination of the compensation ratio. *J. Appl. Phys.* 1980. **51**, No 5. P. 2659.
39. Galavanov V.V. and Siukaev N.V. On mechanism of electron scattering in InP. *phys. status solidi*. 1970. **38**, No 2. P. 523–530.
40. Ferry D.K. First-order optical and intervalley scattering in semiconductors. *Phys. Rev. B*. 1976. **14**. P. 1605–1609.
41. Klad'ko V.P., Chornen'kii S.V., Naumov A.V., Komarov A.V., Tacano M., Sveshnikov Yu.N., Vitusevich S.A., Belyaev A.E. Interface structural defects and photoluminescence properties of epitaxial GaN and AlGaIn/GaN layers grown on sapphire. *Semiconductors*. 2006. **40**, No 9. P. 1060–1065.
42. Mataré H.F. *Defects Electronics in Semiconductors*. Wiley-Interscience, New York, 1971.
43. Blank T.V., Goldberg Yu.A., Konstantinov O.V., Nikitin V.G., Posse E.A. Mechanism of current flow in alloyed ohmic In/GaAs contacts. *Techn. Phys.* 2007. **52**, No 2. P. 285–287.
44. Blank T.V., Gol'dberg Yu.A., Konstantinov O.V., Nikitin V.G., Posse E.A. Peculiarities in the mechanism of current flow through an ohmic contact to gallium phosphide. *Tech. Phys. Lett.* 2004. **30**, No 10. P. 806–809.
45. Gol'dberg Yu.A., Posse E.A. Transition processes occurring under continuous and stepwise heating of GaAs surface-barrier structures. *Techn. Phys.* 2001. **46**, No 9. P. 1128–1132.
46. Blank T.V., Gol'dberg Yu.A., Konstantinov O.V., Nikitin V.G., Posse E.A. The mechanism of current flow in an alloyed In-GaN ohmic contact. *Semiconductors*. 2006. **40**, No 10. P. 1173–1177.
47. Kontsevoi Yu.A., Litvinov Yu.M., Fattakhov E.A. *Plasticity and Strength of Semiconductor Materials and Structures*. Moscow, Radio i Svyaz', 1982 (in Russian).
48. Argunova T.S., Grekhov I.V., Gutkin A.A., Kostina L.S., Belyakova E.I., Kudryavtseva T.V., Kim E.D., Park D.M. Dislocations in silicon structures prepared by direct bonding of surfaces with a relief. *Physics of the Solid State*. 1996. **38**, No 11. P. 1832–1834.
49. Kim E.D., Kim N.K., Kim S.C., Grekhov I.V., Argunova T.S., Kostina L.S., Kudryavtseva T.V. Silicon direct bonding technology employing a regularly grooved surface. *Electron. Lett.* 1995. **31**, No 23. P. 2047–2048.
50. Plößl A. and Kräuter G. Wafer direct bonding: Tailoring adhesion between brittle materials. *Mat. Sci. Eng. R*. 1999. **25**. P. 1–88.
51. Argunova T.S., Andreev A.G., Belyakova E.I., Grekhov I.V., Kostina L.S., Kudryavtseva T.V. Direct bonding of silicon wafers with a regular relief at the interface. *Techn. Phys. Lett.* 1996. **22**, No 2. P. 133–135.
52. Polukhin A.S., Zueva T.K., Solodovnik A.I. Using thermomigration in technology of structures of power semiconductor devices. *Silovaya Elektronika*. 2006. No 3. P. 110–112 (in Russian).
53. Grekhov I.V., Mesyats G.A. Nanosecond semiconductor diodes for pulsed power switching. *Phys.-Uspekhi*. 2005. **48**, No 7. P.703–712.
54. Jayant Baliga B. *Fundamentals of Power Semiconductor Devices*. Springer Science, New York, 2008.
55. Bonch-Bruevich V.L. and Kalashnikov S.G. *Physics of Semiconductors*. 2-nd ed. Nauka, Moscow, 1990 (in Russian) [Bonch-Bruevich V.L. Kalashnikov S.G. *Halbleiterphysik*. Deutscher Verlag der Wissenschaften, Berlin, 1982].
56. *Handbook of Physical Quantities*, ed. by I.S. Grigoriev and E.Z. Meilikhov. CRC Press, Boca Raton, FL, 1996.
57. Samsonov G.V., Dvorina L.A., Rud' B.M. *Silicides*. Moscow, Metallurgiya, 1979 (in Russian).
58. Schroder D.K. *Semiconductor Material and Device Characterization*. New York, Wiley, 2006.
59. Belyaev A.E., Basanets V.V., Boltovets N.S., Zorenko A.V., Kapitanchuk L.M., Kladko V.P., Konakova R.V., Kolesnik N.V., Korostinskaya T.V., Kritskaya T.V., Kudryk Ya.Ya., Kuchuk A.V., Milenin V.V., Ataubaeva A.B. Effect of *p-n* junction overheating on degradation of silicon high-power pulsed IMPATT diodes. *Semiconductors*. 2011. **45**, No 2. P. 253–259.
60. Davydov V.Yu., Klochikhin A.A. Electronic and vibrational states in InN and In<sub>x</sub>Ga<sub>1-x</sub>N solid solutions. *Semiconductors*. 2004. **38**, No 8. P. 861–898.
61. *Indium Nitride and Related Alloys*, Eds. T.D. Veal, C.F. McConville, W.J. Achaff. CRC Press, Boca Raton, FL, 2010.
62. Kovalev A.N. *Semiconductor Heterostructure Transistors*. DomMISiS, Moscow, 2011 (in Russian).
63. Ratnikov V.V., Mamutin V.V., Vekshin V.A., Ivanov S.V. X-ray diffractometric study of the influence of a buffer layer on the microstructure of molecular-beam epitaxial InN layers of different thicknesses. *Phys. Solid State*. 2001. **43**, No 5. P. 949–954.
64. Ren F., Abernathy C.R., Pearton S.J., Wisk P.W. Thermal stability of Ti/Pt/Au nonalloyed ohmic contacts on InN. *Appl. Phys. Lett.* 1994. **64**, No 12. P. 1508–1510.

65. Ren F., Abernathy C.R., Chu S.N.G., Lothian J.R., Pearton S.J. Use of InN for Ohmic contacts on GaAs/AlGaAs heterojunction bipolar transistors. *Appl. Phys. Lett.* 1995. **66**, No 12. P. 1503–1505.
66. Ren F., Vartuli C.B., Pearton S.A., Abernathy C.R., Donovan S.M., MacKenzie J.D., Shul R.J., Zolper J.C., Lovejoy M.L., Boy A.G., Hagerott-Crawford M., Jones K.A. Comparison of ohmic metallization schemes for InGaAlN. *J. Vac. Sci. Technol. A*. 1997. **15**, No 3. P. 802–806.
67. Rudinsky M.E., Gutkin A.A., Brunkov P.N. Capacitance-voltage characteristics of the electrolyte-*n*-InN surface and electron states at the interface. *Semiconductors*. 2010. **44**, No 8. P. 1020–1024.
68. Malkov P.M., Danilin I.B., Zel'dovich A.G., Fradkov A.B. *A Handbook on Physico-Technical Basics of Cryogenics*. Moscow: Energiya, 1973 (in Russian).
69. Bardeen J. Electrical conductivity of metals. *J. Appl. Phys.* 1940. **11**, No 2. P. 88–111.
70. Rinke P., Scheffler M., Qteish A., Winkelkemper M., Bimberg D., Neugebauer J. Band gap and band parameters of InN and GaN from quasiparticle energy calculations based on exact-exchange density-functional theory. *Appl. Phys. Lett.* 2006. **89**. P. 161919.
71. Chin-Yang Chang, Gou-Chung Chi, Wei-Ming Wang, Li-Chyong Chen, Kuei-Hsien Chen, Ren F., Pearton S.J. Transport properties of InN nanowires. *Appl. Phys. Lett.* 2005. **87**. P. 093112.
72. Fistul' V.I. *Heavily Doped Semiconductors*. Plenum Press, New York, 1969.
73. Dykman I.M., Rosenbaum V.M., Vasko F.T. Hot electrons in semiconductors with quasi-relativistic band structure. *phys. status solidi (b)*. 1978. **88**, No 2. P. 385–395.
74. Gantmakher V.F., Levinson Y.B. *Carrier Scattering in Metals and Semiconductors*. North Holland, Amsterdam, 1987.
75. Rauch C., Tuomisto F., King P.D.C., Veal T.D., Lu H., Schaff W.J. Self-compensation in highly *n*-type InN. *Appl. Phys. Lett.* 2012. **101**, No 1. P. 011903.
76. Khanna R., Gila B.P., Stafford L., Pearton S.J., Ren F., Kravchenko I.I., Dariban A., Osinsky A.W. B<sub>2</sub>-based ohmic contacts to *n*-GaN. *Appl. Phys. Lett.* 2007. **90**, No 16. P. 162107.
77. Belyaev A.E., Boltovets N.S., Konakova R.V., Kudryk Ya.Ya., Sachenko A.V., Sheremet V.N., Vinogradov A.O. Temperature dependence of contact resistance for Au–Ti–Pd<sub>2</sub>Si–*n*<sup>+</sup>-Si ohmic contacts subjected to microwave irradiation. *Semiconductors*. 2012. **46**, No 3. P. 330–333.
78. Iucolano F., Greco G., Roccaforte F. Correlation between microstructure and temperature dependent electrical behavior of annealed Ti/Al/Ni/Au ohmic contacts to AlGaIn/GaN heterostructures. *Appl. Phys. Lett.* 2013. **103**, No 20. P. 201604.
79. Brezeanu G., Cabuz C., D. Dascalu, Dan P.A. A computer method for the characterization of surface-layer ohmic contacts. *Solid State Electron.* 1987. **30**, No 5. P. 527–532.
80. *Ion Implantation and Beam Processing*, Eds. J.S. Williams, J.M. Poate. Academic Press, N.Y., 1984.
81. Henisch H.K. *Metal Rectifiers*. Clarendon, Oxford, 1949. Chap. 5. P. 51.
82. Pikus G.E. *Fundamentals of the Theory of Semiconductor Devices*. Moscow, Nauka, 1965. Chap. 2. P. 38 (in Russian).
83. Sachenko A.V., Belyaev A.E., Boltovets N.S., Vinogradov A.O., Kapitanchuk L.M., Konakova R.V., Kostylev V.P., Kudrik Ya.Ya., Klad'ko V.P., Sheremet V.N. The mechanism of contact-resistance formation on lapped *n*-Si surfaces. *Semiconductors*. 2013. **47**. P. 449–454.
84. Sullivan M.V. and Eigler J.H. Electroless nickel plating for making ohmic contacts to silicon. *J. Electrochem. Soc.* 1957. **104**, No 4. P. 226–230.
85. Gershenson M., Logan R.A., Nelson D.F. Electrical and electroluminescent properties of gallium phosphide diffused *p-n* junctions. *Phys. Rev.* 1966. **149**, No 2. P. 580–596.
86. Tsarenkov B.V., Goldberg Yu.A., Izergin A.P., Posse E.A., Ravich V.N., Rafiev T.Yu., Sil'vestrova N.F. Metal-gap surface-barrier structures. *Sov. Phys. Semicond.* 1972. **6**. P. 610.
87. Tsarenkov B.V., Goldberg Yu.A., Gusev G.V., Ogurtsov V.I. Photoelectric properties of Au-*n*-GaAs surface-barrier structures in ultraviolet spectral region. *Sov. Phys. Semicond.* 1974. **8**. P. 264–265.
88. Polukhin A. Using technological factors of thermomigration process. *Silovaya Elektronika*. 2009. No 2. P. 90–92 (in Russian).
89. Grekhov I.V. Power semiconductor electronics and pulsed technics. *Herald of the Russian Acad. Sci.* 2008. **78**, No 2. P. 106–115 (in Russian).
90. Milnes A.G. and Feucht D.L. *Heterojunctions and Metal-Semiconductors Junctions*. Academic, New York, London, 1972.
91. Sugano T., Ikoma T., and Takeisi E. *Introduction into Microelectronics*. Iwanami Shoten, Tokyo, 1985.
92. Penin N.A. Effect of recombination velocity at nonrectifying electrode on frequency properties of *p-n* junction for the case of small alternating voltages. *Radiotekhnika i Elektronika*. 1957. **2**. P. 1053 (in Russian).
93. Avak'yants G.M. and Leiderman A.Yu. Effect of the recombination velocity at the rectifying electrode on the voltage-current characteristics of abrupt *p-n* junction. *Radiotekhnika i Elektronika*. 1964. **9**, No 4. P. 670–674 (in Russian).
94. Leiderman A.Yu. and Karageorgii-Alkalaev P.M. On the theory of semiconductor diode with anti-lock back contact. *Radiotekhnika i Elektronika*. 1965. **10**, No 4. P. 720–726 (in Russian).
95. Sachenko A.V. and Snitko O.V. *Photoeffects in Surface Layers of Semiconductors*. Naukova Dumka, Kiev, 1974 (in Russian).

96. *Physical Methods of Diagnostics in Micro- and Nano-Electronics*, Ed. by A.E. Belyaev and R.V. Konakova. ISMA, Kharkov, 2011 (in Russian).
97. Farenbruch A.L. and Bube R.H. *Fundamentals of Solar Cells Photovoltaic Solar Energy Conversion*. Academic, New York, 1983.
98. Zavrazhnov Yu.V., Kaganova I.I., Mazel' E.Z., and Mirkin A.I. *Powerful High Frequency Transistors*. Moscow: Radio Svyaz', 1985 (in Russian).
99. Glinchuk M.D. and Deygen M.F. On the theory of local electronic centers near semiconductor surface. *Fizika tverdogo tela*. 1963. **5**, No 2. P. 405–412 (in Russian).
100. Palau J.M. and Dumas M. Calculation of semiconductor band bending due to a superficial zone including electronic states: Application to Schottky diodes. *Thin Solid Films*. 1990. **191**, No 1. P. 21–30.
101. Bozhkov V.G., Zaytsev S.E. Model of the close contact metal-semiconductor with the Schottky barrier. *Izvestiya vuzov. Fizika*. 2005. **48**, No 10. P. 77–85 (in Russian).
102. Sachenko A.V., Snitko O.V. Peculiarities of kinetics of photoeffects in semiconductors under arbitrary bending the zones on surface. *Fizika i tekhnika poluprovodnikov*. 1969. **3**, No 7. P. 1415 (in Russian).
103. Spicer W.E., Lindau I., Skeath P., and Su C.Y. Unified defect model and beyond. *J. Vac. Sci. Technol.* 1980. **17**, No 5. P. 1019–1027.
104. Swirhun S.E., Swanson R.M. Temperature dependence of specific contact resistivity. *IEEE Electron Device Lett.* 1986. **EDL-7**, No 3. P. 155–157.
105. Shenai K. Very low resistance nonalloyed ohmic contacts to Sn-doped molecular-beam epitaxial GaAs. *IEEE Trans. Electron Devices*. 1987. **ED-34**, No 8. P. 1642–1649.

#### Authors and CV



**Sachenko A.V.:** Professor, Doctor of Sciences in Physics and Mathematics, Chief Researcher at the Department of Semiconductor Surface Physics and Photoelectricity, V. Lashkaryov Institute of Semiconductor Physics, NAS of Ukraine. The area of scientific interests of Prof. A.V. Sachenko includes physics of semiconductors and metal-semiconductor junction processes.

*V. Lashkaryov Institute of Semiconductor Physics, National Academy of Sciences of Ukraine*

*E-mail: sach@isp.kiev.ua*



**Konakova R.V.:** Professor, Doctor of Technical Sciences, Head of the Laboratory of Physical and Technological Problems of Solid State SHF Electronics, V. Lashkaryov Institute of Semiconductor Physics, NAS of Ukraine. The area of scientific interests of Dr. R.V. Konakova includes physics of metal-semiconductor junctions.

*V. Lashkaryov Institute of Semiconductor Physics, National Academy of Sciences of Ukraine*

*E-mail: konakova@isp.kiev.ua*



**Belyaev A.E.:** Academician of NAS of Ukraine, Professor, Doctor of Sciences in Physics and Mathematics, Head of V. Lashkaryov Institute of Semiconductor Physics, NAS of Ukraine. The area of scientific interests of Prof. A.E. Belyaev includes physics of semiconductors and dielectrics as well as processes in metal-semiconductor junctions.

*V. Lashkaryov Institute of Semiconductor Physics, National Academy of Sciences of Ukraine*

*E-mail: belyaev@isp.kiev.ua*